# Evaluating evapotranspiration rates for corn and cotton in thermo-limited climate of southwest Kansas

by

Umme Fatema Piu

B.Sc., Bangladesh University of Engineering and Technology, 2019

A THESIS

submitted in partial fulfillment of the requirements for the degree

MASTER OF SCIENCE

Carl and Melinda Helwig Department of
Biological and Agricultural Engineering
Carl R. Ice College of Engineering

KANSAS STATE UNIVERSITY
Manhattan, Kansas

2022

Approved by:

Major Professor
Dr. Aleksey Y. Sheshukov

# Copyright

# Abstract

The declining water resources from Ogallala Aquifer in Western Kansas and strong climate warming trends provide opportunities for planting alternative crops that reduce irrigation water needs. For instance, cotton, a drought-tolerant crop that meets these requirements, has lately experienced a rapid growth from 6,500 ha in 2015 to 79,000 ha in 2021 in Kansas. As expansion of cotton and other drought tolerant crops intensifies, a thorough examination of evapotranspiration, water use, and irrigation strategies need to be considered to develop sustainable crop production. The widely used FAO-56 approach for calculating ET rates and crop coefficient has shown that crop coefficient can vary with location, thus, locally specific values need to be determined with a combination of in situ measurements and crop growth modeling. In this study, an approach was developed to estimate crop coefficient and evapotranspiration fluxes using continuous field measurements of radiation fluxes, aerial imagery, remote sensing datasets of vegetation growth, and maximum entropy production (MEP) modeling. The MEP model is based on non-equilibrium thermodynamics that allows the partition of surface radiative fluxes into (turbulent and conductive) heat fluxes as functions of field collected surface net radiation, temperature, and humidity. The MEP model is less sensitive to the uncertainty of the input data and model parameters than other models. Comparison of actual ET from MEP model and crop ET and reference ET from Penman-Monteith model yielded derivation of crop coefficient functions for corn and cotton in a thermo-limited climate of High Plains ecoregion of the United States. The approach was tested on two irrigated fields of cotton and corn in Southwestern Kansas in 2020 and 2021. The results showed cotton's higher tolerance to heat, lower water demand, and lower ET

rates as compared to corn. This makes growing irrigated cotton a viable option as sustainable crop production practice under changing climate in semi-arid regions.

# Table of Contents

# List of Figures

# List of Tables

# Acknowledgements

I would like to thank my advisor Dr. Aleksey Sheshukov for his supports throughout this journey. When I lost my father, he helped me a lot mentally to get back to my regular routine and start my study again. He is one of the best mentors I have ever met in my life, he was always there to listen to my problems and provide guidance. He helped me a lot to understand my potential and motivated me for my future studies. I will be always indebted to him.

I would also like to thank Komlan Koudahe, he helped me a lot with the data and was always there to help.

I would like to thank Dr. Daniel Devlin, Dr. Jonathan Aguilar, and Dr. Landon Marston for their kind consent to become a part of my thesis committee and providing their valuable suggestions.

Finally, I would like to thank my beloved husband, Md Rejwanur Rahman for believing in me and standing by my side in every difficult situation. I want to thank my family, my mom my sister and my brothers especially my younger brother, Abu Horaira Hridhon for always being there for me. Without his support, I would have never got the courage for my graduate studies.

# Dedication

I would like to dedicate this to my late father.

# Chapter 1 - Introduction

## 1.1 Background

The declining water resources of Ogallala Aquifer and strong warming trends in Western Kansas affect sustainable crop production and cause needed development of new measures to reduce irrigation water needs including less water-demanding crops. An efficient irrigation scheduling can be an important factor in better managing crop water demands. Water use by crops can be estimated from knowing precipitation amounts and evapotranspiration rates. Evapotranspiration is a combination of evaporation directly from soil and via transpiration from plants.

Evapotranspiration is an important component in the hydrological cycle, and its rate is highly influenced by weather parameters. Above surface atmospheric variables, such as, solar radiation, air temperature and relative humidity, windspeed, etc., affect the energy transfer at soil or leaf surfaces. Below surface soil characteristics, such as, soil temperature and soil water content, affect the ground heat flux and plant water uptake rates. All these factors are essential for proper estimation of evapotranspiration rates on agricultural fields.

Several methods were developed to estimate evapotranspiration rate based on the energy budget equation. One of the most commonly used methods is the Penman-Montieth model presented in the FAO-56 publication (Allen et al., 2007). This method uses a two-step approach for estimates the actual evapotranspiration rate: (i) first it estimates reference evapotranspiration for a reference vegetation cover using the energy flux balance equation with heat fluxes acquired from weather stations, then (ii) it applies adjustment factors in a form of crop coefficients to adjust the referent Et value to the actual crop specific evapotranspiration. The FAO-56 publication provides generalized crop coefficient curves for each crop that might vary with

location, climatic conditions, and irrigation methods (Koudahe et al., 2021). Crop coefficient function needs to be calibrated for local climatic conditions for a specific crop before it can be used in the FAO-56 approach. For established cash crops in a well-studied region crop coefficient functions are usually known and validated (Lamm et al., 1995). However, for the new crops even in a traditionally agricultural region the crop coefficient functions may not be properly represented in the FAO-56 tables and are required to be refined. One example of such new crops in a traditional agricultural region is cotton in Southwest Kansas.

Crop coefficient functions can be developed using the measurements of actual evapotranspiration and reference evapotranspiration. For the reference ET, a weather station outside of the agricultural field with measurements of solar radiation, air temperature and relative humidity, windspeed, and shallow soil temperature are often sufficient. For the actual evapotranspiration on the agricultural field, a more sophisticated meteorological equipment is required. One example could be a flux tower with eddy covariance fluxes that is expensive and provide measurements that can be uncertain if atmospheric turbulence is weak. A cost-effective theoretical and measuring approach needs to be developed for accurate estimation of energy fluxes and ET rates.

Recent studies showed that soil or leaf surface temperature responds had stronger correlation with canopy evapotranspiration condition than air temperature. This relationship can make surface or skin temperature a better proxy to the ET rate than other atmospheric variables including the ones determined by the eddy covariance approach (Good et al., 2017, Mildrexler et al., 2011,Panwar et al., 2019). The new model was developed using the Maximum Entropy

Production (MEP) theory to account for such correlation. MEP is an unconventional dynamic-statistical model of surface heat fluxes proposed by Wang & Bras, 2009,2011 and Wang et al., 2014. MEP model solves for the four energy fluxes at the surface (net radiation, sensible heat, ground heat, and ET fluxes) using data on net radiation, surface (or skin) temperature, and surface specific humidity (El Sharif et al., 2019). This novel approach requires fewer parameters to measure and showed similar (or even smaller) uncertainty in ET estimates than the traditional FAO-56 approach.

ET rates can be highly affected by the crop productivity level with lower transpiration rates caused by higher crop water stress. The crop water stress index (CWSI) is an indicator of the crop water stress. The theoretical CWSI was developed by Jackson et al. (1981) and based on the energy balance analysis. This approach characterizes plant water condition and estimates crop productivity, water stress, and irrigation timing (O'Shaughnessy et al., 2012). For efficient irrigation scheduling, the irrigation timing when crop is slightly under stress is very important.

With the declining water storage in the Ogallala aquifer, alternative crops that optimize and reduce irrigation water needs should be considered in Southwest Kansas. Cotton is a drought-tolerant crop that needs less water and its fiber and oil have high commodity values. Cotton can be used as an alternative crop or rotational crop that optimizes and reduces irrigation water needs. In recent years, the acreage of cotton production (irrigated and non-irrigated) in Kansas has experienced a rapid growth, increasing from 16,000 acres in 2015 to 182,000 acres in 2020 (USDA, 2021). Expanding cotton production in southwestern Kansas could generate several positive benefits to the producer, the rural community, and the Ogallala Aquifer.

## 1.2 Objectives

In this study, we aimed at estimating energy fluxes, ET rates, and crop coefficient functions for two crops, corn, and cotton, in a semi-arid region of Western Kansas. We combine a traditional FAO-56 Penman-Monteith approach with a novel framework based on the maximum entropy production (MEP) model. Two sites near Garden City, KS with two different crops (corn and cotton) were monitored during two growing seasons in 2020 and 2021. Specific objectives for this study are to:

1. Estimate the energy fluxes and the ET rates by low-cost observational setup and novel modeling approach,
2. Develop crop-specific crop coefficient functions for corn and cotton that are suitable to climatic conditions of Southwest Kansas, and
3. Evaluate water stress for corn and cotton during growing seasons of 2020 and 2021 for optimal irrigation scheduling.

## 1.3 Document organization

The thesis consists of the five chapters. Specific topics discussed in each chapter are summarized as follows:

(i) **Chapter 1 – Introduction:** This chapter highlights a background of the problem, specifies objectives, and presents the scope of the study.

(ii) **Chapter 2 – Literature Review:** This chapter presents an overall review of previous studies relevant to this research. The discussed studies were primarily focused on different methods of estimating ET rates.

(iii) **Chapter 3 – Methodology:** This chapter describes the sites, presents the experimental setups, and details model development.

(iv) **Chapter 4 – Results and Discussions:** This chapter contains the results from data collection and the results obtained from applying methods described in Chapter 3 for corn and cotton.

(v) **Chapter 5 – Conclusions and Recommendations:** This chapter concludes this study and provides recommendations for future work.

# Chapter 2 - Literature Review

## 2.1 Agriculture in U.S and Kansas

Agriculture is an art and science of cultivating soil, growing crops, and raising livestock. This includes a preparation of plant and animal products for people to use and distribute to markets. It plays a vital role in the economics and livelihoods of many people around the world.

The growth of agriculture contributed to the rise of civilizations over the centuries. According to world bank's survey which was released in 2021, in 2019, agriculture contributed 3.55%, industry contributed approximately 24.79% and services contributed about 65.04% to the global gross domestic product (Global GDP 2014-2024 | Statista n.d.). There is a wide difference in the contribution of agriculture to national GDPs between highly and least developed countries. In the developed countries, it accounts for 1.3% of GDP, while 26.3% in the least developed ones (The World Bank Group, 2018). Although agriculture is a very small fraction of the GDPs in developed economies, it is important to note that the overall product output of this sector in such countries is significantly higher than those of many developing countries.

Economy of the US is the largest in the world (World Bank, 2016) and agriculture accounts for just 1% of the U.S. Gross Domestic Product (OECD,2011). Around 40% of the U.S. land is used as farmland (Nickerson et al., 2012), and as a result agriculture has become important part of the socioeconomics and livelihoods of large rural areas of the country. Annual crops and livestock produced from U.S. farms are valued at $143 and $153 billion respectively (US EPA, 2015). The main crops grown in the U.S. by acreage are corn, soybeans, wheat, cotton, sorghum, rice, and hays (US EPA, 2015).

Kansas is one of the most important agricultural states in the US, ranking 7th among the other states for total agricultural production (Netstate, 2021). Agriculture is a critical part of Kansas's past, and it is a key economic driver in the present, but it also holds great potential for the future. In terms of the revenue generated, Kansas's top five agricultural products are cattle and calves, wheat, corn for grain, soybeans, and hays, among them wheat is the largest one that accounts for about 12% of the state's total agricultural production. In fact, Kansas is the number 1 wheat-producing state, generating about 15% of the nation's total crop. Corn for grain is another valuable Kansas crop, contributing about 9% to the state's total agricultural revenue. Soybeans are also a valuable crop in Kansas, followed by sorghum grain and hays (Netstate, 2021). It was estimated that in 2019, 72 agriculture and agriculture-related sectors directly contributed $47.3 billion in output and supported about 135,786 jobs for Kansas economy (KDA, 2019). Table 2.1 shows summary of total crops for Kansas in 2020.

**Table 2.1: Crops - Planted, Harvested, Yield, Production, Price (MYA), Value of Production Sorted by Value of Production in Dollars (USDA/NASS 2020)**

| Commodity | Planted All Purpose Acres | Harvested Acres | Yield | Production | Price per Unit | Value of Production in Dollars |
|---|---|---|---|---|---|---|
| CORN | | | | | | |
| CORN, GRAIN | | 5720000 | 134 BU / ACRE | 766,480,000 BU | 4.35 $ / BU | 3.3E+09 |
| CORN, SILAGE | | 250000 | 19.5 TONS / ACRE | 4,875,000 TONS | | |
| CORN | 6100000 | | | | | |
| SOYBEANS | | | | | | |
| SOYBEANS | 4800000 | 4750000 | 41 BU / ACRE | 194,750,000 BU | 10.7 $ / BU | 2.07E+09 |
| WHEAT | | | | | | |
| WHEAT | 6600000 | 6250000 | 45 BU / ACRE | 281,250,000 BU | 4.53 $ / BU | 1.27E+09 |

| | | | | | | |
|---|---|---|---|---|---|---|
| WHEAT, WINTER | 6600000 | 6250000 | 45 BU / ACRE | 281,250,000 BU | 4.53 $ / BU | 1.27E+09 |
| SORGHUM | | | | | | |
| SORGHUM, GRAIN | | 2800000 | 85 BU / ACRE | 238,000,000 BU | 8.85 $ / CWT | 1.15E+09 |
| SORGHUM, SILAGE | | 60000 | 15 TONS / ACRE | 900,000 TONS | | |
| SORGHUM | 3000000 | | | | | |
| HAY & HAYLAGE | | | | | | |
| HAY & HAYLAGE | | 2665000 | 2.33 TONS / ACRE, DRY BASIS | 6,222,000 TONS, DRY BASIS | | 6.81E+08 |
| HAY & HAYLAGE, (EXCL ALFALFA) | | 2120000 | 1.97 TONS / ACRE, DRY BASIS | 4,184,000 TONS, DRY BASIS | | 3.93E+08 |
| HAY & HAYLAGE, ALFALFA | 85000 | 545000 | 3.74 TONS / ACRE, DRY BASIS | 2,038,000 TONS, DRY BASIS | | 2.87E+08 |
| HAY | | | | | | |
| HAY | | 2590000 | 2.28 TONS / ACRE | 5,893,000 TONS | 128 $ / TON | 6.48E+08 |
| HAY, (EXCL ALFALFA) | | 2050000 | 1.9 TONS / ACRE | 3,895,000 TONS | 96 $ / TON | 3.66E+08 |
| HAY, ALFALFA | | 540000 | 3.7 TONS / ACRE | 1,998,000 TONS | 147 $ / TON | 2.82E+08 |
| COTTON | | | | | | |
| COTTON, UPLAND | 195000 | 184000 | 783 LB / ACRE | 300,000 480 LB BALES | 0.583 $ / LB | 82637000 |
| COTTON, COTTONSEED | | | | 99,000 TONS | 196 $ / TON | 19110000 |
| COTTON, PIMA | | | | | (NA) $ / LB | |
| COTTON | 195000 | 184000 | 783 LB / ACRE | 300,000 480 LB BALES | | |
| SUNFLOWER | | | | | | |
| SUNFLOWER | 73000 | 70000 | 1,465 LB / ACRE | 102,540,000 LB | 21.4 $ / CWT | 21513000 |
| OATS | | | | | | |
| OATS | 140000 | 16000 | 52 BU / ACRE | 832,000 BU | 3.05 $ / BU | 2454000 |
| BARLEY | | | | | | |
| BARLEY | 16000 | 6000 | 51 BU / ACRE | 306,000 BU | 3.7 $ / BU | 872000 |
| CANOLA | | | | | | |
| CANOLA | 5000 | 2800 | 1,790 LB / ACRE | 5,012,000 LB | 12.2 $ / CWT | 655000 |

| | | | |
|---|---|---|---|
| HAYLAGE | | | |
| HAYLAGE, ALFALFA | 15000 | 5.3 TONS / ACRE | 80,000 TONS |
| HAYLAGE, (EXCL ALFALFA) | 90000 | 6.5 TONS / ACRE | 585,000 TONS |
| HAYLAGE | 105000 | 6.33 TONS / ACRE | 665,000 TONS |

## 2.2 Climate Condition in Kansas

Kansas is located in the center of the United States, and experiences three different types of climate. The western half of Kansas is represented by a semi-arid steppe (Köppen climate classification BSk) with hot summers and cold winters, where atmosphere draws more water from the soil than it gives back in the form of a rain. A significant eastern part of this state has hot and humid summers and falls under the humid continental (Köppen Dfa) type. Southeastern Kansas has a humid subtropical type (Köppen Cfa) with mild winters. The topography of the state mainly consists of fertile farmlands in the west and forests in the east. The western part of Kansas lies in the great central plain of the US. A major part of the state is covered by the Missouri, Kansas, and Arkansas rivers, along with their tributaries. Altitude differences and the effect of the Rocky Mountains have a large impact on precipitation (Atlas, n.d.). Figure 2.1 and Figure 2.2 show annual precipitation and average temperature for Kansas from 1991 to 2020. From southeastern Kansas to southwestern Kansas, precipitation varies from more than 45 inches to less than 18 inches and temperature varies from more than 58° F to less than 51° F (Kansas Mesonet, 2019).

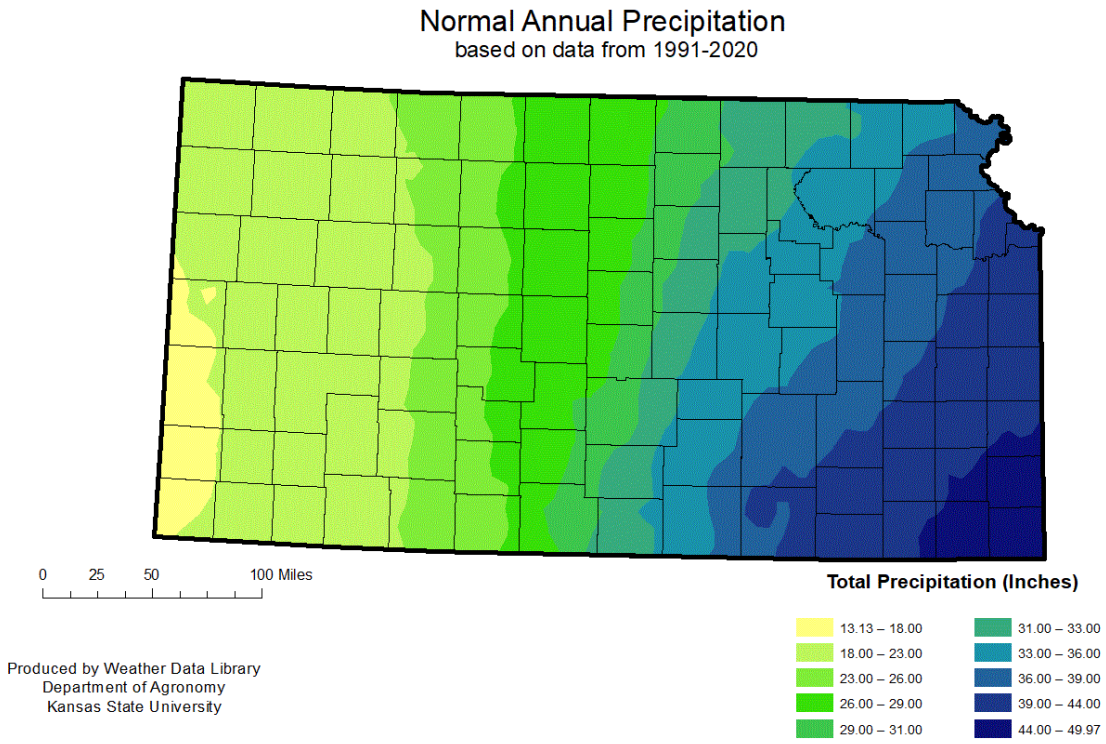


**Figure 2.1: Annual average precipitation in Kansas (Kansas Mesonet, 2019)**

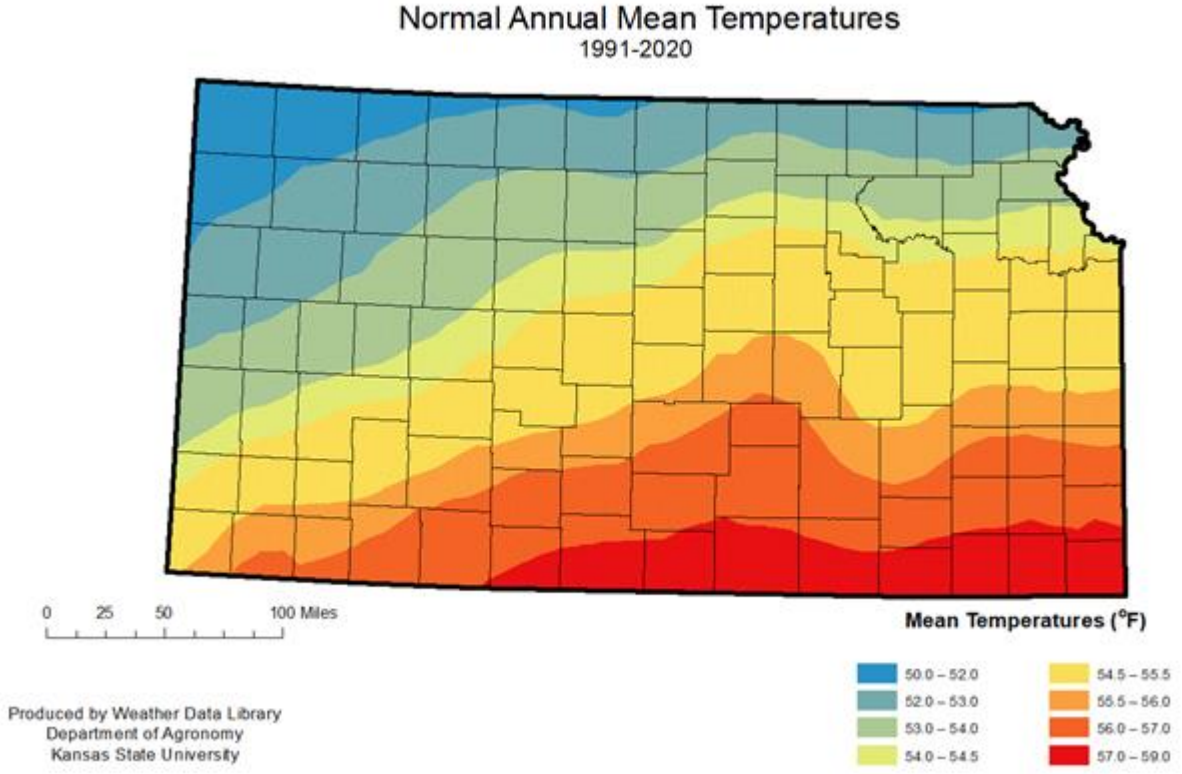


**Figure 2.2: Annual average temperature in Kansas (Kansas Mesonet, 2019)**

## 2.3 Corn Production in Kansas

Corn plays a vital role in Kansas agricultural economy. It is the second largest crop in Kansas history. According to USDA/NASS Crop Values Report, in 2020 corn production was 766 million bushels with a yield of 134 bushels per acre and 5.72 million acres that was valued at $3.296 billion (USDA/NASS 2020 State Agriculture Overview for Kansas, n.d.). Figure 2.3 shows the county level crop production data for Kansas in 2020.

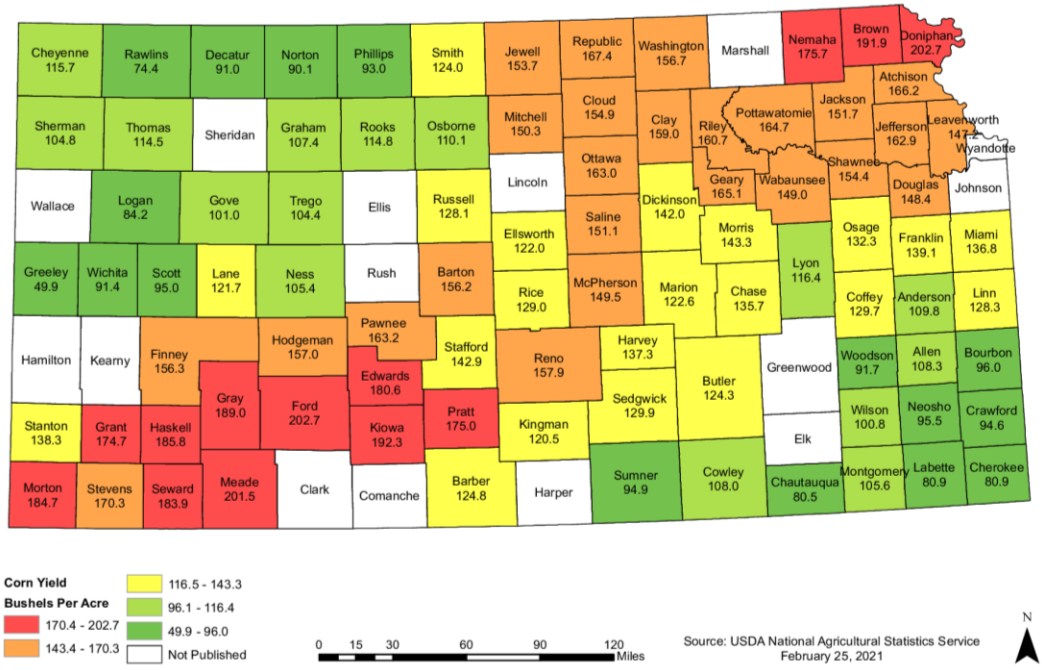


**Figure 2.3: Corn yield for Kansas in 2020 (United States Department of Agriculture, 2016)**

A mid-season corn hybrid requires approximately 2700 Growing Degree Days (GDD) from Table 2.2 to reach maturity stage from the time of planting, for which the length of growing season is approximately 120 days. It can be more or less than 120 days as the number of days required to reach maturity depends on location, date of planting, and the weather condition in a particular growing season. Average net seasonal irrigation requirements for corn in Kansas range from about 5 inches in the east to nearly 16 inches in the west considering 80 percent chances of

rainfall. Corn yield response to irrigation is significant. In western Kansas most prevalent soil type is silt loam, a high water-holding capacity soil type; as a result, irrigation capacity here is needed only about 0.25 inches per day under most conditions to provide full water capacity (Holman & Foster, 2017).

**Table 2.2: Growing Degree Days (GDD) required for a mid-season maturity corn hybrid to reach different growth stages from the time of planting (Hoeft, 2000)**

| Stage | GDD |
|---|---|
| VE-Emergence | 125 |
| V6 - Tassel initiation | 475 |
| VT - Tassel emergence | 1150 |
| Silking | 1400 |
| R4 - Dough stage | 1925 |
| R5 - Dent stage | 2450 |
| R6 - Physiological maturity or black-layer | 2700 |

Data from F. R. Lamm et al., 1995 and Hall, 2014 were used to develop crop coefficient curve for corn in Kansas for different growth stages (Figure 2.4).

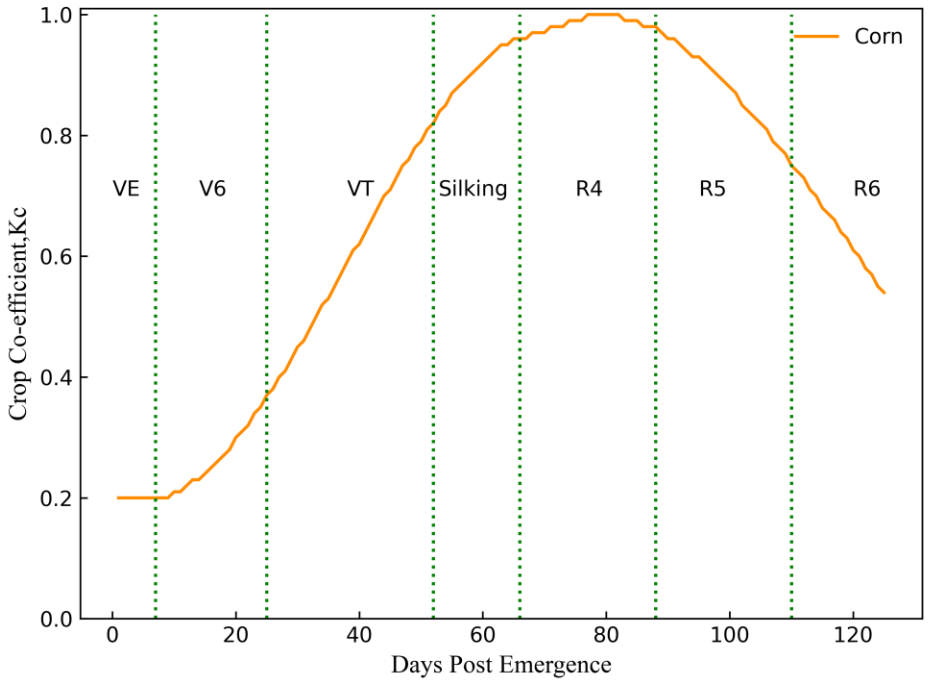


**Figure 2.4: Crop Coefficient for Corn in Kansas**

## 2.4 Cotton Production in Kansas

Cotton is a comparatively new crop in Kansas that has become one of the fastest growing crops with acreage and its production increasing every year. The cotton sector is smaller in production than other Kansas crops and ranked 15th nationwide as of 2018, but production in the state has increased significantly since 1996. Cotton offers farmers a highly water-efficient crop which works well as part of a rotation management system (Haag et al., 2013). Figure 2.5 shows county level Cotton production in Kansas.

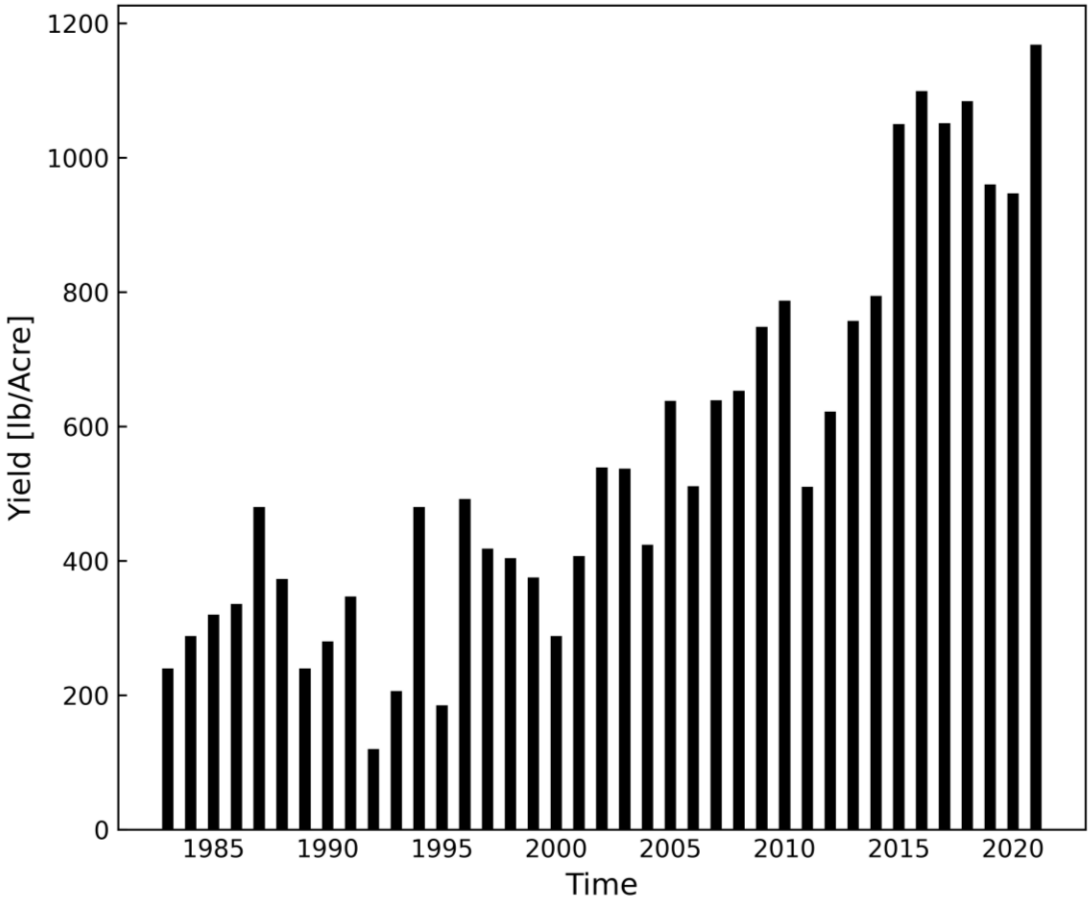


**Figure 2.5: Cotton Yield for Kansas in from 1980 to 2021 (United States Department of Agriculture, 2016)**

Cotton is a perennial plant which is heat-unit sensitive, and approximately 2,200 to 2,600 GDD (Table 2.3) is required for a set boll to open. Once the plant reaches bloom stage, the

response to heat units is less significant and night temperatures and light intensity become more critical in reaching the maturity stage. As it is a drought-tolerant crop, it produces higher farm-level economic value per inch of applied water than any other crop in southwest Kansas. Compared to corn, alfalfa and soybeans, profitable cotton yields can be reached under irrigation with about one-half to one-third of the water usages of these crops (National Cotton Council, 2002).

**Table 2.3: The average number of days and heat units required for various growth stages of cotton in the Mid-South(Oosterhuis, 2015)**

| Growth Stage | Days | Heat Units |
|---|---|---|
| Planting to Emergence | 4 to 9 | 50 to 60 |
| Emergence to First Square | 27 to 38 | 425 to 475 |
| Square to Flower | 20 to 25 | 300 to 350 |
| Planting to First Flower | 60 to 70 | 775 to 850 |
| Flower to Open Boll | 45 to 65 | 850 to 950 |
| Planting to Harvest Ready | 130 to 160 | 2200 to 2600 |

Figure 2.5 indicates that cotton is relatively new in Kansas, so we do not have that much information about its water usages. During the flowering stage cotton is sensitive to limited water condition. To meet crop evapotranspiration during that period proper irrigation scheduling is needed. FAO-56 publication provides generalized crop coefficients for each crop, but crop water use varies with location, climatic conditions, and irrigation methods. As a result, FAO-56 generalized crop coefficients are not appropriate for all regions, and so local crop coefficient values need to be estimated (Koudahe et al., 2021). Figure 2.6 is produced by using data from Ko et al., 2009, and represents crop coefficient for cotton at Uvalde, Texas for different growing stages.

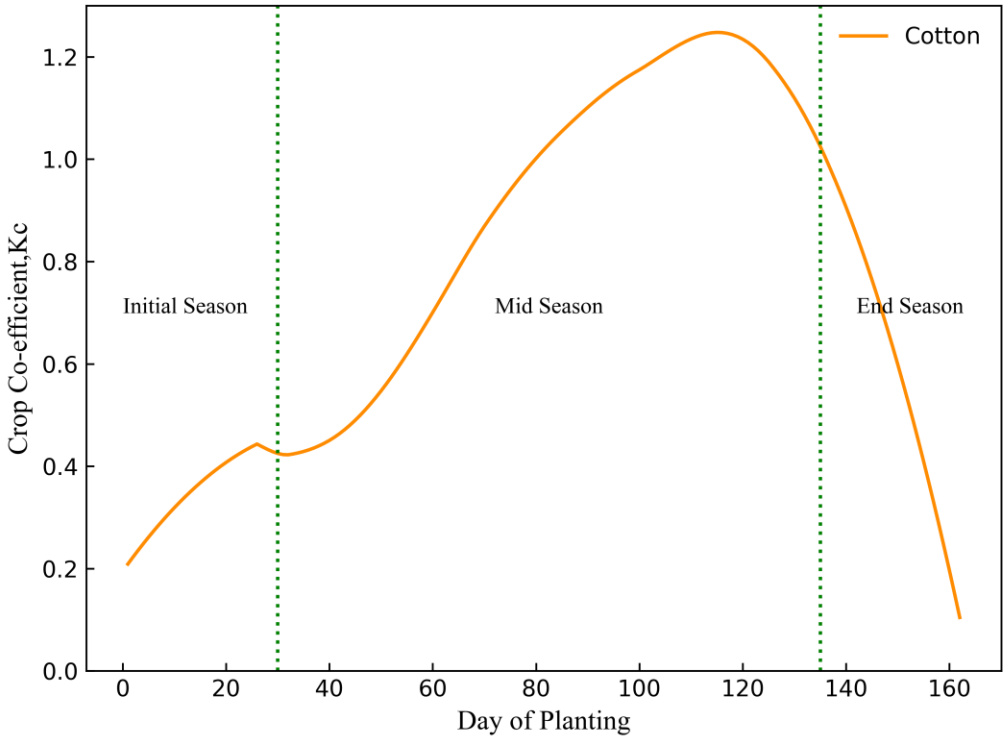


**Figure 2.6: Crop coefficient for Cotton in Texas**

## 2.5 Energy Balance

Land surface energy balance is important for the climate system. It regulates Earth's critical zone hydrometeorological processes where the subsurface is closely coupled with the atmosphere (Brooks et al., 2015). The exchange of energy between the Earth's surface and the overlying atmosphere involves four important processes: radiative exchanges with the atmosphere, ground heat flux, sensible heat fluxes and latent heat fluxes (evapotranspiration) in the lower atmosphere. It can be represented as Equation 2.1.

$$R_n = H + G + \lambda ET \qquad \text{Equation 2.1}$$

where, net radiation, $R_n = SW_{net} + LW_{net} = SW_{in} - SW_{out} + LW_{in} - LW_{out}$

Sensible heat flux =H

Ground heat flux = G

Latent heat flux= λET

Figure 2.7 represents the exchange of energy between Earth's surface and the atmosphere.

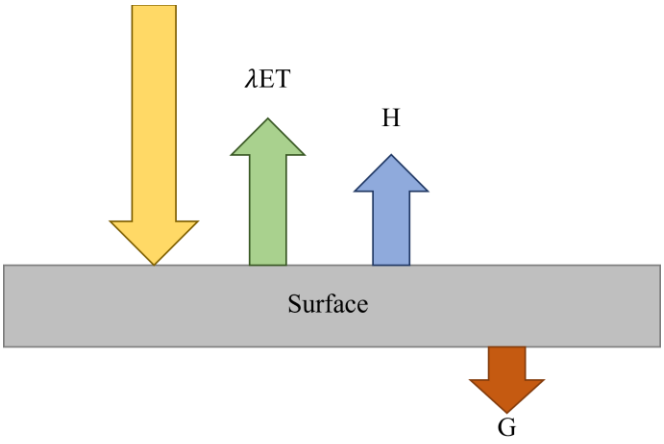


**Figure 2.7: Schematic diagram of land surface energy budget**

### 2.5.1 Radiation Fluxes

Sun continuously emits energy in the form of electromagnetic radiation. Our earth can absorb only a small portion of this energy. This energy is dissipated mainly by warming up the air, warming up the ground, evaporation of water, photosynthesis and some of the portion reflects to the atmosphere.

Emitted energy from the earth's surface does not go directly out to space rather it is reabsorbed by clouds and gases in the atmosphere. Some portion of it gets redistributed by convection. In fact, more energy is released into the atmosphere through condensation.

The balance of incoming sunlight and outgoing longwave radiation are affected by the daily change of temperature and the seasonal changes of weather. In winter when days are short,

the peak temperatures can occur 2-3 hours after noon whereas in summer when days are longer, it can be 4 to 5 hours after noon to reach the highest temperature(North Carolina Climate Office, 2020).

### 2.5.2 Ground Heat flux

The amount of thermal energy that moves through an area of soil in a unit of time is the soil heat flux or ground heat flux. Soil temperature is a key factor that affects the chemical and biological processes in the soil. It is an important component in energy balance at the land surface, particularly over relative dry land surface and over a daily time scale (Sauer & Horton, 2015).

### 2.5.3 Sensible Heat Flux

The loss of energy by the surface as heat transfer to the atmosphere is referred as sensible heat flux. The magnitude of the sensible flux depends on the difference in temperature between air and water and the atmospheric removal.

### 2.5.4 Latent Heat Flux/ Evapotranspiration

Evapotranspiration (ET) is used to describe the water loss process by plant, waterbody, and land surface. Evaporation occurs when water changes to vapor on either soil or plant surfaces, and transpiration refers to water loss through leaves of plants. In a practical situation, we cannot differentiate between evaporation and transpiration, so they are described together as evapotranspiration (Schwalbe, 2017).

Evapotranspiration is a major component in hydrological cycle. Accurate measurements of ET over field, watershed, and regional scales enhance efficiency of water resources usages as well as protect the environment and water quality. ET estimation is also crucial for water allocation, irrigation management, evaluating the effects of changing land us, environmental

assessment, and development of best management practices to protect surface and groundwater (Irmak, 2008).

## 2.6 Evolution of Different Evapotranspiration Methods

There are several methods that were developed to estimate evapotranspiration. The pioneer for developing an equation for evaporation was John Dalton (1766-1844). He developed an equation to estimate evaporation from large water bodies like lakes and reservoirs where the evaporation rate was calculated as the product of vapor pressure deficit and a factor "K". This factor depends on wind speed. It was a breakthrough for ET estimation approach, and over time other ET methods were developed (Subedi & Chávez, 2015). Table 2.4 summarizes major ET estimation methods.

**Table 2.4: Evolution of Different Evapotranspiration Methods**

| Methods | Description | References |
|---|---|---|
| Blaney-Criddle Method | one of the oldest and simple empirical methods to estimate reference crop evapotranspiration by using temperature data | (Kumar et al., 2011) |
| Thornthwaite Method | PET is estimated by using air temperature, and estimation is based on a 12-hour day (amount of daylight) and a 30-day month | (Sellinger, 1996) |
| Hargreaves Equation | only requires a few parameters including minimum, maximum and mean temperature, and extraterrestrial radiation and it does not require wind speed | (Hargreaves & Allen, 2003) |
| Christiansen Method | uses pan evaporation data to relate with crop consumptive use | (Christiansen, 1968) |
| Priestley Taylor Method | simplification of Penman's formula considering evaporation from a wet surface under conditions of minimal advection | (Agam et al., 2010) |

| | | |
|---|---|---|
| Original Penman Equation | combines the surface energy balance equation with an aerodynamic equation, basis for several ET models | (Temesgen et al., 2005) |
| Penman Monteith Equation | introduced some crop resistance terms in the original Penman equation, it is physically based, and it does not require local calibrations | (Monteith et al., 1965) |
| FAO 56 Penman-Monteith Equation | based on the Penman-Monteith equation, defines the reference crop as a hypothetical crop with an assumed height of 0.12 m having a surface resistance of 70 s/m and an albedo of 0.23 | (Allen et al, 1998) |
| ASCE-EWRI Standardized Penman Monteith Evapotranspiration Equation | based on the Penman-Monteith equation, with some simplification and standardization on the aerodynamic and surface resistances, applicable for both tall (alfalfa) and short (grass) reference surfaces, allows to estimate ET at both hourly and daily basis | (Allen et al., 2018) |

### 2.6.1 Blaney-Criddle Method

The Blaney-Criddle method is an empirical method which was first developed in 1942. It is one of the oldest and simple method to estimate reference crop evapotranspiration and uses measured temperature data mainly. The developed mathematical model is given by Equation 2.1 (Kumar et al., 2011).

$$u = kf \qquad \text{Equation 2.2}$$

$$U = \sum kf = KF \qquad \text{Equation 2.3}$$

where, u = monthly consumptive use, in inches

f = TF × p / 100 is the monthly consumptive use factor

TF = mean monthly temperature, in degrees Fahrenheit (ºF)

p = monthly percentage of daytime hours of the year

k = empirical consumptive use crop coefficient for monthly period

U = seasonal consumptive use (or evapotranspiration), in inches

F = sum of the monthly consumptive use factors for the period (sum of the products of mean monthly temperature and monthly percentage of daytime hours of the year)

K = empirical consumptive use crop coefficient for irrigation season or growing period.

However, this method is not very accurate. It provides only a rough estimate, especially under extreme climatic conditions. In windy, dry, sunny areas, the ETo can be underestimated up to 60%, while in calm, humid, clouded areas it overestimates ET by up to 40% (Management, 2012).

### 2.6.2 Thornthwaite Method

In 1948, Thornthwaite and Mather had developed a PET estimation method based solely on air temperature during 12-hour daylight in 30-day period (Sellinger, 1996)

$$PET = 16(10T_a/I)^a \qquad \text{Equation 2.4}$$

where, PET = potential evapotranspiration rate, in mm per month

Ta = mean monthly air temperature, in degrees Celsius (ºC)

I = summation of the 12 monthly heat index i, where i = (Ta / 5)1.514

a = an empirical coefficient, which is calculated using Equation 2.5,

$$a = 0.675 * 10^{-6} I^3 - 77.1 * 10^{-6} I^2 + 0.01792\, I + 0.49239 \qquad \text{Equation 2.5}$$

This method is widely used due to its empirical nature and simple approach. In many parts of the world the method is still used to estimate irrigation water requirement, but its limitations include parameter an estimation based on local climate (Trajkovic et al., 2019).

### 2.6.3 Hargreaves Equation

Hargreaves and Samani in 1975 introduced a simple evapotranspiration model that only requires a few easily accessible parameters, such as, minimum, maximum and mean temperatures, extraterrestrial radiation, and does not require wind speed.

$$ET_0 = 0.0075\ R_s T_F \qquad \text{Equation 2.6}$$

where, $ET_0$ = potential ET for a grass reference surface in the same units as Rs

$R_s$ = global solar radiation at the surface in equivalent water evaporation, usually mm of evaporation

$T_F$ = mean air temperature in degrees Fahrenheit (ºF)

The equation was revised over the years (Hargreaves & Allen, 2003). In 1985 Hargreaves et al. proposed a modified version of Equation 2.7 for degrees Celsius(°C)

$$ET_0 = 0.0022 R_a (\mathrm{TC} + 17.8)\ TR^{0.5} \qquad \text{Equation 2.7}$$

Hargreaves equation is empirical, simple, and easy to use. Bautista et al., 2009, compared the results of the Hargreaves equation with the FAO 56 PM equation (Allen et al., 1998), considering FAO 56 PM as the standard method. Hargreaves method compared well with the FAO 56 PM method with a resulting coefficient index of 0.82.

### 2.6.4 Christiansen Method

In 1968, Christiansen developed a simple method Equation 2.8 to estimate pan evaporation and crop evapotranspiration. The reasons for using pan evaporation data were to utilize the work previously conducted on its relation with crop consumptive use.

$$E = KR_aC \qquad \text{Equation 2.8}$$

where, E= a generalized form to apply to evapotranspiration,

K=a dimensionless constant developed empirically from data analysis,

$R_a$ =the extraterrestrial radiation, expressed as equivalent depth of evaporation in the same units as E.

C=a dimensionless coefficient related to climatic parameters which is expressed as the product of any number of sub coefficients in Equation 2.9 that are functions of specific climatic parameters that are found to have a significant effect on evapotranspiration (Christiansen, 1968).

$$C = C_T C_W C_H C_S C_E \qquad \text{Equation 2.9}$$

where, CT= coefficients for air temperature

CW= coefficients for wind speed

CH= coefficients for relative humidity

CS= coefficients for sunshine percentage

CE= coefficients for elevation

The value of K was adjusted so that all coefficients were equal to unity for standard and approximate mean values of the parameter they represent (Christiansen, 1968).

This method is purely empirical and can estimate ET monthly but is not reliable for daily or shorter time steps (Subedi & Chávez, 2015).

### 2.6.5 Priestley Taylor Method

The Priestley and Taylor (1972) approach is a simplification of Penman's formulation of evapotranspiration fluxes (Penman 1948). It assumes that the equilibrium term $\lambda E_{eq}$ (Slatyer and McIlroy 1961) is significantly larger than the aerodynamic term $\lambda E_a$ which is formulated in Equation 2.10 (Agam et al., 2010).

$$\lambda E = \alpha \lambda E_{eq} \qquad \text{Equation 2.10}$$

where, $\alpha$= is the Priestley–Taylor coefficient.

It considers evaporation from a wet surface under conditions of minimal advection and referred to it as Priestly Taylor for partial equilibrium.

$$\lambda E = \alpha \frac{\Delta (R_n - G)}{\Delta + \gamma} \qquad \text{Equation 2.11}$$

$\alpha$ depends on the surface type, climate, and season and it can range from 1.15 to 1.50. For water surfaces under condition of minimal advection, the approximated value of $\alpha$ is 1.26. The value of $\alpha$ will vary for different crops and open water bodies. This method is more suitable to find the ET rate on a large scale which is more related to hydrological modeling with minimum advective condition. Due to fewer parameters and variables, this method is simpler to use than the Penman Monteith approach (Subedi & Chávez, 2015).

### 2.6.6 Original Penman Equation

Penman (1948) used a combination of the surface energy balance equation and an aerodynamic equation to calculate ET. Several ET estimation models, for example, FAO 56 PM

equation, ASCE-EWRI Standardized PM equation, CIMIS Penman method are based on the Penman equation, Equation 2.12 (Temesgen et al., 2005):

$$ET = \frac{\Delta(R_n - G) + k_w(e_s - e_a)f(u)\gamma}{\lambda(\Delta + \gamma)} \qquad \text{Equation 2.12}$$

where, f(u) = wind speed function

$k_w$ = unit coefficient (6.43 for ET in mm/d or 0.268 for ET in mm/h)

### 2.6.7 Penman-Monteith Equation

Monteith in 1965introduced crop resistance terms in the original Penman equation 2.12 which later became known as the "Penman-Monteith" (PM) ET equation. The equation is physically based (Temesgen et al., 2005) (Allen et al, 1998) and incorporates aerodynamic and surface resistance terms instead of wind speed:

$$\lambda E = \frac{\Delta(R_n - G) + \rho C_p \frac{(e_s - e_a)}{r_a}}{\Delta + \gamma\left(1 + \frac{r_s}{r_a}\right)} \qquad \text{Equation 2.13}$$

FAO 56 PM equation and the ASCE Standardized Reference PM ET equations are based on the Penman Monteith Equation 2.13 (Allen et al, 1998).

### 2.6.8 FAO 56 Penman-Monteith Equation

The FAO 56 PM equation is a modification to the Penman-Monteith equation, that uses specific coefficients for a reference crop. The reference crop is represented by a hypothetical crop of 0.12 m height with surface resistance of 70 sm-1 and an albedo of 0.23. The crop resembles the evaporation of an extensive surface of green grass with uniform height, actively growing, and without any water stress.

$$ET_0 = \frac{0.408\Delta(R_n - G) + \left(\frac{900\gamma}{T_a + 273}\right) u_2(e_s - e_a)}{\Delta + \gamma(1 + 0.34u_2)} \quad \text{Equation 2.14}$$

where, $ET_0$ = grass reference ET (mm/d),

$R_n$ = net radiation at the crop surface (MJ/m$^2$/d),

G = soil heat flux density (MJ/m$^2$/d)

### 2.6.9 ASCE-EWRI Standardized Penman Monteith Evapotranspiration Equation

The ASCE Standardized Reference Evapotranspiration Equation (Equation 2.15) is based on the Penman-Monteith equation using simplified and standardized aerodynamic and surface resistances. This equation is applicable for both tall (alfalfa) and short (grass) reference surfaces. A grass reference crop is defined same as FAO 56, and a full cover alfalfa reference crop is defined as an extensive, uniform surface of dense, actively growing vegetation with a height of 0.50 m, and under no water stress (Allen et al., 2018). The equation is as follows,

$$ET_{sz} = \frac{0.408\Delta(R_n - G) + u_2\gamma C_n \left(\frac{(e_s - e_a)}{T_a + 273}\right)}{\Delta + \gamma(1 + C_d u_2)} \quad \text{Equation 2.15}$$

where, $ET_{sz}$ = standardized reference crop evapotranspiration for short crop (grass) ($ET_{os}$) or tall crop (alfalfa) ($ET_{rs}$) surfaces (mm/d or mm/h),

$R_n$ = calculated net radiation at the crop surface (MJ/m$^2$/d or MJ/m$^2$/h),

G = soil heat flux density at the soil surface (MJ/m$^2$/d or MJ/m$^2$/h)

The values for $C_n$ and $C_d$ are determined in Table 2.5.

**Table 2.5: Values for $C_n$ and $C_d$, (Allen et al., 2018)**

| Calculation | Short Reference | | Tall Reference | | Units for | Units for |
|---|---|---|---|---|---|---|
| Time Step | $ET_o$ | | $ET_r$ | | $ET_o$ , $ET_r$ | $R_n$, G |
| | $C_n$ | $C_d$ | $C_n$ | $C_d$ | | |
| Daily | 900 | 0.34 | 1600 | 0.38 | mm $d^{-1}$ | MJ $m^{-2}$ $d^{-1}$ |
| Hourly daytime | 37 | 0.24 | 66 | 0.25 | mm $d^{-1}$ | MJ $m^{-2}$ $d^{-1}$ |
| Hourly nighttime | 37 | 0.96 | 66 | 1.7 | mm $d^{-1}$ | MJ $m^{-2}$ $d^{-1}$ |

## 2.7 Remote Sensing for Evapotranspiration

Remote sensing is one of the feasible means to provide spatially distributed ET fluxes over larger land surfaces (Choudhury et al., 1994, Jackson et al., 1987). The use of remote sensing to estimate ET has been developed by using two approaches: (a) land surface energy balance method that uses remotely sensed surface reflectance in the visible (VIS) and near-infrared (NIR) portions of the electromagnetic spectrum and surface temperature (radiometric) from an infrared (IR) thermal band, and (b) reflectance based crop coefficient ($K_{cr}$) and reference ET approach where the crop coefficient ($K_c$) is related to vegetation indices derived from canopy reflectance values.

The land surface energy balance approach relies on the basis that ET is represented by the change of the state of water using available energy in the environment to vaporize (Su et al., 2005).For these models satellite sensed radiances are converted into land surface characteristics such as albedo, leaf area index, vegetation indices, surface emissivity and surface temperature to estimate ET as a residue of the land surface energy balance equation, Equation 2.1.

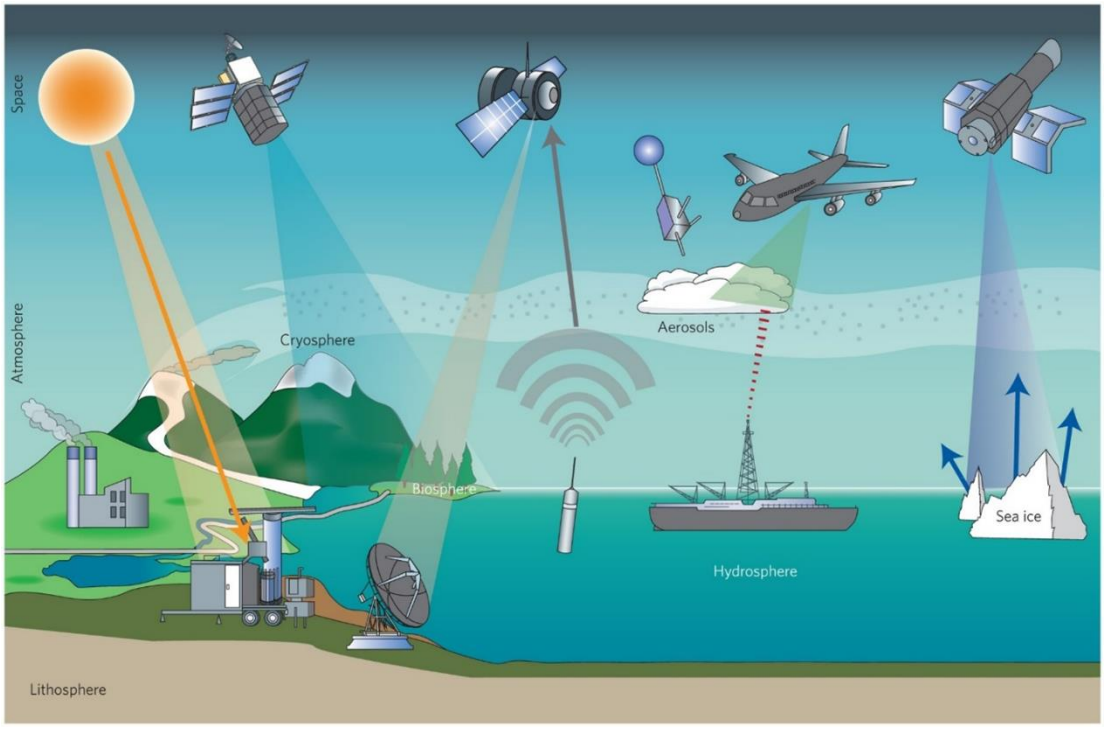


**Figure 2.8: A schematic diagram of different remote sensing measurements** (Yang et al., 2013)

The VI-basal crop coefficient approach provides daily values directly by using FAO methodology, based on the concepts of crop coefficient and reference ET. Advantage of this approach is that satellite imagery in the reflective bands is more readily available than thermal band data at higher spatial resolution (Gonzalez-Dugo et al.,2009). However, without coupling with a soil water balance, this method cannot account for soil evaporation or the reduction of transpiration of plants under water stress conditions. Whereas surface-temperature-based approaches can readily capture stress effects without requiring precipitation and soil texture information (Anderson et al., 2007).

Over the past three decades, numerous remote sensing-based ET mapping algorithms were developed that provide economical, and efficient tool for ET estimations at field and

regional scales. ET maps is useful for crop water management and irrigation performance, climate change impact assessment, hydrological modeling, groundwater recharge prediction, and land use planning. Some of the commonly used remote sensing-based ET algorithms are listed below:

1. Surface Energy Balance Algorithm for Land (SEBAL; Bastiaanssen et al., 1998)
2. Mapping Evapotranspiration at High Resolution with Internalized Calibration (METRIC; Allen et al., 2007)
3. Surface Energy Balance System (SEBS; Su et al., 2005)
4. Two-Source Model (TSM; Norman et al., 1995)
5. Surface Energy Balance Index (SEBI; Menenti & Choudhury, 1993)
6. Simplified Surface Energy Balance (SSEB; Senay et al., 2013)
7. Trapezoid Interpolation Model (TIM; Jiang & Islam, 2001)

Accuracy of ET estimates by remote sensing varies from 67 to 97% for daily ET and above 94% for seasonal ET which implies that remote sensing technology with appropriate algorithms has the potential to estimate ET at regional scale adequate for irrigation scheduling (Gowda et al., 2008).

## 2.8 Maximum Entropy Production

The Maximum Entropy Production (MEP) method is an unconventional dynamic-statistical model of surface heat fluxes proposed by Wang & Bras, 2009,2011 and Wang et al., 2014. The model is built on the Bayesian probability theory, information theory and atmospheric boundary layer turbulence theory. The MEP model allows $E$, $H$, and $Q$ over the Earth-atmosphere interface to be simultaneously solved in terms of analytical functions of surface

radiation fluxes, temperature, and humidity as the most probable partition of radiation fluxes while maintaining the surface energy budget.

MEP differs from conventional bulk transfer models as it predicts surface fluxes without using temperature and humidity gradients, wind speed, and surface roughness as input variables and always closing the surface energy budget using the energy balance equation as a mathematical constraint of the MEP solution of the surface fluxes. It solves the surface fluxes using only net radiation, surface temperature, and surface specific humidity (El Sharif et al., 2019).

Two different versions of the MEP model can be distinguished, one is for soil evaporation, while the other one is for plant transpiration. Both were used to estimate subdaily evaporation over bare soil and transpiration over dense vegetation under humid to moderately limited water availability conditions (Wang & Bras, 2011).

The formulation of the MEP model is described in Wang & Bras, 2011 for the case of land surfaces, and in Wang et al., 2014 for the case of water-snow-ice surfaces. The MEP model uses fewer model parameters than existing models that are independent of wind speed. The modeling errors of the MEP heat fluxes are bounded by the measurement errors of surface radiative fluxes. Tests of the MEP model using field observations provide evidence that the MEP model accurately predicts surface heat fluxes over both land and water-snow-ice surface at field scales (J. Wang & Bras, 2009,2011 , Wang et al., 2014 ). The MEP model applies to a full range of soil moisture conditions from residual water content to saturation. Published tests of the MEP model showed that it matches or outperforms other existing models (Nearing et al., 2012, Yang & Wang, 2014).

# Chapter 3 - Methodology

## 3.1 Study Area

A research field of Southwest Research and Extension Center of Kansas State University, near Garden City, Kansas (latitude 32.024°, longitude -100.826°, elevation of 885 m above sea level) was used for this study. A field was divided in half into the western and eastern parts and had two different crops (corn and cotton) grown in each half. The soil in the field is classified as a Ulysses silt loam (Oker et al., 2018). A four-span center pivot system with four irrigation technologies (LEPA, LESA, MDI1, and MDI2) was used to irrigate the crops in both halves of the main circle, while a northeast corner was used for non-irrigated or rainfed cotton. All three parts of the field had low-profile energy budget towers installed. The towers were located under Low Elevation Sprinkler Application (LESA) irrigation zone.

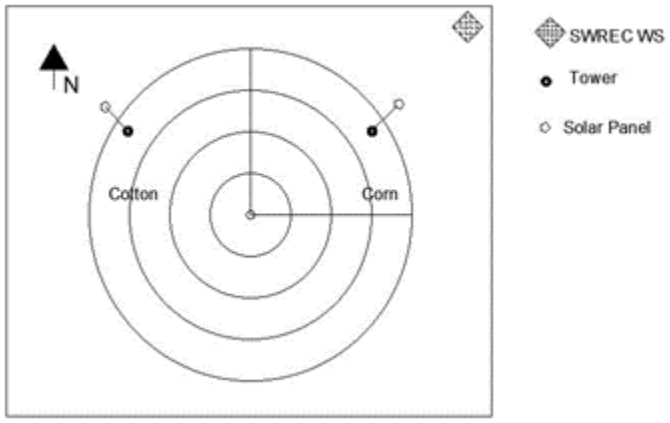


**Figure 3.1: Schematic Diagram of the Field for 2020 Season**

The irrigated cotton and corn were rotated to the opposite half of the circle every year to imitate crop rotation. Such crop rotation done in 2021 helped managing soil and fertility, reduce erosion, improve soil's health, and increase nutrients available for crops (NRCS, 2013).

## 3.2 Climate Condition

Figure 3.2 and Figure 3.3 show monthly average precipitation and temperature from 1991 to 2021 for Garden City, KS. Both total precipitation and average temperature increase from March to June while starting to decline in July. June was the hottest month with maximum temperature around 33° C.

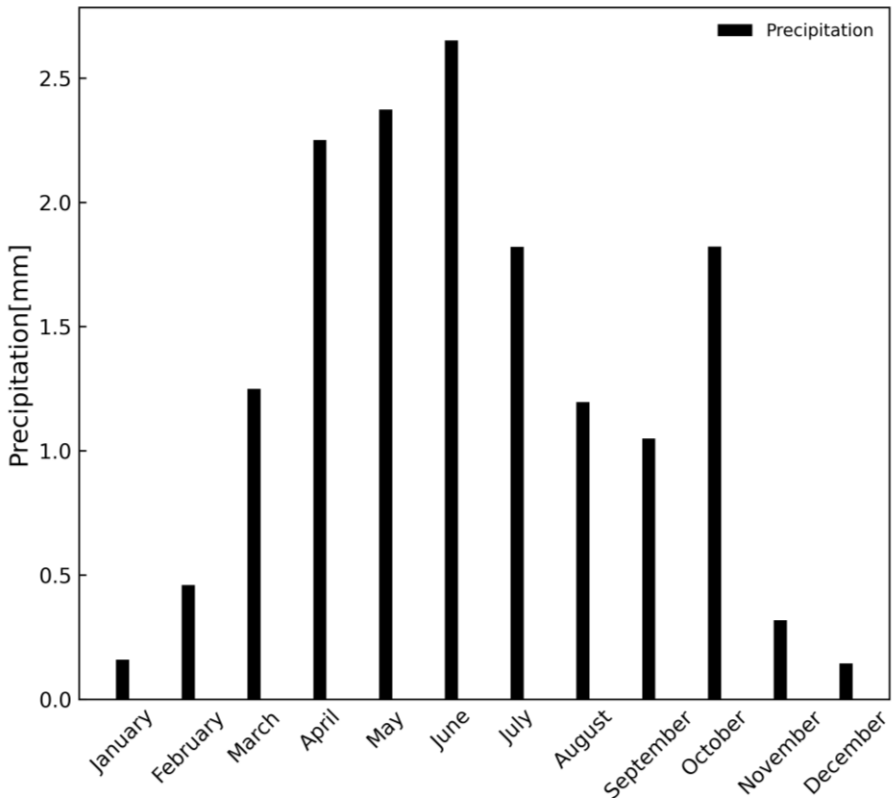


**Figure 3.2: Monthly average total precipitation in Garden City, KS from 1991 to 2021**

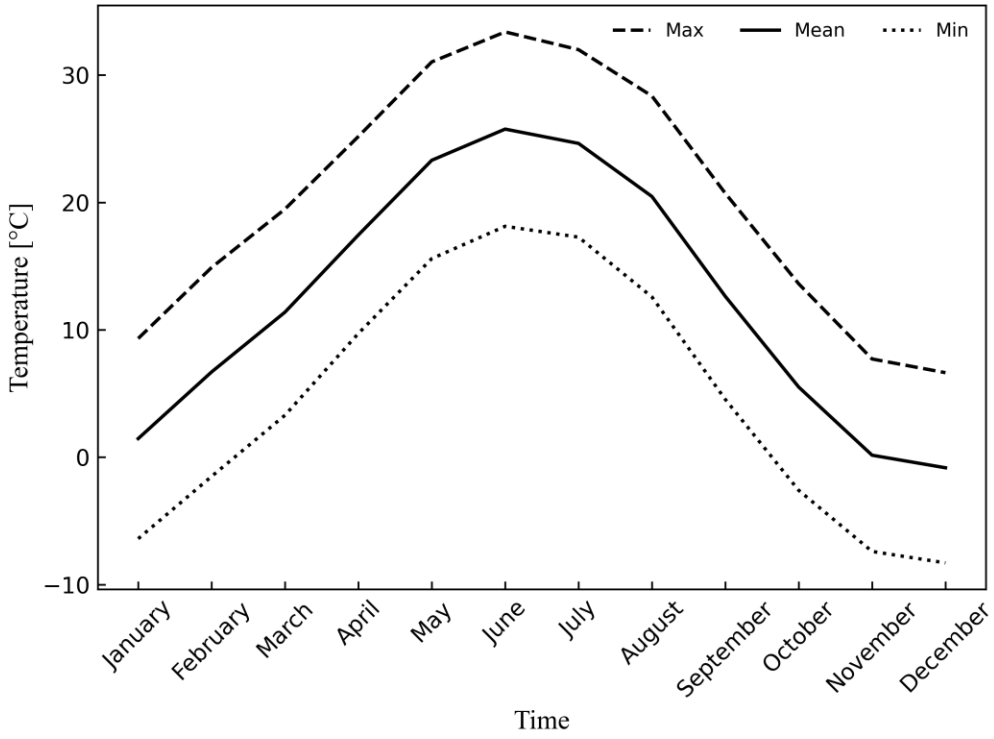


**Figure 3.3: Monthly average daily temperature in Garden City, KS from 1991 to 2021**

## 3.3 Experimental field setup

Continuous observations of incoming and outgoing shortwave and longwave radiation and net radiation from three field towers were conducted in 2020 and 2021. Figure 3.4 shows the instrumentational setup at two irrigated fields (cotton and corn).

Four-channel radiometers were setup at 2 m height for short vegetation crops (cotton all season and corn in June and July) and 3.5 m for tall vegetation crops (corn in August to November). The sensor height ensured at least 1.5 m of clearance between crop canopy and the instrument. Having such open distance below the sensor ensured that 99% of the input to the sensors comes from a circular area with a radius of approximately 20-30 m (Kipp & Zonen, 2014).

Additionally, air temperature at the convective boundary layer, relative humidity, precipitation, and wind speed (~2 m height) were collected from all sites. Infrared radiometer was installed on top of the tower to cover a land circular area of approximately 20-30 m and measure average skin canopy or surface temperature. Subsurface soil temperature and volumetric soil water content sensors (at 5, 10, 20, 40, and 60 cm depth) were placed under irrigated crop within the field near the tower. Ground heat flux was measured at 2 to 5 cm below soil surface with three heat flux sensors. Table 3.1 provides a list of equipment that were used, and Table 3.2 provides a list of collected variables.

**Figure 3.4: Instrumentational setup of energy budget towers in cotton (left image) and corn fields (right image).**

**Table 3.1 : List of Field Equipment**

| Sensor | Description |
|---|---|
| Apogee_SN500SS | 4-Channel Net Radiometer |
| Apogee_SI-111 | Infrared Radiometer |
| CS_Hygrovue-5 | Temperature and Relative humidity |
| CS | Rain Gauge |
| CS_CS655 | Water Content Reflectometer |
| Met One/014A | Anemometer |
| Hukseflux_HFP01 | Soil Heat flux Plate |
| CS_CR1000X | Panel Temperature and Solar Panel Voltage |

**Table 3.2: List of Variables**

| Variables | Elevation/Depth |
|---|---|
| Incoming Shortwave | 200 cm/350 cm |
| Outgoing Shortwave | 200 cm/350 cm |
| Incoming Longwave | 200 cm/350 cm |
| Outgoing Longwave | 200 cm/350 cm |
| Net Radiation | 200 cm/350 cm |
| Albedo | 200 cm/350 cm |
| Air Temperature | 20 cm/180 cm |
| Relative Humidity | 20 cm/180 cm |
| Canopy Temperature | 200 cm/350 cm |
| Precipitation | 180 cm |
| Wind speed | 180 cm |
| Volumetric Water Content | 5 cm/10 cm/20 cm/40 cm/60 cm |
| Soil Temperature | 5 cm/10 cm/20 cm/40 cm/60 cm |
| Soil Heat Flux | 5 cm |

## 3.4 Data Processing

Raw data files were prepared from data collected from the sensors, then missing values were replaced with NAN. There were some overlapping days which were removed. Extreme outliers were replaced with NAN.

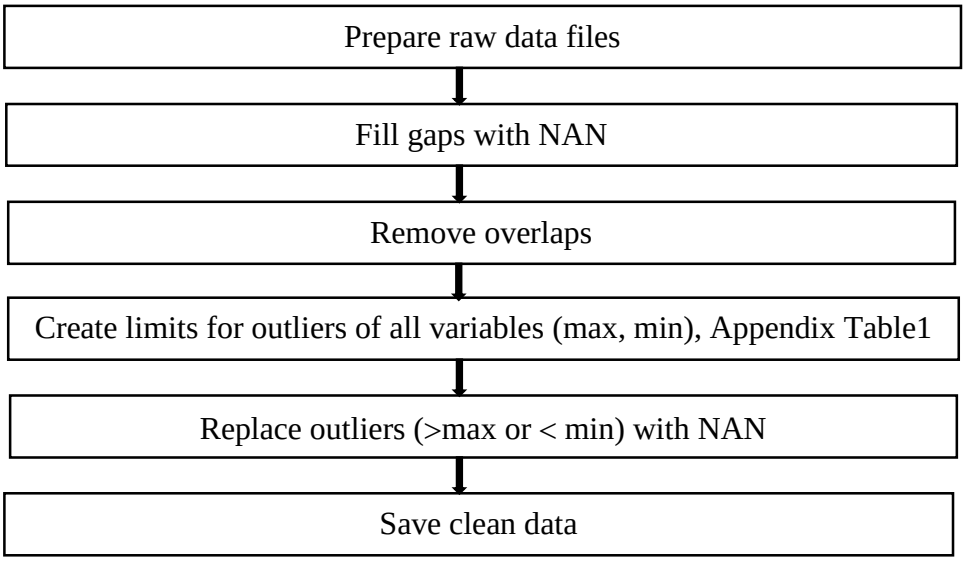


## 3.5 FAO Penman Monteith Equation

In 1948, the energy balance equation by Penman was combined with the mass transfer method resulted in an equation to compute the evaporation from an open water surface from standard climatological records of sunlight, air temperature, air relative humidity, and wind speed. The equation was called Penman-Monteith form of the ET equation:

$$\lambda ET = \frac{\Delta(R_n - G) + \rho_a c_p \frac{(e_s - e_a)}{r_a}}{\Delta + \gamma(1 + \frac{r_s}{r_a})} \qquad \text{Equation 3.1}$$

where, Rn is the net radiation, G is the soil heat flux, ($e_s$ - $e_a$) represents the vapour pressure

deficit of the air, $\rho_a$ is the mean air density at constant pressure, $c_p$ is the specific heat of the

air, $\Delta$ represents the slope of the saturation vapor pressure-temperature relationship, $\gamma$ is the psychrometric constant, and $r_s$ and $r_a$ are the (bulk) surface and aerodynamic resistances.

The Penman-Monteith equation formulated in Equation 3.1 includes all parameters that govern energy exchange and corresponding latent heat flux (evapotranspiration) from uniform expanses of vegetation. Most of the parameters are measured or can be readily calculated from weather data. The equation can be utilized for a direct calculation of any crop evapotranspiration since surface and aerodynamic resistances are crop specific.

The transfer of heat and water vapor from the evaporating surface into the air above the canopy is determined by the aerodynamic resistance, $r_a$.

$$r_a = \frac{1}{\kappa^2 u}\left[\ln\left(\frac{z-d_0}{z_{0m}}\right)\ln\left(\frac{z-d_0}{z_{0v}}\right)\right] \qquad \text{Equation 3.2}$$

where, $d_0 = 0.66\ H$ , $z_{0m} = 0.123\ H$ , $z_{0v} = 0.1\ z_{0m}$ and H represents average canopy height in meters.

The 'bulk' surface resistance describes the resistance of vapor flow through transpiring crop and evaporating soil surface. Where the vegetation does not completely cover the soil, the resistance factor should include the effects of the evaporation from the soil surface. If a crop does not transpire at a potential rate, the resistance depends also on the water status of the vegetation. An acceptable approximation to a much more complex relation of the surface resistance of dense full cover vegetation is

$$r_s = \frac{r_1}{LAI_{active}} \qquad \text{Equation 3.3}$$

where, $LAI_{active} = 0.5\ LAI$ , and the stomatal resistance, $r_l$, of a single leaf has a value of about 100 s $m^{-1}$ under well-watered conditions.

The Penman-Monteith combination method was suggested to be a new standard for reference evapotranspiration FAO in May 1990. The reference crop was defined as a hypothetical crop with height of 0.12 m, a surface resistance of 70 s m-1 and an albedo of 0.23 which minimizes the shortcomings of the previous FAO Penman method and values were more consistent with actual crop water use data.

Using the original Penman-Monteith Equation 3.1 and the equations of the aerodynamic resistance Equation 3.2 and surface resistance Equation 3.3, the FAO Penman-Monteith method to estimate reference ET can be derived as

$$ET_{ref} = \frac{0.408\Delta(R_n - G) + \gamma \frac{900}{T + 273} u_2 (e_s - e_a)}{\Delta + \gamma(1 + 0.34u_2)} \qquad \text{Equation 3.4}$$

where, $ET_{ref}$ = reference evapotranspiration (mm $d^{-1}$)

$R_n$ = net radiation, (MJ $m^{-2}$ $d^{-1}$)

G = the soil heat flux, (MJ $m^{-2}$ $d^{-1}$)

($e_s$ - $e_a$) = the vapor pressure deficit of the air, (kPa)

$e_s$ = saturation vapor pressure of the air, (kPa)

$e_a$ = actual vapor pressure of the air, (kPa)

$\Delta$=slope of the saturation vapor pressure temperature relationship, (kPa $^oC^{-1}$)

$\gamma$= psychrometric constant, (kPa $^oC^{-1}$)

### 3.5.1 Crop Evapotranspiration

Crop evapotranspiration, ETc, is calculated by multiplying the reference crop evapotranspiration, ETo, by a crop coefficient, $K_c$

$$ET_c = K_c\ ET_o \qquad \text{Equation 3.5}$$

Most of the effects of the various weather conditions are incorporated into the $ET_o$ estimate. The reference $ET_o$ is defined and calculated using the FAO Penman-Monteith Equation 3.4. Therefore, as $ET_o$ represents an index of climatic demand, $K_c$ varies predominately with the specific crop characteristics and only to a limited extent with climate. This enables the transfer of standard values for $K_c$ between locations and between climates. This has been a primary reason for the global acceptance and usefulness of the crop coefficient approach and the $K_c$ factors developed in past studies.

The crop coefficient, $K_c$, is the ratio of the crop $ET_c$ to the reference $ET_o$; it integrates the effect of characteristics that distinguish a typical field crop from the grass reference which has a constant appearance and a complete ground cover. So, different crops will have different $K_c$ coefficients. The changing characteristics of the crop over the growing season also affect the $K_c$ coefficient. Finally, as evaporation is an integrated part of crop evapotranspiration, conditions affecting soil evaporation also influence $K_c$.

The $K_c$ in Equation 3.5 predicts $ET_c$ under standard conditions. This represents the upper envelope of crop evapotranspiration and represents conditions where no limitations are placed on crop growth or evapotranspiration due to water shortage, crop density, or disease, weed, insect or salinity pressures. The $ET_c$ predicted by $K_c$ and $ET_o$ can be additionally adjusted if necessary to

non-standard conditions where any environmental condition or characteristic is known to have an impact on or to limit $ET_c$. Figure 3.5 shows schematic diagram crop coefficient which was published in (Allen et al.,1998)

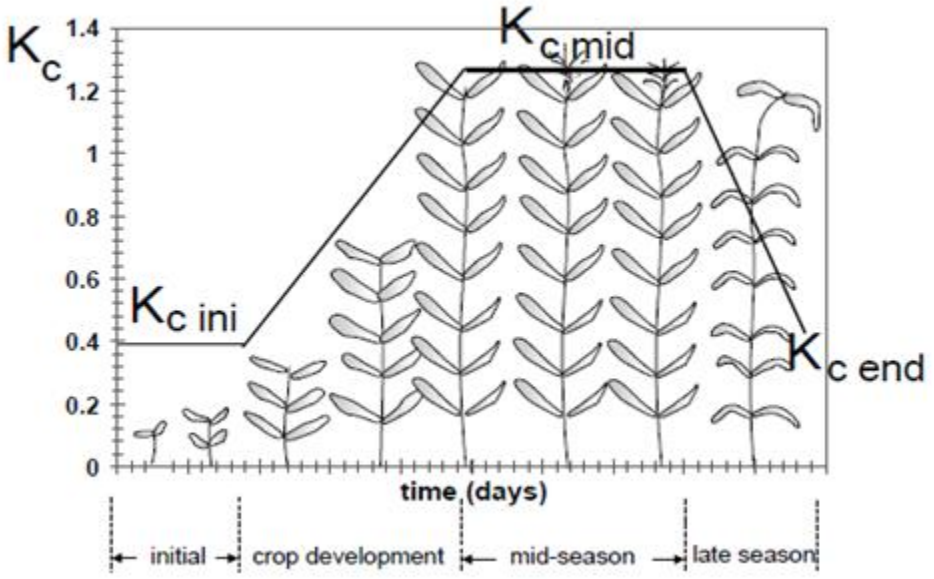


**Figure 3.5: Variation of the crop coefficient during a crop growing season (Allen et al., 1998)**

The $K_c$ varies with crop, leaf area, phonological stage, etc. And it is usually determined by using experimental data.

As the crop develops, the ground cover, crop height and the leaf area change. Due to the differences in evapotranspiration during various growth stages, the $K_c$ for a given crop will vary over the growing period. The growing period can be divided into four distinct growth stages: initial, crop development, mid-season and late season as shown in Figure 3.5.

## 3.6 Maximum Entropy Production (MEP)

The maximum entropy production (MEP) model was recently developed to model land surface fluxes, including soil evaporation and vegetation transpiration. This model is based on the principles of nonequilibrium thermodynamics and the theory of Bayesian probabilities. MEP requires few input data as compared to other models and its form ensures that the closure of the surface energy balance is always fulfilled (Hajji et al., 2018)

Two different versions of the MEP model can be distinguished: (i) MEP-Ev for evaporation from a bare soil and (ii) MEP-Tr for plant transpiration. Both models have already been used successfully to estimate sub daily evaporation over bare soil (MEP-Ev) and transpiration over dense vegetation (MEP-Tr) under humid to moderately limited water availability conditions (Jingfeng Wang & Bras, 2011).

The formulation of the MEP solution was obtained for land surface fluxes (ground heat flux G, sensible heat flux H, and ET expressed as latent heat flux) under the constraint of energy conservation at the land surface:

$$E + H + G = R_n \qquad \text{Equation 3.6}$$

where, Rn is net radiation at the land surface.

The entropy production function D is formulized in terms of surface fluxes and it characterize the physics behind the ET processes, including turbulent transport in the atmospheric boundary layer. The entropy production function D is derived from the MEP theory (Wang and Bras 2009, 2011) and can be expressed as

$$D(E,H,G) \equiv \frac{2G^2}{I_s} + \frac{2H^2}{I_a} + \frac{2E^2}{I_e} \qquad \text{Equation 3.7}$$

where, $I_s$, $I_a$, and $I_e$ are the thermal inertia parameters ($Wm^{-2}K^{-1}s^{1/2}$) associated with the corresponding fluxes: ground heat flux, sensible heat flux, and evaporative flux, respectively. Is characterizes a thermal property of soil varying with moisture content (Verhoef, 2004). The entropy production function D may be understood using the analogy of an electrical circuit where the electric current and conductance corresponds to land surface fluxes and thermal inertia parameters, respectively. These three thermal inertia parameters ($I_s$, $I_a$, and $I_e$) are key elements of D.

Parameter, $I_s$ is the thermal inertia of the land surface (i.e., soil or leaf surfaces). For leaf surfaces, this parameter can be neglected since the thermal inertia of the leaf matrix is two orders of magnitude smaller than that of soil. For soil surfaces, $I_s$ may be parameterized using an empirical equation, Equation 3.8 according to Wang and Bras (2011),

$$I_s = I_{ds} + \sqrt{\theta}\, I_w \qquad \text{Equation 3.8}$$

where, $I_{ds}$ is the thermal inertia of dry soil that can be calculated by using Equation 3.9.

$$\mathrm{I} = \sqrt{kpc_h} \qquad \text{Equation 3.9}$$

where, k is thermal conductivity ($Wm^{-1}K^{-1}$), ρ is material density ($kgm^{-3}$), and $c_h$ is specific heat capacity ($Jkg^{-1}K^{-1}$).

θ is the soil water content, and $I_w$ is the thermal inertia of water that can be obtained from Equation 3.10.

$$I_w = \sqrt{\rho_w c_w k_w} \qquad \text{Equation 3.10}$$

where, $\rho_w$ is the water density ($10^3$ $kgm^{-3}$), $k_w$ is heat conductivity of water ($0.58Wm^{-1}K^{-1}$), and $c_w$ is specific heat of water ($4.183x10^3$ $Jkg^{-1}K^{-1}$).

Parameters $I_a$ and $I_e$, introduced in Equation 3.7 characterize the turbulent transport of heat and water vapor in the boundary layer, respectively. They are parameterized based on using an extremum solution of the Monin-Obukhov similarity theory (Jingfeng Wang & Bras, 2011) as follows:

$$I_a = I_0 |H|^{\frac{1}{6}} \qquad \text{Equation 3.11}$$

$$I_e = \sigma I_a \qquad \text{Equation 3.12}$$

where, $\sigma$ is a dimensionless parameter characterizing the phase-change related state of the evaporating surface which is given by Equation 3.13.

$$\sigma = \frac{\lambda^2 q_s}{c_p R_v {T_s}^2} \qquad \text{Equation 3.13}$$

where, $\lambda$ is the heat of vaporization of liquid ($2.5x10^6$ $JKg^{-1}$), $R_v$ is the gas constant of water vapour (461 $JKg^{-1}$ $K^{-1}$), $c_p$ is the specific heat of air at constant pressure (1.004 $JKg^{-1}$ $K^{-1}$), $T_s$ is the surface (skin) /soil temperature and surface specific humidity qs.

Equation 3.14 for the case of water/snow surface is a function of Ts according to the Clausius-Clapeyron equation since water vapor right above water/snow surface is assumed to be saturated at surface temperature.

$$q_s = \varepsilon \frac{e_o}{P_o} exp\left(\frac{\lambda}{R_v}\left(\frac{1}{T_o} - \frac{1}{T_s}\right)\right) \qquad \text{Equation 3.14}$$

where, ε (= 0.62) is the ratio of molecular weight of water vapor to that of dry air, P the atmospheric pressure, $T_0$ is representative environment temperature (~300 K), $e_0$ saturation vapor pressure at temperature $T_0$.

The postulated σ function in Equation 3.15 may be justified by the limiting cases of dry and saturated soil. For the case of dry soil, σ=0 as $q_s = 0$ ( Wang & Bras, 2011).For the case of saturated soil, σ becomes

$$\sigma = \frac{\Delta}{\gamma} \qquad \text{Equation 3.15}$$

where, Δ is the slope of the saturation water vapor pressure curve at surface temperature $T_s$ and γ the psychrometric constant (Brutsaert, 1982).

Parameter $I_0$ in Equation 3.16 is referred to as apparent thermal inertia of air and is only dependent upon external parameters such as such as z and $T_0$ ( Wang & Bras, 2009).

$$I_o = \rho\, c_p \sqrt{C_1 \kappa z}\left(C_2 \frac{\kappa z g}{\rho c_p T_0}\right)^{\frac{1}{6}} \qquad \text{Equation 3.16}$$

$$C_1 = \begin{cases} \sqrt{3}/\alpha \ , \ unstable \\ 2/(1+2\alpha) \ , \ stable \end{cases} \qquad \text{Equation 3.17}$$

$$C_2 = \begin{cases} \gamma_2/2 \ , \ unstable \\ 2\beta \ , \ stable \end{cases}$$ Equation 3.18

where, ρ is the air density (1.22 $kgm^{-3}$), κ is the von Kármán constant (0.4), z is the distance above the surface(m), g is the gravitational acceleration (9.81$ms^{-2}$) and $C_1$ and $C_2$ are coefficients related to the universal constants in the empirical functions (α, β, $\gamma_2$ in Table 3.3) representing the effect of the stability on the mean profiles of wind speed and (potential) temperature within the surface layer (Businger et al., 1971).

**Table 3.3: Summary of the Extremum Solution Based on Monin-Obukhov Similarity Theory**

| | Stable | Unstable |
|---|---|---|
| $\Theta_z$ | $\left(\alpha + \frac{1}{2}\right)\frac{1}{2\beta}\frac{T_0}{g}\left(\frac{u_*}{\kappa z}\right)^2$ | $-\frac{2}{\sqrt{3}}\frac{\alpha}{\gamma_2}\frac{T_0}{g}\left(\frac{u_*}{\kappa z}\right)$ |
| $\frac{H}{\rho c_p}$ | $-\frac{1}{2\beta}\frac{T_0}{g}\frac{u_*^3}{\kappa z}$ | $\frac{1}{\gamma_2}\frac{T_0}{g}\frac{u_*^3}{\kappa z}$ |

The constants are taken as α~0.75 or 1, β~4.7, $\gamma_2$~ 9.

### 3.6.1 Non-vegetated Land Surface

Over non-vegetated surfaces, ET consists of only bare soil evaporation. In this case, the parameter σ in Eq 3.13 is a function of soil surface temperature Ts and soil surface specific humidity $q_s$. Finding a maximum D in Equation 3.7 over all possible combinations of E, H, and G under the constraint of conservation of energy (Equation 3.6) for a given net radiation $R_n$, the following nonlinear equations are obtained,

$$G = \frac{B(\sigma)}{\sigma}\frac{I_s}{I_0}H|H|^{-\frac{1}{6}}$$ Equation 3.19

where, $I_0$ is defined in Eq 3.16 and σ in 3.13.

$$E = B(\sigma)H$$ Equation 3.20

B(σ) in Equation 3.19 and Equation 3.20 is recognized as the reciprocal Bowen ratio in terms of σ as a function of $q_s/T_s^2$. It can be obtained from Equation 3.21 as

$$B(\sigma) = 6(\sqrt{1 + \frac{11}{36}\sigma - 1})$$ Equation 3.21

Substituting G and E into Eq 3.6, it transforms into a nonlinear equation for H:

$$R_n = B(\sigma)H + H + \frac{B(\sigma)}{\sigma}\frac{I_s}{I_0}H|H|^{-\frac{1}{6}}$$ Equation 3.22

### 3.6.2 Vegetated Land Surface

For fully vegetated surfaces covered with a closed canopy, only transpiration ($T_r$) is considered for the estimation of ET (Wang & Bras, 2011). In this case, the MEP for transpiration version of the model is applied. This version is derived as a special case of the MEP for evaporation model when $I_s$ =0, for which ground heat flux G at the soil surface does not enter MEP formalism. And G, the heat flux through the leaf matrix is negligible compared to sensible and latent heat fluxes (H and $T_r$) at the leaf scale. When $I_s$ =0, Equation 3.6 becomes

$$R_n = T_r + H$$ Equation 3.23

which leads to

$$T_r = \frac{R_n}{1 + B^{-1}(\sigma)}$$ Equation 3.24

$$H = \frac{R_n}{1 + B(\sigma)} \qquad \text{Equation 3.25}$$

where $B(\sigma)$ is given in Eq 3.21 and $\sigma$ in Eq 3.13 except $T_s$ and $q_s$ here represent leaf temperature and specific humidity at the leaf surface, respectively. Equation 3.24 and Equation 3.25 are referred to as the 'MEP model of transpiration' ( Wang & Bras, 2011).

### 3.6.3 Partially Vegetated Land Surface

The use of the MEP model described above is restricted to specific sites of either bare soil or fully vegetated surface and the periods of non-growing or growing seasons when these conditions are applied. In a broad range of sites, the surface can be partially vegetated. In that scenario evapotranspiration consists of soil evaporation as well as plant transpiration. To estimate the total ET, it is necessary to combine MEP for evaporation (bare soil) and MEP for transpiration (fully vegetated). This can be achieved by using a vegetation index $f_{veg}$ which is defined as the fraction of soil covered with vegetation. When the of effect rainfall is neglected for evaporation, the combined MEP-ET model to calculate total ET can be obtained from Equation 3.26 (Hajji et al., 2018).

$$ET = \left(1 - f_{veg}\right)E_v + f_{veg}T_r \qquad \text{Equation 3.26}$$

where, Ev is soil evaporation which is obtained from Equation 3.20 and Tr is plant transpiration which is obtained from Equation 3.26. The vegetation index $f_{veg}$ may be determined using the normalized difference vegetation index (NDVI) as shown in Equation 3.27, as it is an indicator of the chlorophyll activity of the vegetation (Hajji et al., 2018).

$$f_{veg} = \frac{NDVI - NDVI_{min}}{NDVI_{max} - NDVI_{min}} \qquad \text{Equation 3.27}$$

where, $NDVI_{max}$ and $NDVI_{min}$ correspond to NDVI values for dense vegetation and bare soil and the vegetation index, $f_{veg}$ varies between 0 (bare soil) and 1 (fully vegetated condition).

## 3.7 Normalized Difference Vegetation Index (NDVI)

Normalized Difference Vegetation Index (NDVI) is related to the proportion of photosynthetically absorbed radiation, and can be calculated using spectral reflectance from visible red and near infrared band using Equation 3.28 (Rouse et al., 1973; Sellers, 2007).The NDVI considers the difference between red and near infrared reflectance of vegetation canopies to assess the presence of green vegetation. As vegetation preferentially absorbs solar radiation in the red portion of the light spectrum for photosynthesis and strongly reflects it in the near infrared, so NDVI reflects the balance between the energy received and emitted by vegetation.

$$NDVI = \frac{NIR - R}{NIR + R} \qquad \text{Equation 3.28}$$

For this study, NDVI data was collected from Sentinel-2 online database (spatial resolution 10 m, band 4 for red and band 8 for near infrared) using Copernicus Open Access Hub (https://scihub. copernicus. eu /dhus/#/home ). The data is downloaded at the weekly scale, with daily NDVI obtained by applying linear interpolation between weekly records.

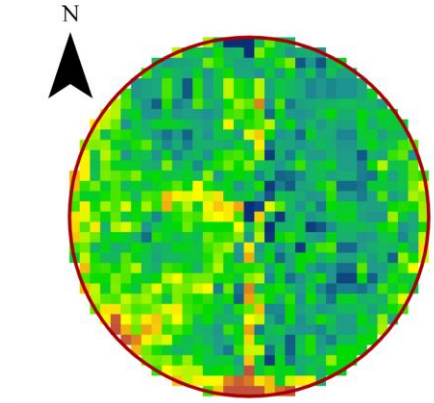


field_gardencity

**20_May2020**

**Value**

High : 1

Low : 0

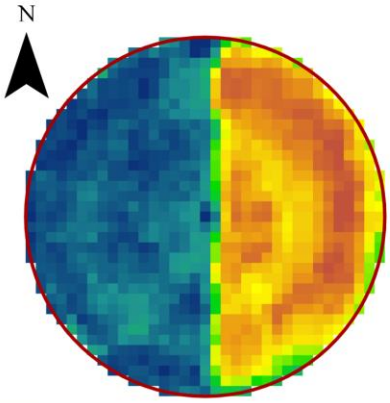


field_gardencity

**24_June2020**

**Value**

High : 1

Low : 0

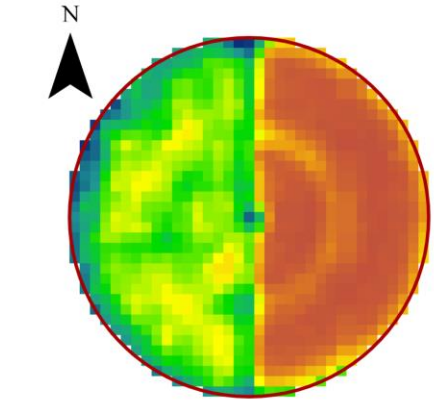


field_gardencity

**24_July2020**

**Value**

High : 1

Low : 0

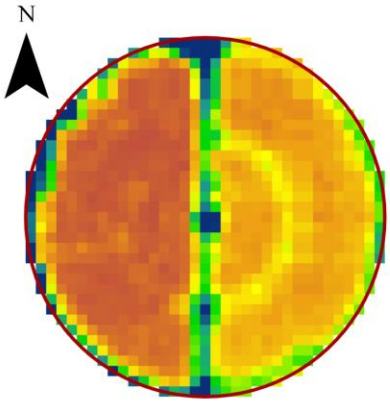


field_gardencity

**23_August2020**

**Value**

High : 1

Low : 0

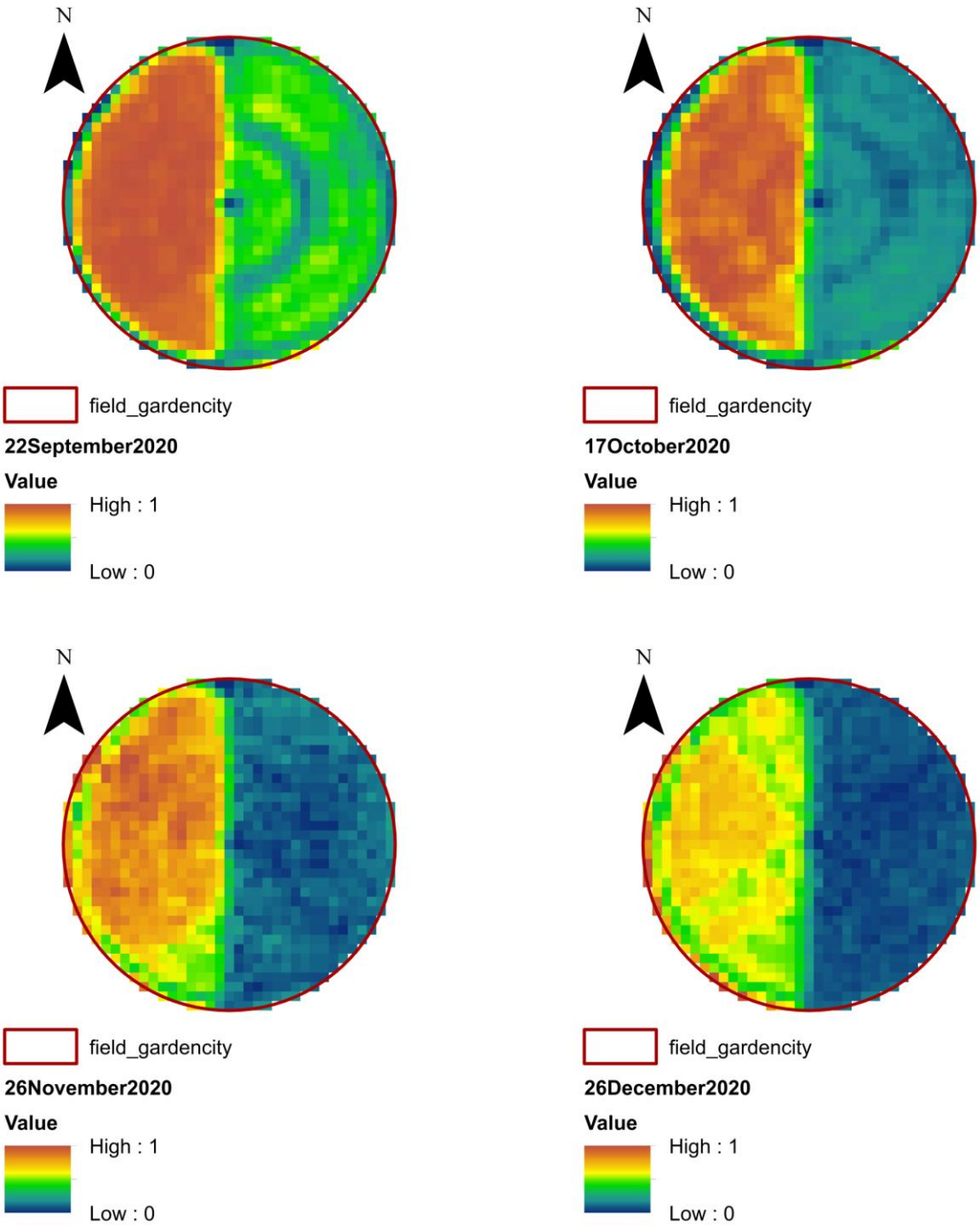


**Figure 3.6: Maps of NDVI over the experimental site for season 2021 for corn and cotton**

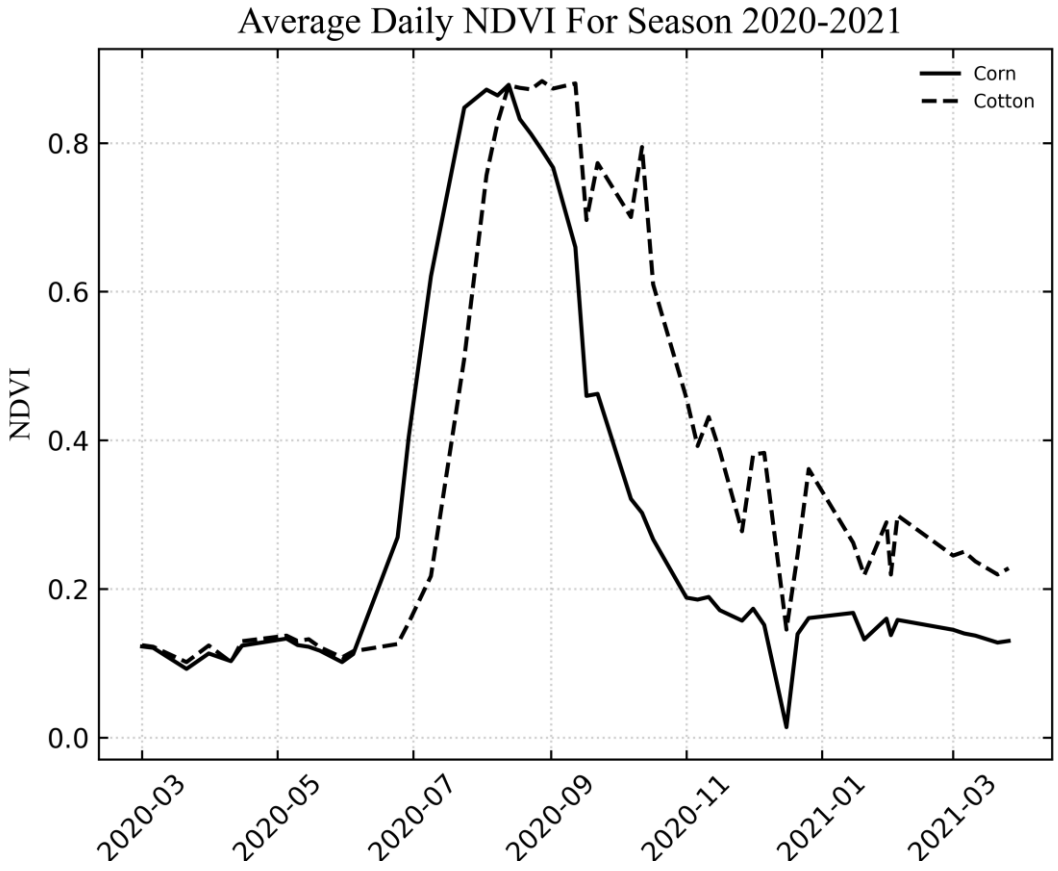


**Figure 3.7: NDVI curve for corn and cotton during growing season 2020 and non-growing season 2021**

## 3.8 Ground Heat Flux Calculation

Ground soil heat flux, G is an important component of the surface energy budget, but it is difficult to measure. Accurate determination of G is required to evaluate surface energy balance (Heusinkveld et al., 2004; De Silans et al., 1997; Roxy et al., 2014) and to estimate soil evaporation (Heitman et al., 2010; Kampf et al., 2005; Yao et al., 2013).

For our study, we are directly measuring G at 5 cm depth (Table 3.2) by using three individuals Hukseflux_HFP01 heat flux plates. Since for surface energy budget G needs to be known at the surface, an additional procedure is needed to transfer the measured flux at 5 cm depth to the surface.

### 3.8.1 Soil Heat Flux and Storage

Soil heat flux at the surface is calculated by adding the measured flux at a fixed depth, d, to the energy stored in the layer above the heat flux plate. The specific heat of the soil and the change in soil temperature, $\Delta T_s$, over the output interval, t, are required to calculate the stored energy. The soil heat flux at the surface is given by Equation 3.29:

$$G_{sfc} = G_{5cm} + S \qquad \text{Equation 3.29}$$

where, $G_{sfc}$ is the soil heat flux at surface [W/m$^2$], $G_{5cm}$ is the soil heat flux at 5cm depth [W/m$^2$] and S is the soil heat storage [W/m$^2$]. The storage term is then given by Equation 3.30.

$$S = \frac{\Delta T_s C_s d}{t} \qquad \text{Equation 3.30}$$

The heat capacity of the soil is calculated by adding the specific heat of dry soil to that of the soil water as given by Equation 3.31:

$$C_s = \rho_b (C_d + \theta_m C_w) = \rho_b C_d + \theta_v \rho_w C_w \qquad \text{Equation 3.31}$$

$$\theta_m = \frac{\rho_w}{\rho_b} \theta_v \qquad \text{Equation 3.32}$$

where, $C_s$ is the heat capacity of moist soil, $\rho_b$ is bulk density, $\rho_w$ is the density of water, $C_d$ is the heat capacity of a dry mineral soil, $\theta_m$ is soil water content on a mass basis, $\theta_v$ is soil water content on a volume basis, and $C_w$ is the heat capacity of water.

For the study area soil properties data was collected from Web Soil Survey (https://websoilsurvey. sc.egov.usda.gov/App/HomePage.htm). Table 3.4 shows the percentage of soil components at depth 1-25 cm.

**Table 3.4: Percentage of Soil Components**

| Map unit symbol | Map unit name | Clay (percent) | Sand (percent) | Silt (percent) | Total percentage | Acres in AOI | Percent of AOI |
|---|---|---|---|---|---|---|---|
| 1856 | Ulysses silt loam, 0 to 1 percent slopes | 26.6 | 19.2 | 54.2 | 100 | 25.8 | 0.841 |
| 1857 | Ulysses silt loam, 1 to 3 percent slopes | 23 | 25 | 52 | 100 | 4.6 | 0.151 |
| 1968 | Buffalo Park-Ulysses silt loams, 3 to 6 percent slopes, eroded | 22.7 | 20.7 | 56.7 | 100.1 | 0.2 | 0.008 |
| Totals for Area of Interest | | 24.1 | 21.63 | 54.3 | 100.03 | 30.7 | 1 |

## 3.9 Crop Water Stress Index

Crop Water Stress Index (CWSI) is used for characterizing plant water stress and scheduling irrigation. It is a thermal-based stress index which incorporates incoming solar radiation, relative humidity, air temperature, wind speed, canopy resistance at potential evapotranspiration, and crop height. All these measurements are taken once daily or over a short period of time, around solar noon or after cloud-free conditions. Equation 3.39 shows a generalized formula to estimate CWSI (O'Shaughnessy et al., 2012).

$$CWSI = \frac{(T_c - T_a) - (T_c - T_a)_{ll}}{(T_c - T_a)_{ul} - (T_c - T_a)_{ll}} \qquad \text{Equation 3.33}$$

where, $(T_c - T_a)$ is the measured difference between crop canopy temperature and air temperature, $(T_c - T_a)_{ll}$ is the lower limit representing the temperature difference for a well-watered crop, shown in Equation 3.40, and $(T_c - T_a)_{ul}$ is the upper limit representing the

temperature difference between the crop canopy and ambient air when the plants are severely stressed, shown in Equation 3.41 (Jackson et al., 1988).

$$(T_c - T_a)_{ll} = \left(\frac{r_a R_n}{\rho C_p}\right)\left(\frac{\gamma}{\Delta + \gamma}\right) - \frac{e_s - e_a}{\Delta + \gamma} \qquad \text{Equation 3.34}$$

$$(T_c - T_a)_{ll} = \frac{r_a (R_n - G)}{\rho C_p} \qquad \text{Equation 3.35}$$

# Chapter 4 - Results and Discussions

## 4.1 Data Collection and Processing

The data from two growing seasons in 2020 and 2021, and one non-growing season in 2021 was collected, processed, and analyzed for both corn and cotton sites. The data included the variables specified in Table 3.2 in Chapter 3. All variables were collected every 10 minutes and aggregated for 30-minute or 60-minute intervals. Various figures below present diurnal graphs and daily distributions during the growing seasons.

Figure 4.1 shows diurnal distributions of radiation fluxes (incoming solar radiation, net radiation, and ground heat flux) collected from in-situ sensors at two sites, two growing seasons, and one non-growing season: corn and cotton in 2020 and 2021. The fluxes are calculated for the entire seasons. Radiation fluxes show higher values during the growing seasons than non-growing season with the highest values at noon being 21% higher on average. Net radiation is normally negative during night times and positive during day times when the sun is up. Ground heat fluxes are positive when soil is heating up and negative at night. On average, solar radiation represents 155% of net radiation while ground heat flux is about 15% of daily net radiation.

Incoming solar radiation is similar for both corn and cotton during growing seasons 2020 (maximum ~700 $Wm^{-2}$) and 2021 (maximum ~700 $Wm^{-2}$) and non-growing season 2021 (maximum ~550 $Wm^{-2}$). In growing season 2020, net radiation for both crops were similar but in growing season 2021, cotton had higher net radiation than corn.

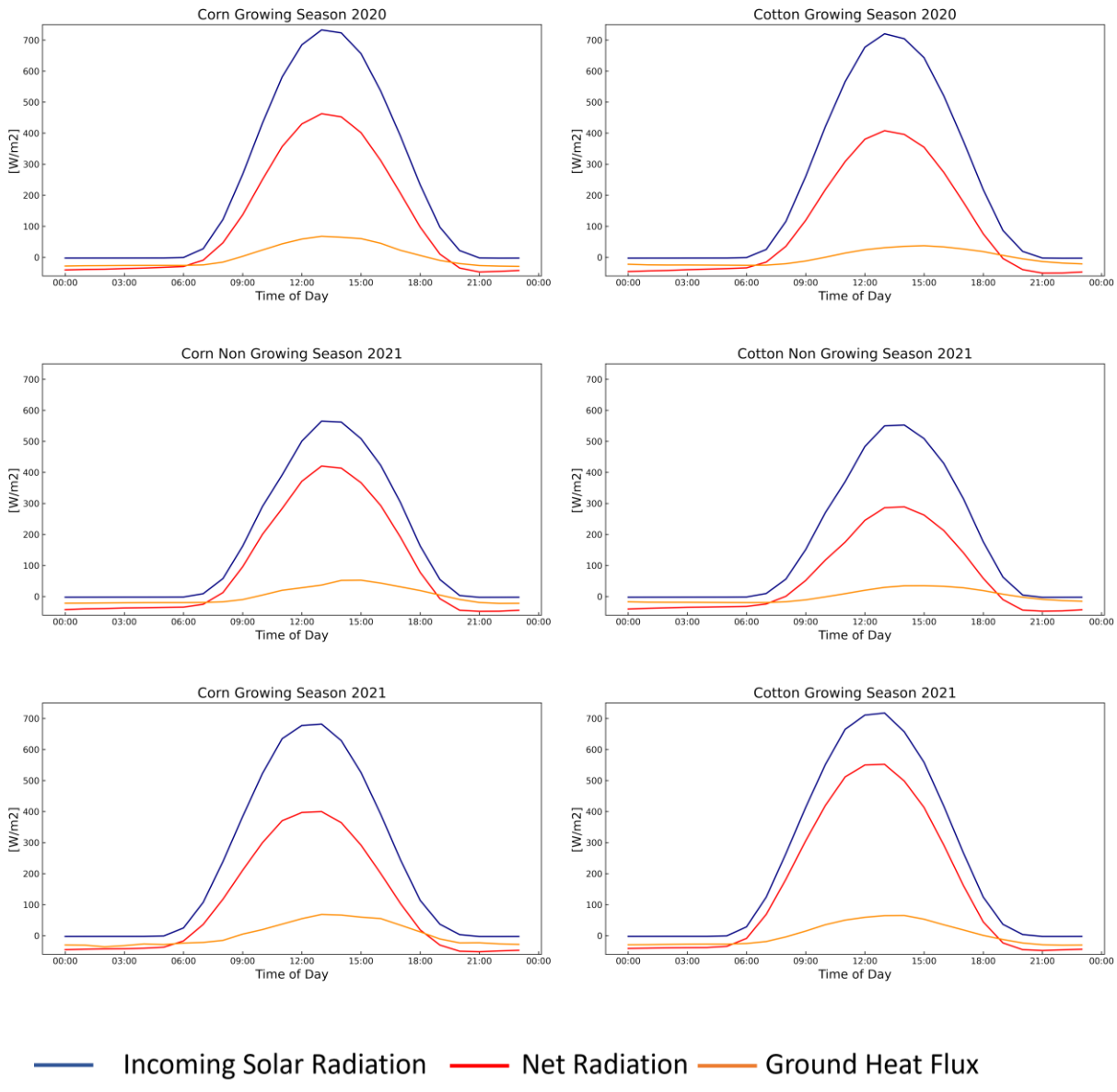


**Figure 4.1: Radiation fluxes (Incoming short radiation, net radiation and ground heat flux) during growing (2020, 2021) and non-growing (2021) seasons for corn and cotton.**

Figure 4.2 shows diurnal distributions of temperature (air, canopy, and soil) for corn and cotton. Canopy temperature was always reaching higher values than other temperatures due to radiation heating, while temperature of the soil at 2 cm depth had the lowest values. There was a shift in temperature reaching maximum values toward the later part of the day by 3 hours from

the air temperature to the soil temperature. Temperature distributions are similar during growing and non-growing seasons, but the values are lower for the non-growing season.

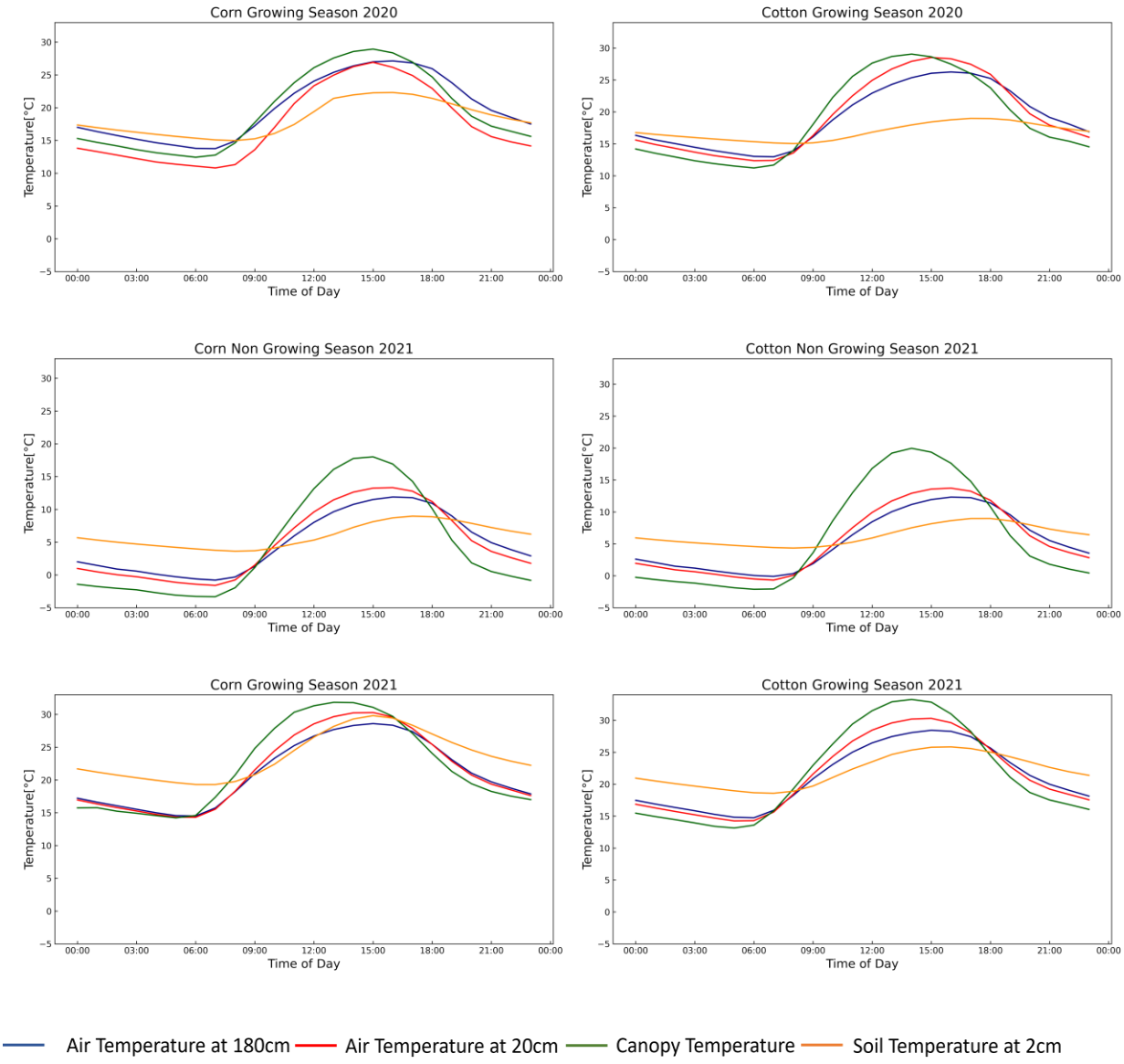


**Figure 4.2: Temperature (air temperature, canopy temperature and soil temperature) during growing (2020 ,2021) and non-growing (2021) seasons for corn and cotton.**

Figure 4.3 shows time series of daily average radiation fluxes (incoming short-wave radiation, net radiation, and ground heat flux) for corn during growing season 2020 and 2021. Incoming

solar radiation was higher during 2020 than 2021 resulting in higher net radiation and ground heat fluxes in 2020.

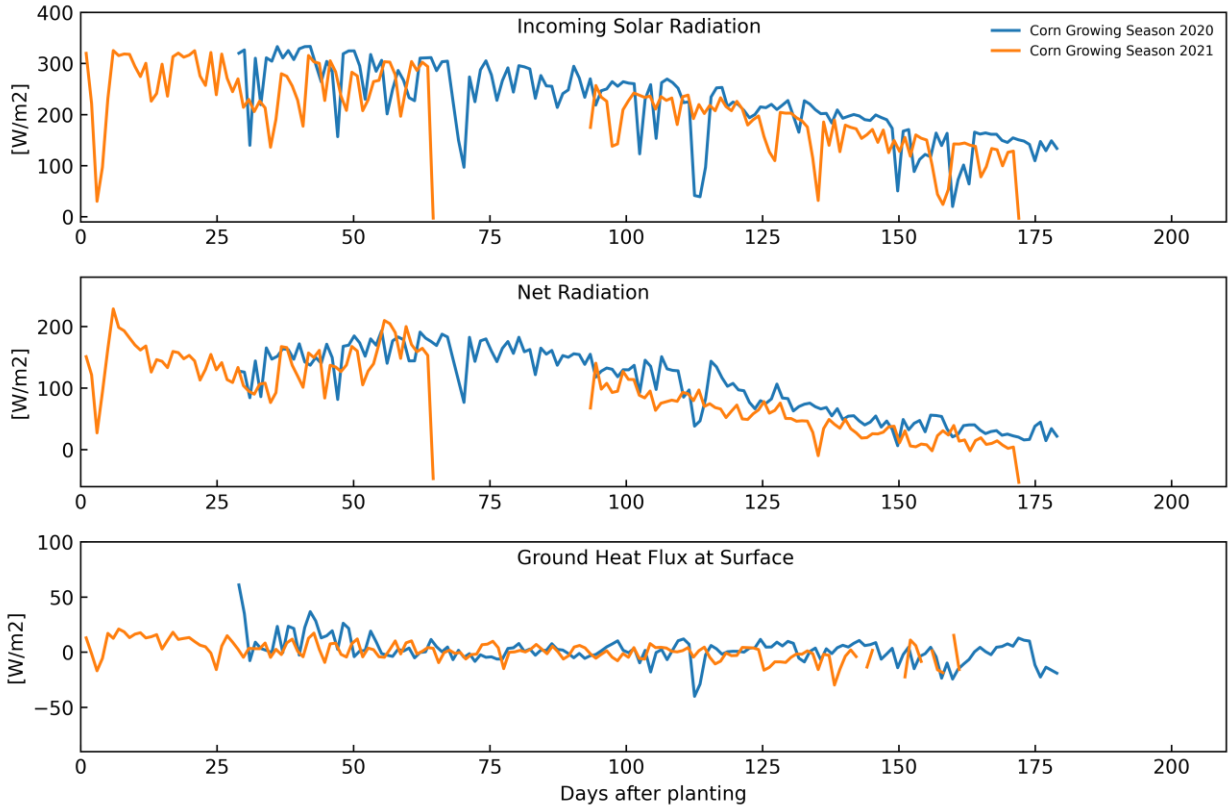


**Figure 4.3: Distribution of radiation fluxes during growing seasons (2020 and 2021) for corn**

Figure 4.4 shows time series of daily temperature (air temperature, canopy temperature, and soil temperature) distributions for corn during growing season 2020 and 2021. Year 2021 was warmer than 2020 that results in higher canopy temperature and soil temperature in 2021 than in 2020. All temperatures followed a similar pattern for both years with some fluctuations affected by atmospheric conditions.

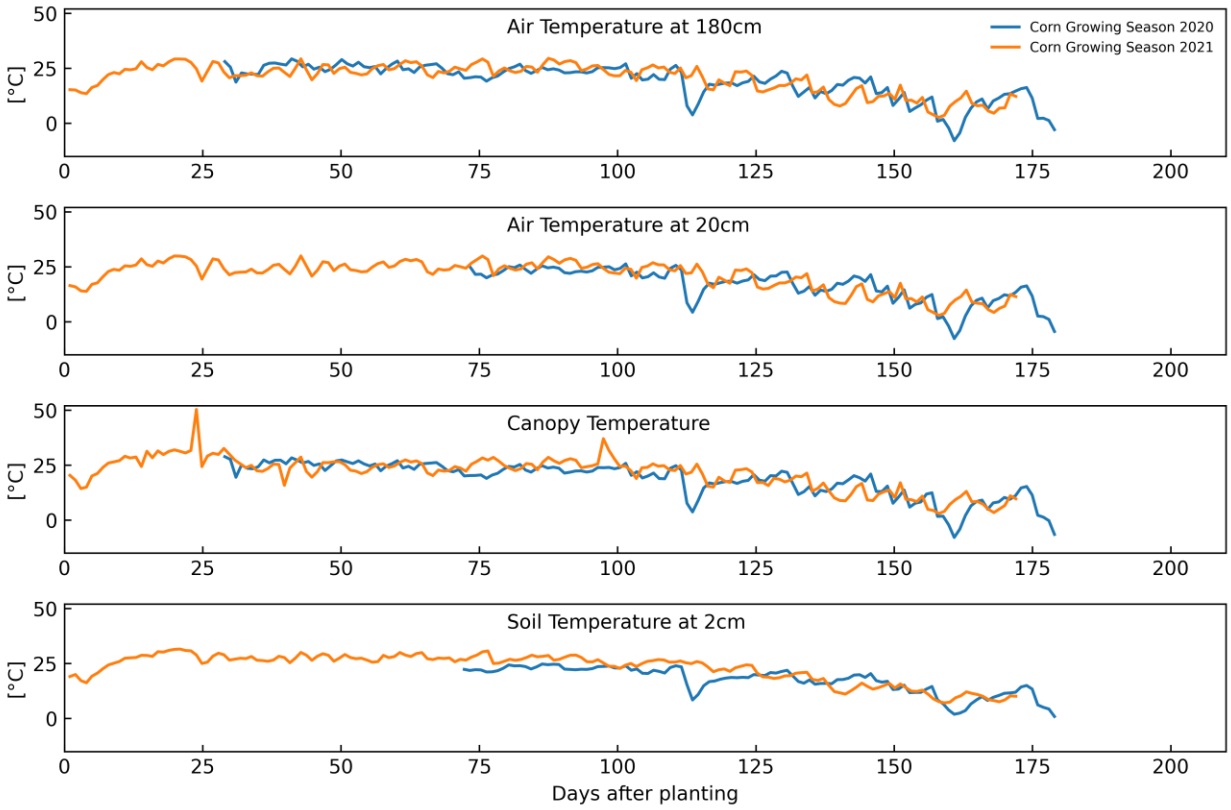


**Figure 4.4: Distribution of temperatures during growing seasons (2020 and 2021) for corn**

Figure 4.5 shows time series of daily distributions of radiation fluxes (incoming short-wave radiation, net radiation, and ground heat flux) for cotton during growing season 2020 and 2021. Incoming solar radiation was similar during 2020 and 2021 but net radiation was higher in 2021 than 2020 for cotton, and it is different than in corn (Figure 4.3). Slight differences in solar radiation for the same year for corn and cotton can be attributed to corn tower raised higher to 3m height to provide a 1.5 to 2 m clearance with corn canopy during its mature stage.

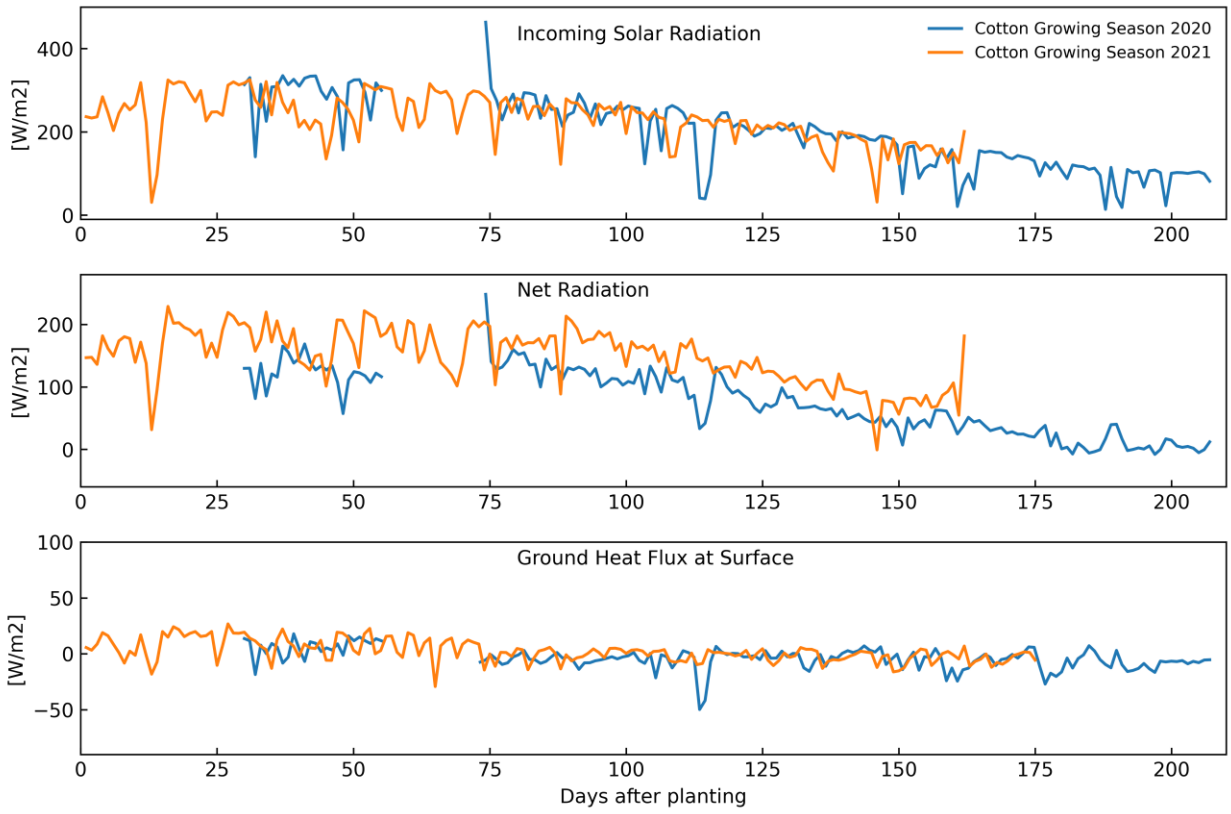


**Figure 4.5: Distribution of radiation fluxes during growing seasons (2020 and 2021) for cotton**

Figure 4.6 shows time series of daily temperature (air temperature, canopy temperature, and soil temperature) distributions for cotton during growing seasons 2020 and 2021. Year 2021 was warmer than 2020 and resulted in higher canopy temperature and soil temperature. The distributions follow similar trends with corn (Figure 4.4).

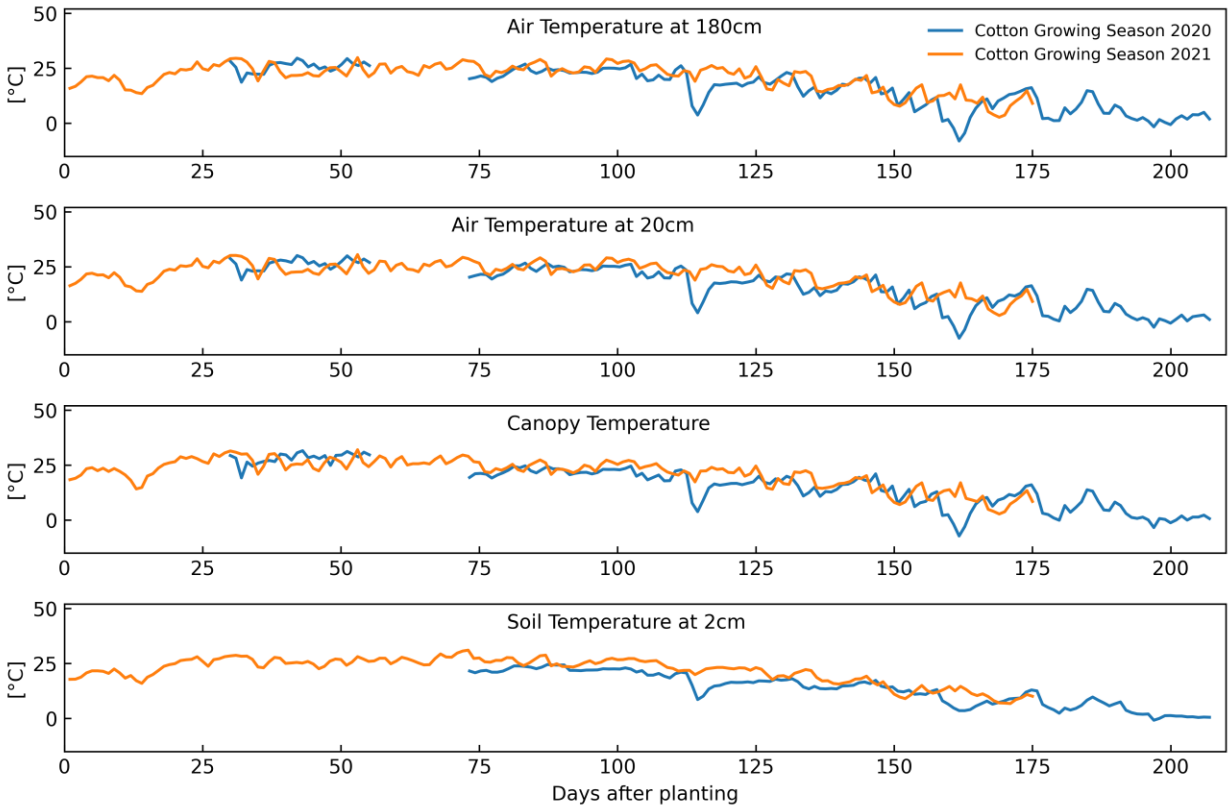


**Figure 4.6: Distribution of temperatures during growing seasons (2020 and 2021) for cotton**

The growing season in 2020 was extended into December for cotton due to extreme wet conditions in the field and accounted for 207 days, while it took 169 days in 2021 (Table 4.1). Total heat units were similar for both crops, but precipitation was drastically different. Season 2021 was warmer and dryer than 2020, which resulted in shorter growing season for both crops (Table 4.1).

**Table 4.1: Summary of corn and cotton production during growing seasons in 2020 and 2021.**

| Growing season | Crop | Growing days | P (in) | Irrigation (in) | Heat Units (ºC) | P days | Irrigation Days |
|---|---|---|---|---|---|---|---|
| 2020 | Cotton | 207 | 11.63 | 2.75 | 1198.9 | 28 | 3 |
| | Corn | 155 | | 2.75 | 1824.43 | | 3 |
| 2021 | Cotton | 169 | 6.76 | 5.75 | 1165.1 | 21 | 6 |
| | Corn | 141 | | 5 | 1839.2 | | 5 |

### 4.1.1 Comparison of daily time series

#### 4.1.1.1 Corn vs Cotton

Incoming solar radiation, net radiation, air temperature (at 20 cm and 180 cm), relative humidity (at 20 cm and 180 cm), canopy temperature, soil temperature at 5 cm depth, soil water content at 5 cm depth were compared for both corn and cotton during growing seasons 2020 and 2021 to verify the data collected from both stations. Table 4.2 summarizes a comparison statistics and Figure 4.7 shows comparisons scatter plots. Coefficient of determination, $r^2$ is less for net radiation though incoming solar radiation is highly correlated which indicates the other radiation fluxes (outgoing short wave, incoming long wave, and outgoing long wave) contributing to net radiation are different for each crop (corn and cotton). Also, water content has the lowest $r^2$ value due to different irrigation scheduling, and different water up taking rates by each crop.

**Table 4.2: Summary of variable comparison (cotton vs corn)**

| Variables | $R^2$ | RMSE |
|---|---|---|
| Incoming solar radiation | 0.94 | 20.04 |
| Net radiation | 0.746 | 28.62 |
| Air temperature at 20 cm | 0.999 | 0.34 |
| Air temperature at 180 cm | 0.996 | 0.64 |
| Relative humidity at 20 cm | 0.985 | 1.61 |
| Relative humidity at 180 cm | 0.962 | 2.58 |
| Canopy temperature | 0.966 | 2.09 |
| Soil temperature at 5 cm depth | 0.984 | 1.24 |
| Water content at 5 cm depth | 0.243 | 0.08 |

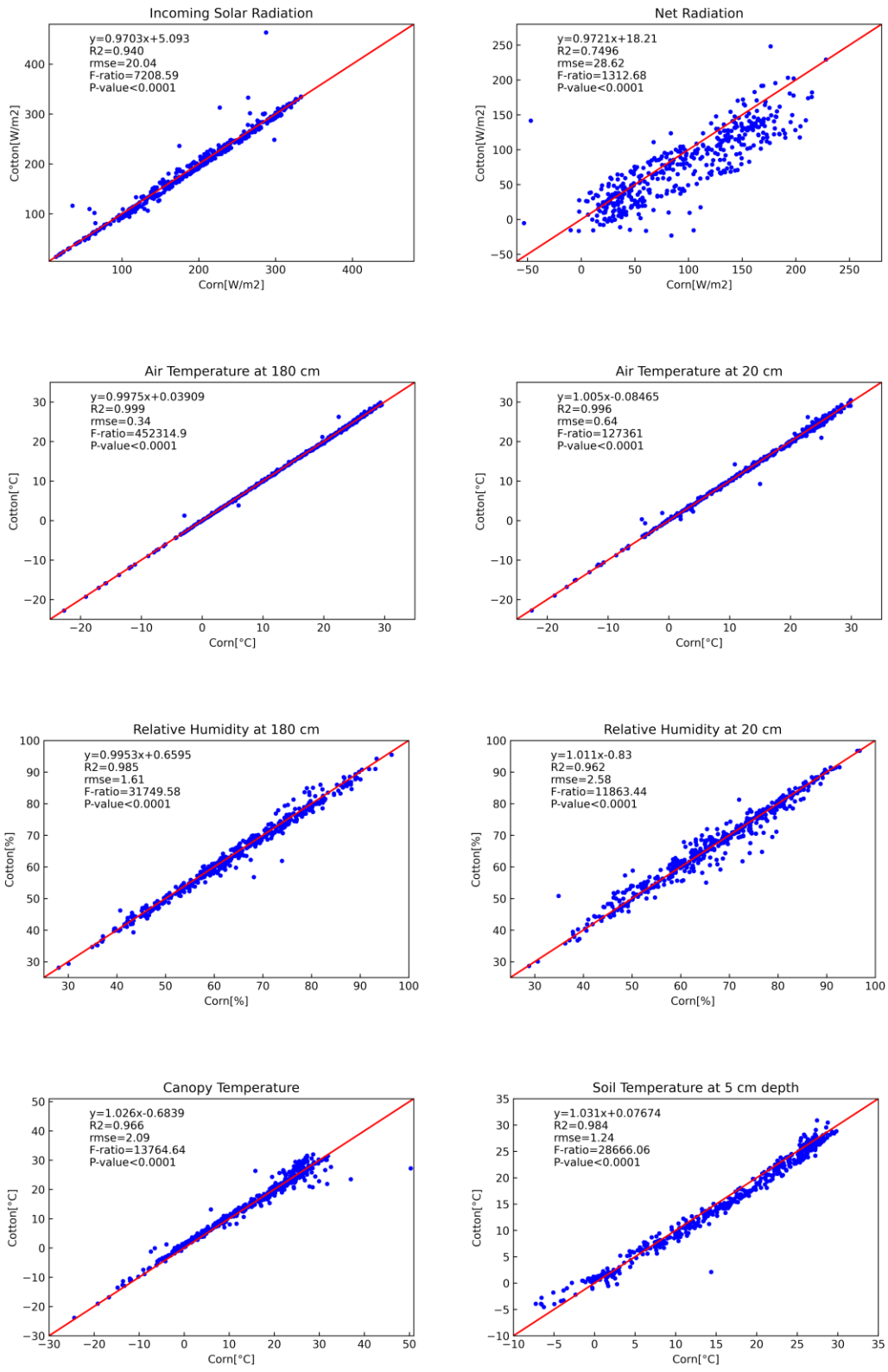


**Figure 4.7: Cotton vs corn meteorological parameters comparisons**

#### 4.1.1.2 Mesonet Vs Corn and Cotton

Incoming solar radiation and air temperature at both sites (corn and cotton) were compared during the growing season 2020 and 2021 with the data from the nearest Mesonet station to validate the data collection. Table 4.3 shows summary of the comparison and Figure 4.8 shows the comparison scatter plots. Higher $r^2$ indicates higher similarities of the data with Mesonet, validating the data collected at both stations.

**Table 4.3: Summary of variable comparison (mesonet vs (cotton and corn))**

| Mesonet | Variables | $R^2$ | RMSE |
|---|---|---|---|
| Corn | Incoming solar radiation | 0.911 | 24.59 |
| | Air temperature | 0.992 | 0.96 |
| Cotton | Incoming solar radiation | 0.939 | 20.27 |
| | Air temperature | 0.991 | 0.99 |

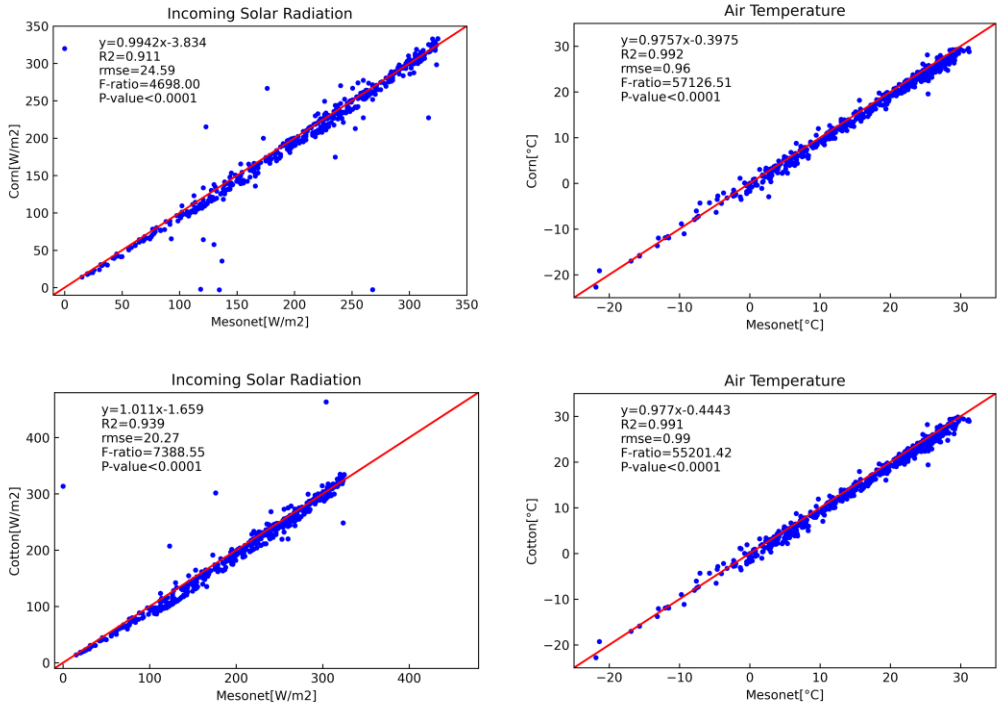


**Figure 4.8: Radiation and air temperature comparison with mesonet**

## 4.2 Reference Evapotranspiration

Reference evapotranspiration was calculated using FAO 56 Penman-Monteith equation (Allen et al, 1998) using data collected at the two in-field sites and compared with the data from the nearest Mesonet station (shown in Figure 4.9). We note that the calculated reference ET was not used for calculating crop coefficient but was only presented here to ensure that reference ET is robust to the environmental conditions observed in the actual sites. Higher $r^2$ indicates higher similarities of the calculated results with Mesonet.

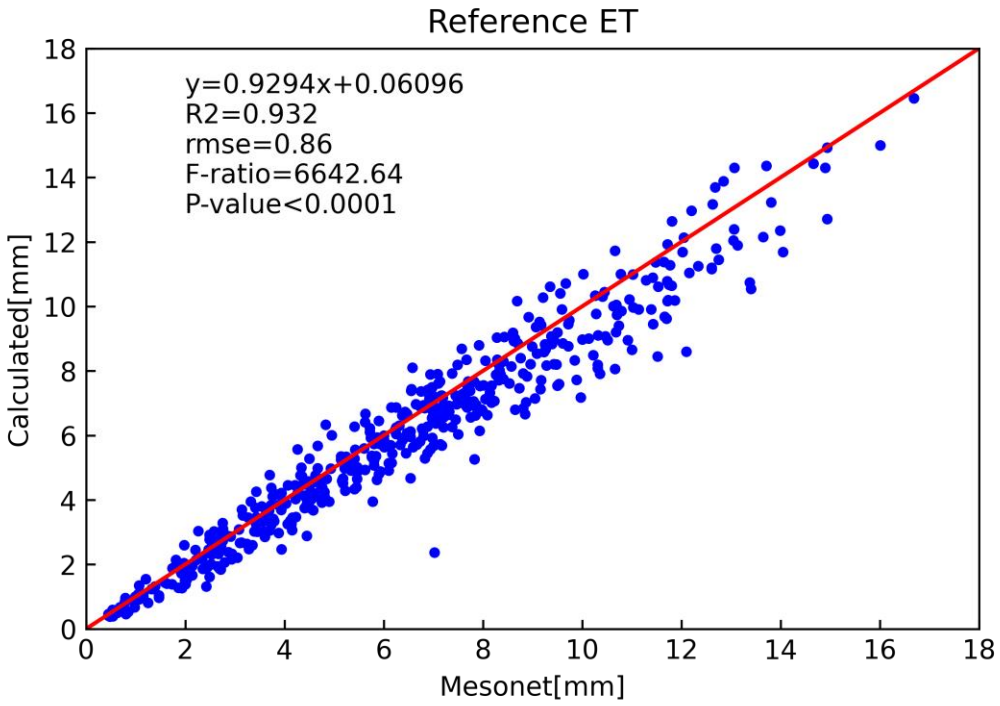


**Figure 4.9: Reference ET comparison**

## 4.3 Crop Evapotranspiration

### 4.3.1 NDVI

Weekly NDVI values aggregated from pixeled data in each field in 2020 and 2021 were interpolated and the NDVI graphs for corn and cotton are shown in Figure 4.10. The bell-shaped graphs are similar for corn and cotton, but corn showed a much shorter initial stage of plant

growth, about 25 days after planting for corn to about 50 days for cotton. There was a shift in NDVI reaching maximum values for cotton from corn by 25 days in 2020 and 50 days in 2021. After harvest at the end of growing season NDVI values were found to be at a higher value than at the beginning of the growing season. It happens likely due to amount residue on the ground left after harvest.

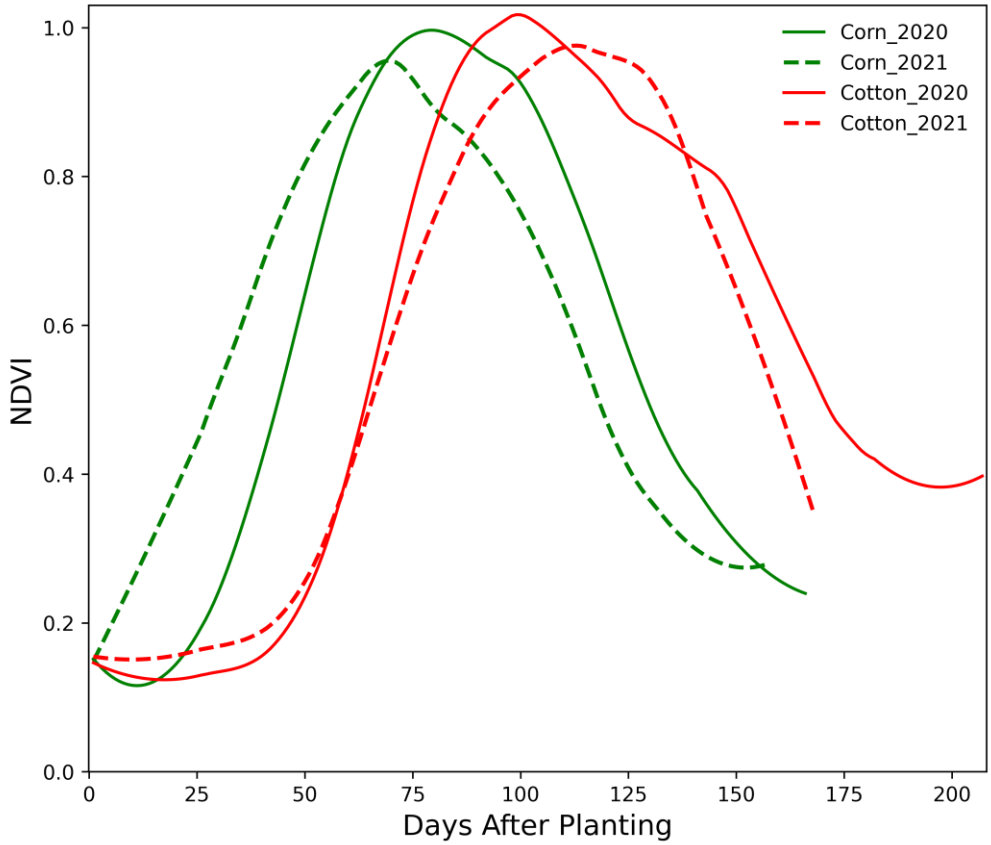


**Figure 4.10: NDVI for corn and cotton during growing seasons (2020,2021)**

### 4.3.2 Soil thermal inertia calibration

Soil thermal inertia needs to be calibrated before using it in the MEP model. Since soil thermal properties are difficult to properly evaluate, the value of I_s was calibrated by testing a range of its values and comparing the calculated ground heat flux by MEP with the observed value at soil surface re-constructed from 5 cm depth measurements during the non-growing

season. During non-growing season, a bare soil Penman-Monteith equation for ET under saturated soil condition can be used without crop coefficient adjustments. ET calculated from the MEP model was compared with actual the ET using Equation 3.1.

We used soil thermal inertia defined in Equation 3.9 as an initial estimate by substituting the book values of soil thermal properties. This was used as an initial value of I_s and applied during the non-growing season 2021. Figure 4.11 shows scatter plot of ET values and optimized ground heat flux. ET comparison shows high coefficient of determination, $r^2 \sim 0.97$. The optimized value of $I_s$ was found at 1141 with $r^2 \sim 0.84$.

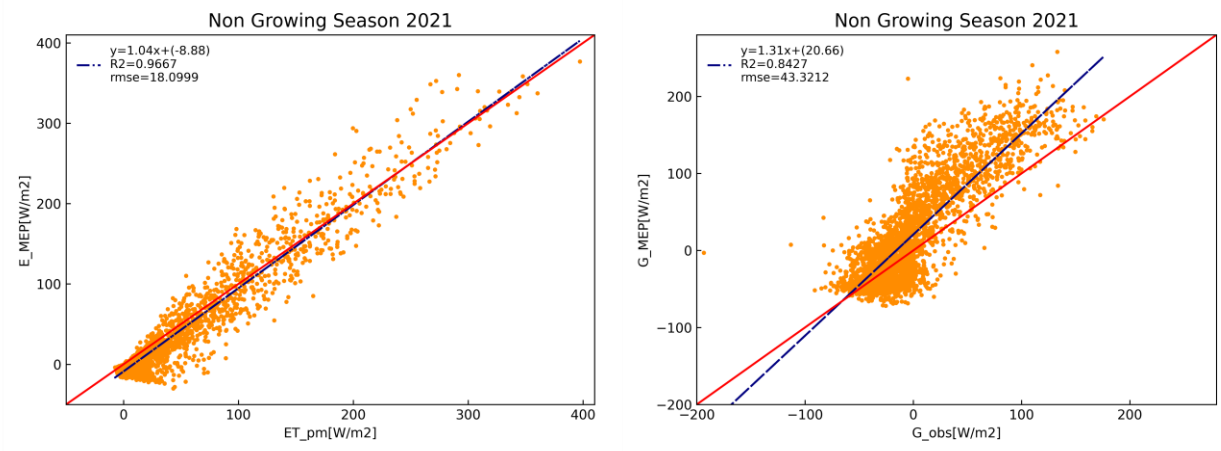


**Figure 4.11: Soil thermal inertia verification during non-growing season 2021**

### 4.3.3 Ref ET vs Actual ET

The optimized MEP model was applied to the sites during the growing seasons in 2020 and 2021. Figures 4.12 and 4.13 show time series of daily reference ET and actual ET for corn and cotton calculated by using the MEP model during growing season 2020. Seven days average data is presented in Figure 4.13. Actual ET reached its maximum value at the development stage

and started to decline at the mid stage. Maximum actual ET was higher for corn than cotton. ET was higher for corn during initial and development stages while cotton ET rates were higher during the maturity stage. During the period from 60 to 75 days, cotton ET was not calculated due to equipment damage in the field, thus zero values in Figures 4.12 which was later recalculated by using 2021 crop coefficient for cotton. In Figure 4.13 cross marked line shows the recalculated ET calculation.

Figure 4.14 and Figure 4.15 show the portion of evaporation and transpiration from MEP model used in actual ET calculation.

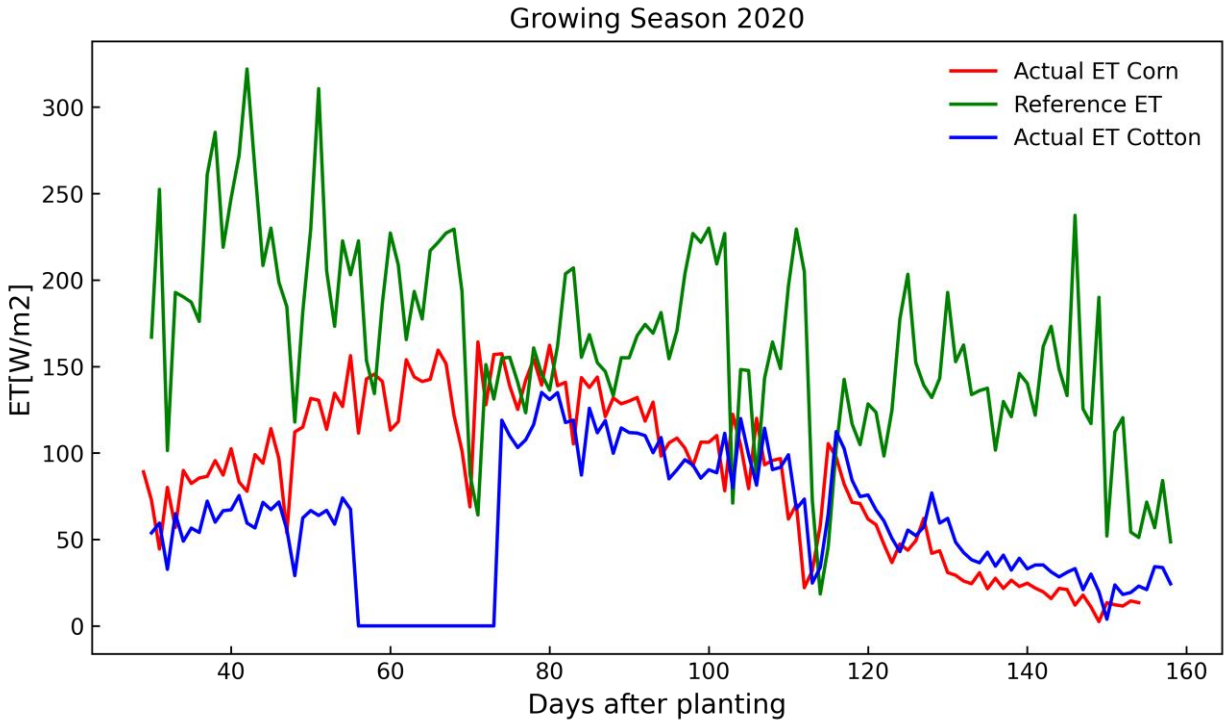


**Figure 4.12: Reference ET with actual ET from MEP for corn and cotton during season 2020 (daily)**

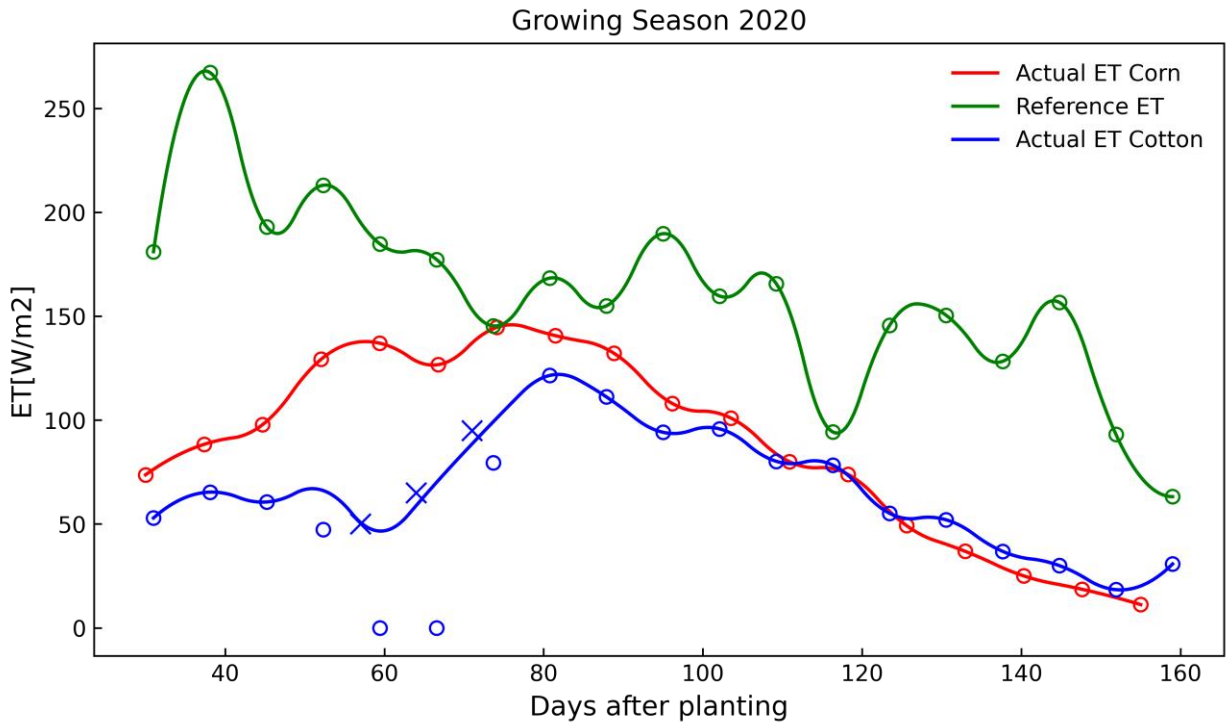


**Figure 4.13: Reference ET with actual ET from MEP for corn and cotton during season 2020 (seven days average)**

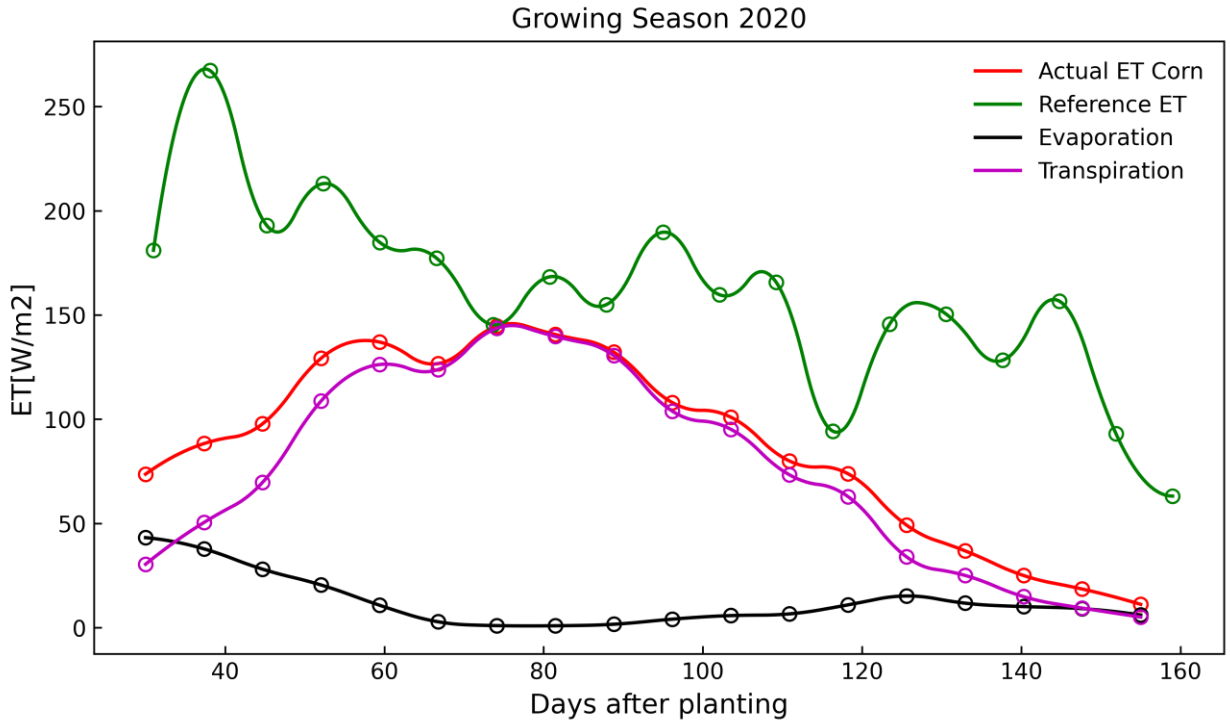


**Figure 4.14: Reference ET with actual ET, evaporation, and transpiration from MEP for corn during season 2020 (seven days average)**

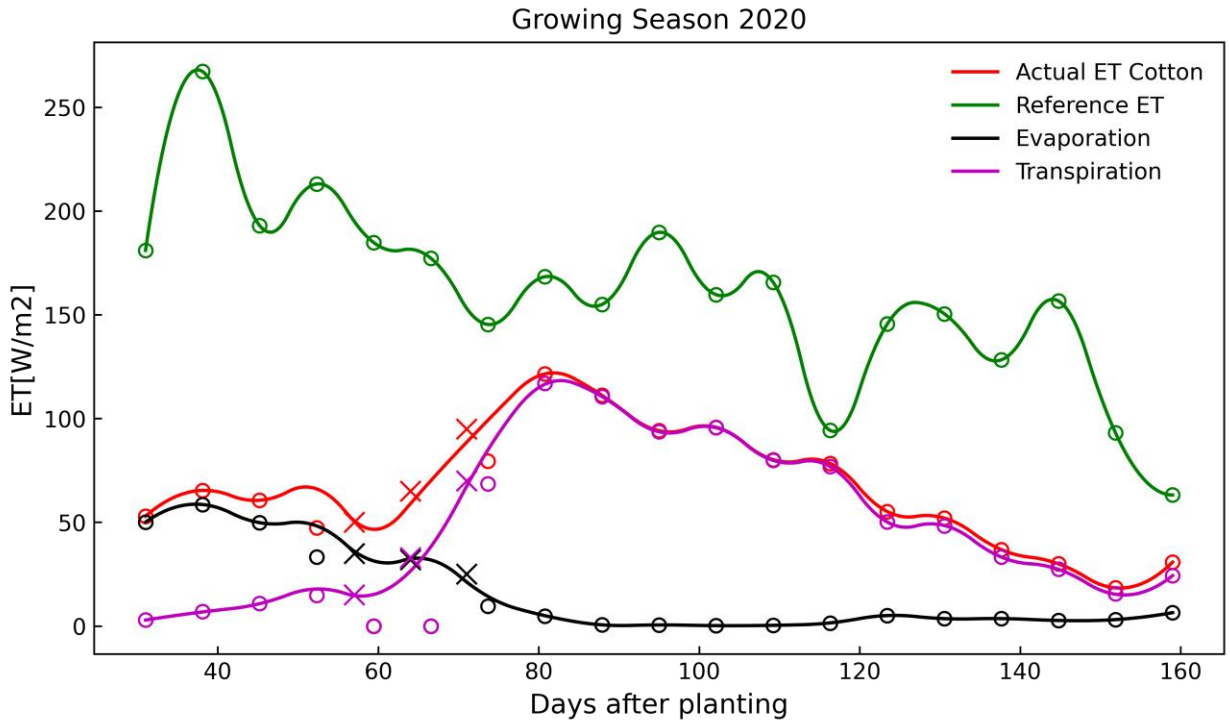


**Figure 4.15: Reference ET with actual ET, evaporation, and transpiration from MEP for cotton during season 2020 (seven days average)**

Figures 4.16 and 4.17 show daily reference ET and actual ET for corn and cotton by using MEP model during growing season 2021. Figure 4.17 shows seven-day average values. Actual ET reached its maximum value at the development stage and started to decline at the mid stage. Maximum actual ET was higher for corn than cotton also for this season but smaller during the maturity stage. The pattern is similar for 2020 and 2021. During August 2021, an equipment failure at the corn site caused lack of ET calculations, thus ET shows as zero in Figures 4.16 which was later recalculated by using 2020 crop coefficient for corn. In Figure 4.17 cross marked line shows the recalculated ET calculation.

Figure 4.18 and Figure 4.19 show the portion of evaporation and transpiration from MEP model used in actual ET calculation.

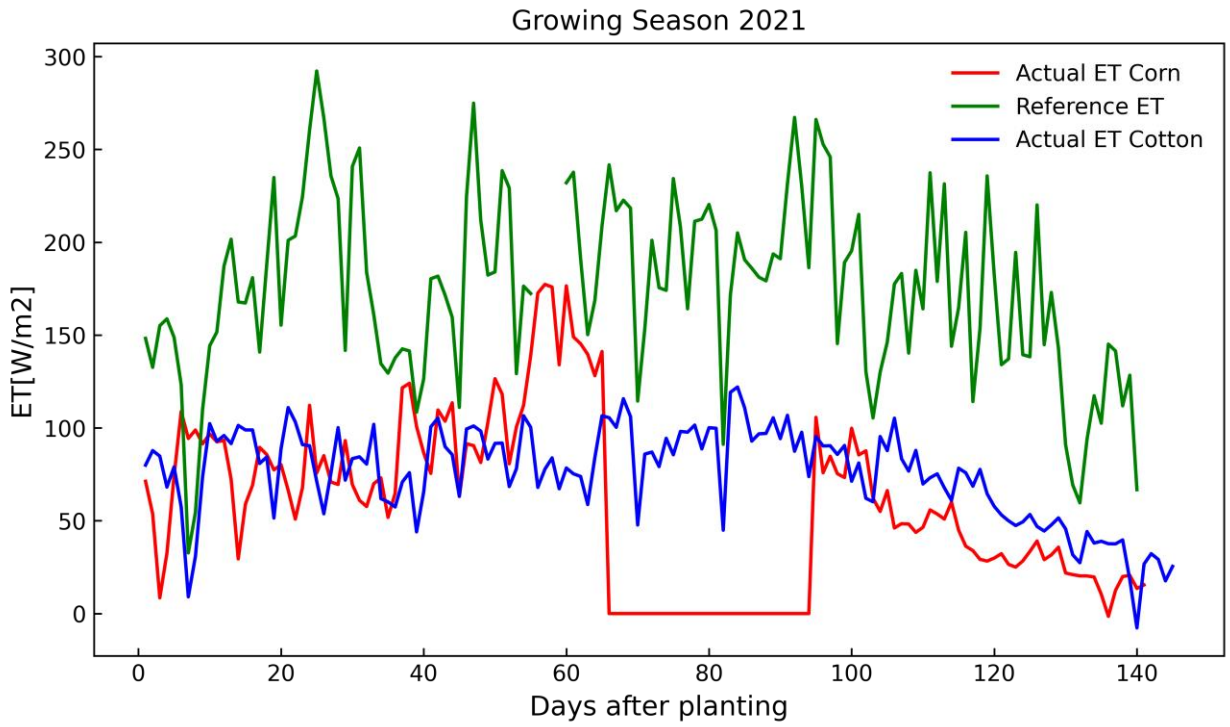


**Figure 4.16: Reference ET with actual ET from MEP for corn and cotton during season 2021(daily)**

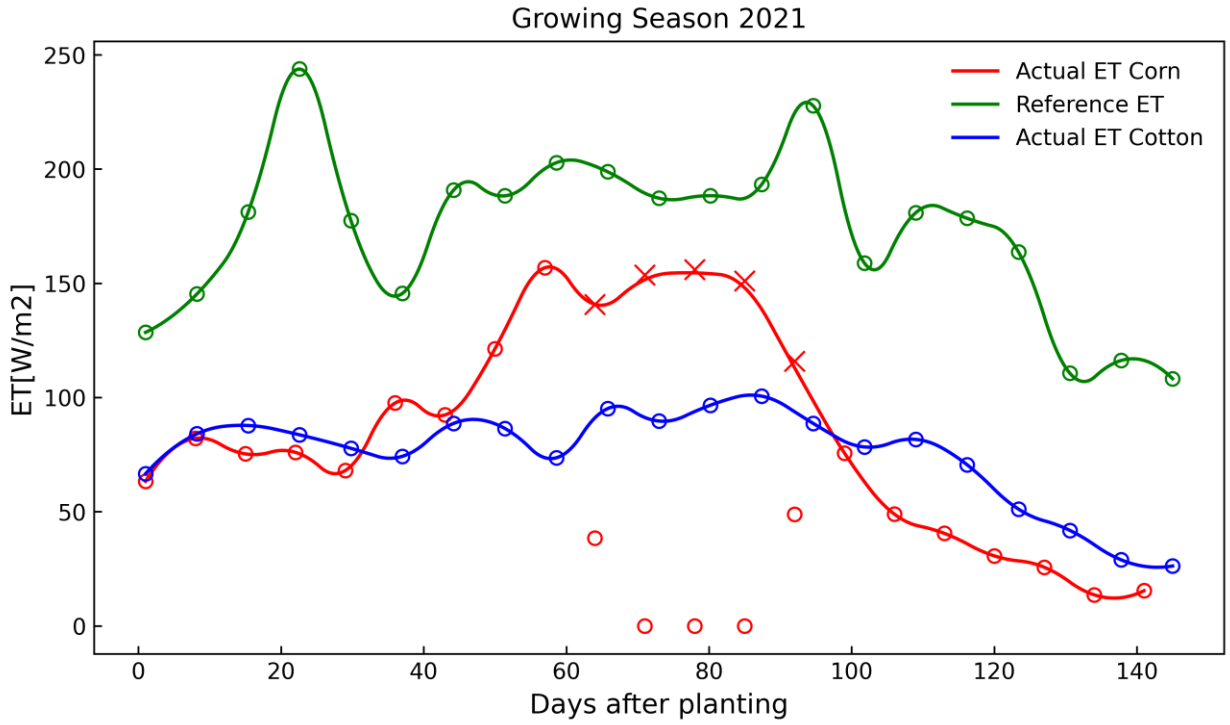


**Figure 4.17: Reference ET with actual ET from MEP for corn and cotton during season 2021 (seven days average)**

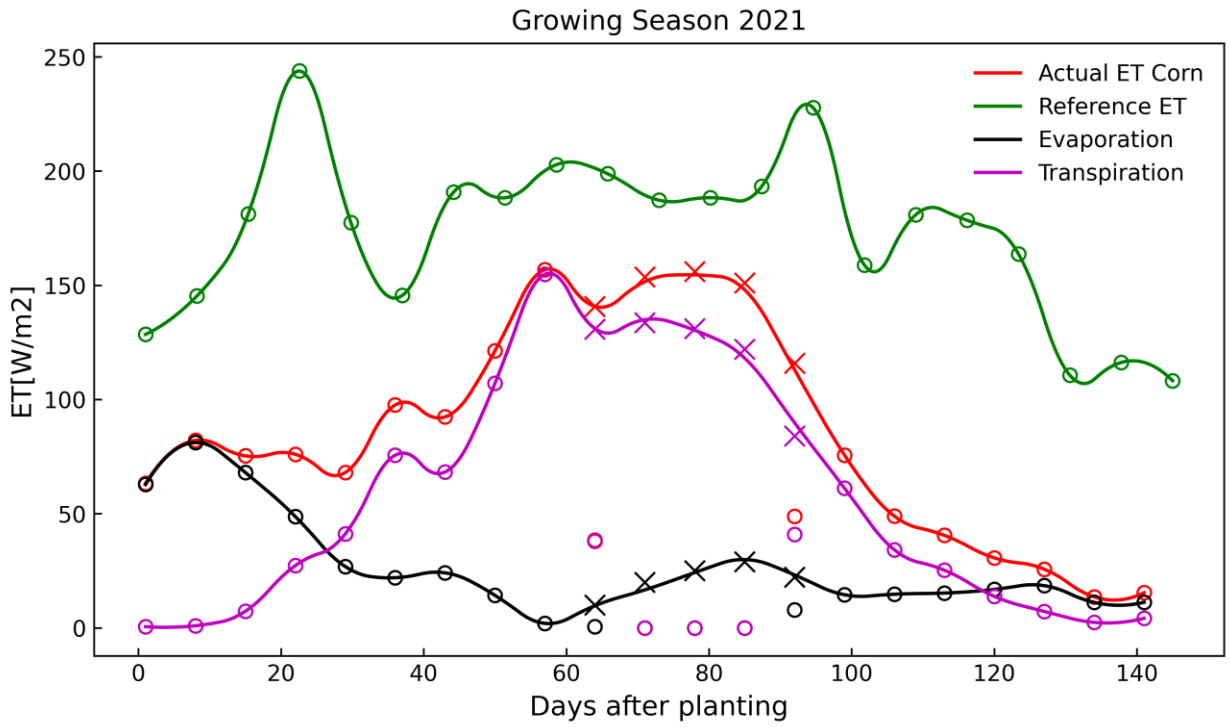


**Figure 4.18: Reference ET with actual ET, evaporation, and transpiration from MEP for corn during season 2021 (seven days average)**

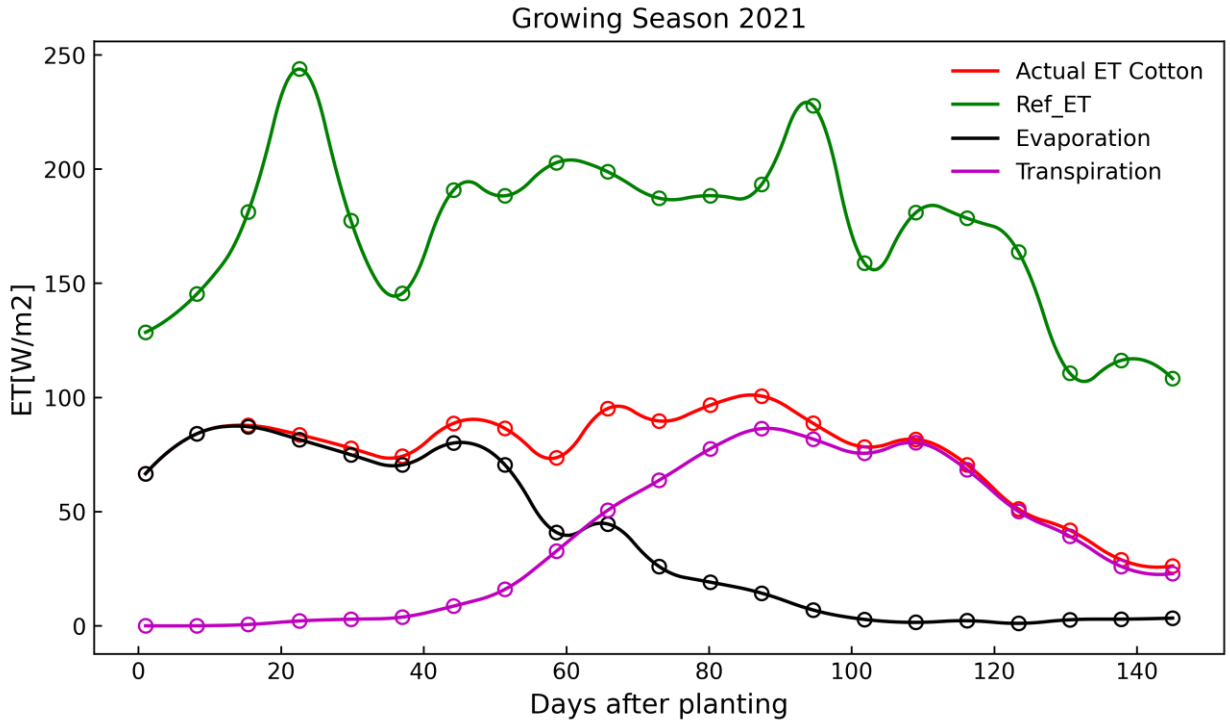


**Figure 4.19: Reference ET with actual ET, evaporation, and transpiration from MEP for cotton during season 2021 (seven days average)**

Table 4.4 shows the summary of seasonal ET for both crops during growing season 2020 and growing season 2021. For both season ET was less for cotton than corn. ET calculation was stopped right after first freezing temperature.

**Table 4.4: Summary of seasonal ET for Corn and Cotton in growing season 2020 and 2021**

| Growing season | Crop | Growing days | Total ET [mm] | Total Evaporation[mm] | Total Transpiration[mm] |
|---|---|---|---|---|---|
| 2020 | Cotton | 207 | 311.5 | 78 | 233.5 |
| | Corn | 155 | 387.65 | 55.85 | 331.8 |
| 2021 | Cotton | 169 | 387.15 | 192.94 | 194.21 |
| | Corn | 141 | 441.16 | 136.88 | 304.29 |

### 4.3.4 Crop Coefficient:

Figure 4.16 shows daily crop coefficient calculated for corn from reference ET and actual ET values during growing seasons 2020 and 2021. Crop coefficient reached value of 1.2 at the mid stage in 2020 and 1.1 in 2021 though there are some missing values during the mid-stage.

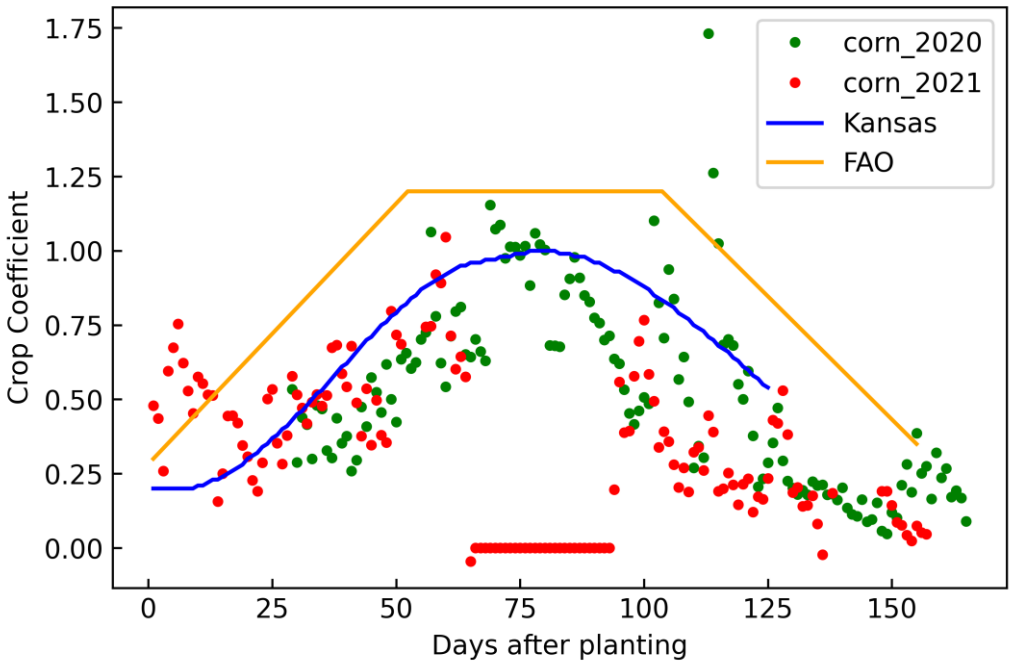


**Figure 4.20: Crop co-efficient for corn during growing season 2020 and 2021**

Figure 4.17 shows the crop coefficient for cotton calculated from reference ET and actual ET during growing season 2020 and 2021. Crop coefficient reached value of 0.8 at the mid stage in 2020 and 0.7 in 2021 during the mid-stage.

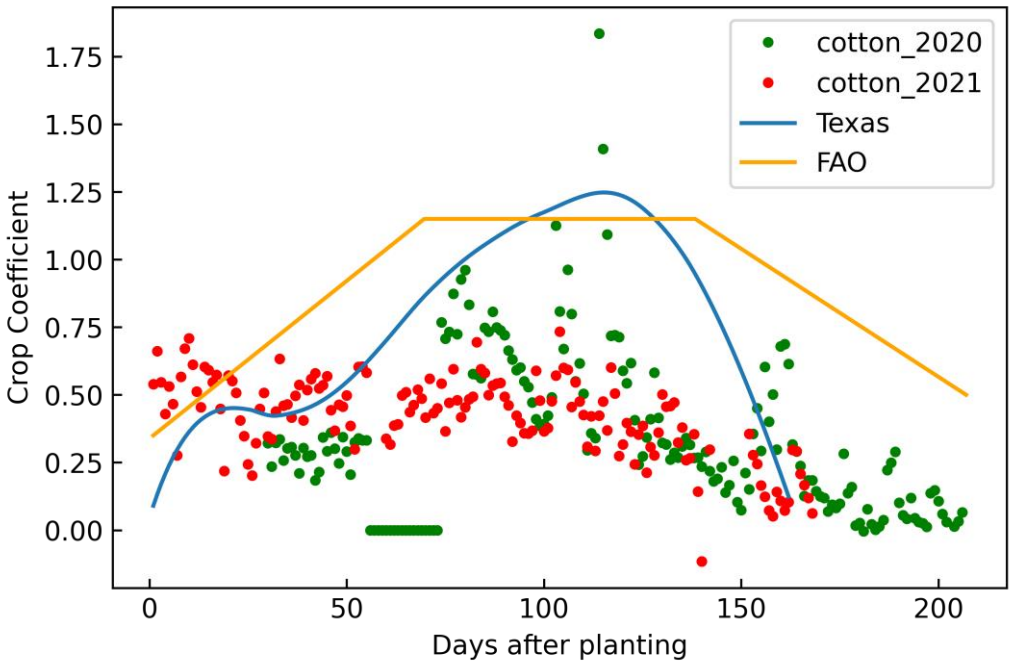


**Figure 4.21: Crop coefficient for cotton during growing season 2020 and 2021**

## 4.4 Crop Water Stress Index

Figure 4.18 shows the crop water stress index for corn during growing seasons 2020 and 2021. The index fluctuated throughout the entire season reaching values >0.45 for 52 days especially during 2021. 0.45 is used as threshold for CWSI (O'Shaughnessy et al., 2012).

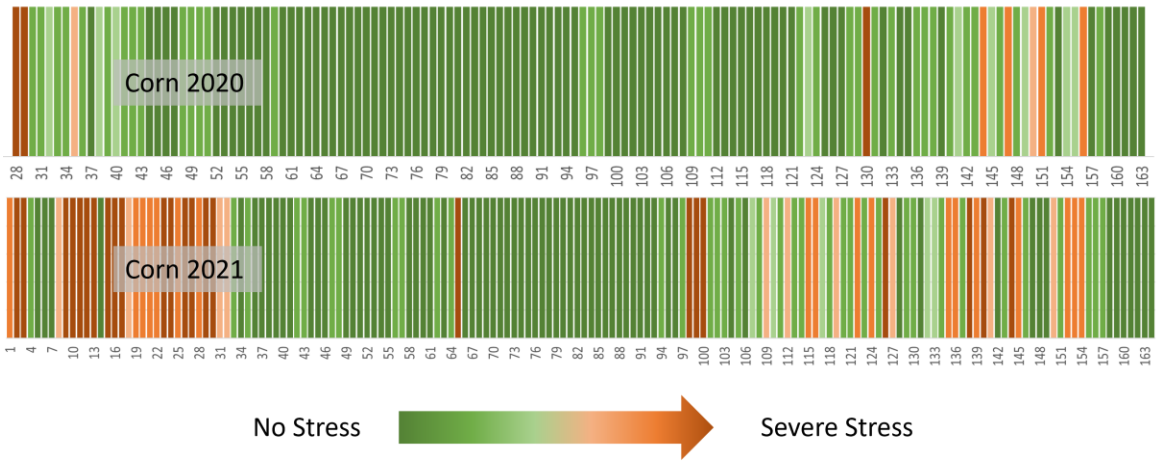


**Figure 4.22: Crop water stress index for corn during growing season 2020 and 2021**

Figure 4.19 shows the crop water stress index for cotton during growing seasons 2020 and 2021. The index fluctuated throughout the entire season reaching values >0.45 for 50 days during 2020.

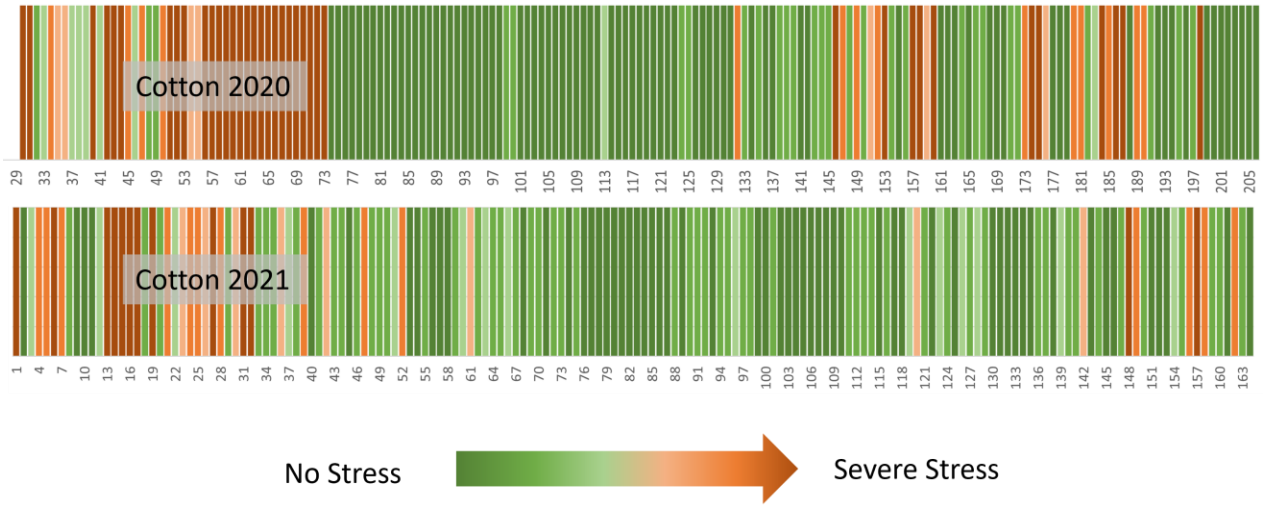


**Figure 4.23: Crop water stress index for cotton during growing season 2020 and 2021**

Table 4.5 shows the summary of total stressed days faced by both crops during growing season 2020 and 2021.

**Table 4.5: Summary of stressed days for corn and cotton during growing season 2020 and 2021**

| Growing season | Crop | Stressed Days | | |
|---|---|---|---|---|
| | | Initial Season | Mid-Season | End Season |
| 2020 | Cotton | N/A | 35 | 24 |
| | Corn | N/A | 3 | 6 |
| 2021 | Cotton | 12 | 15 | 8 |
| | Corn | 20 | 11 | 22 |

## 4.5 Discussion

The result for the optimizing Is showed good comparison of MEP and PM ET with R2=0.97. The ground heat flux from MEP model was higher at higher values resulting in overestimating ground heat flux mainly during the middle of the day, but R2 was good at 0.84. The reason for overestimation was soil being unsaturated during actual observation condition. The difference of 20 to 50 W/m2 appears to be in line with the flux being poorly transmitted through an unsaturated soil.

The reference ET calculated by the PM method showed significantly higher values than actual ET at all crop growth stages throughout the entire season (Figure 4.13 and Figure 4.15). This indicates that additional calibration of the MEP and adjustment of the PM models might be needed to resolve the issue of not matching the ET fluxes during the mature crop stage. It is more evident from the crop coefficient graphs (Figure 4.17).

Crop coefficient reached maximum value of 1.2 at the mid stage in 2020 and 1.1 in 2021 for corn. These values appear to be larger than reported in the literature, i.e. for Kansas by Lamm et al., 1995 but similar to FAO suggested Kc (Allen et. al 1998). But for cotton crop coefficient reached maximum value of 0.8 at the mid stage in 2020 and 0.7 in 2021 that appear to

be lower than reported in the literature, i.e., for panhandle region of Texas (Kcmax = 1.3 to 1.4). Actual ET and reference ET were calculated by two different methods, for actual ET the theory of maximum entropy production was used that is based on the energy balance while for reference ET FAO-based PM approach was used that has series of assumptions on the values of various physical parameters from empirical considerations. The empirical parameters in PM method were generally estimated by the experiments conducted in the locations with conditions that might be different from the semiarid conditions of southwest Kansas. Regardless of this, additional research on cotton growth characteristics and verification of both models are needed.

The cotton water stress index (CWSI) was calculated for corn and cotton daily during growing season 2020 and 2021. Corn was under stress in 9 days out of 166 days after planting in 2020, and 52 days out of 157 days though there were some missing values in 2020. Cotton was under stress in 50 days out of 207 days after planting in 2020, and 35 days out of 168 days though we have some missing values in 2020 for cotton. Both crops became stressed during the development stage and stayed stressed during most mid and late stages. Occasional rainfall events saturated soil and caused crops not to be stressed but the stressed condition quickly returned if the crop was not irrigated. Year 2021 was below average precipitation with only 6.76 inches of rainfall over 21 precipitation events during the growing season (Table 4.1).

Cotton generates more profits with less irrigation groundwater than corn. With equal distribution of well capacities, cotton generate 30.8% more profits and use 26.6% less irrigation groundwater. Cotton tends to be more profitable than corn, it also tends to exhibit slightly more

risk than corn which may be due to low yielding years that suffered from cool weather and had a reduction of accumulated heat units.

# Chapter 5 - Conclusions and Recommendations

The integrated MEP model was capable of estimating the actual ET rates for corn and cotton during growing seasons 2020 and 2021. The reference ET were found to be higher than actual ET values by MEP especially during the mid-stage. This leads to the need of further adjustment of the crop coefficient. It can also indicate that more effort needs to be applied to better calibrate the MEP model parameters, i.e., soil thermal inertia and NDVI.

Crop coefficient was calculated as a ratio of actual ET by the MEP model and reference ET by the MP method. Corn had higher ET rates and higher crop coefficient than those for cotton. These higher values result in water demands higher for corn. It also supports the notion that adoption of cotton as an alternative crop to corn may reduce groundwater withdrawals and extend the economic life of the aquifer.

Crop water index graphs showed that cotton was under more stress during growing mid and late stages than corn. Since cotton is a drought tolerant crop, it can withstand more stress than corn.

More studies, experimental, theoretical, and modeling, are needed to fully evaluate cotton water use in Southwest Kansas. One application can relate to how rainfed cotton growth would differ from irrigated cotton growth under thermally limited semi-arid climate.

Maximum entropy production model takes fewer input parameters (temperature, relative humidity, and net radiation) than the other models. MEP requires temperature and relative

humidity to be measured close to the leaf surface for better representation of heat exchange there. For this study canopy temperature was measured by infrared radiometer, which is accurate, while relative humidity was measured either at 20 cm for bare soil option or at 180 cm for fully vegetated option. During crop development stage and canopy raising in height, these two measurements may not be very representative and interpolated value can be more accurate.

NDVI values were acquired from online remote sensing database and interpolated for the entire field. Using NDVI as a weighting factor between fully vegetated canopy and bare soil for actual ET calculation by the MEP model can be confused by the presence of residue and fluctuate during the season. This poses a need to develop a different weighting factor or better adjust NDVI readings to get more accurate ET results. Ground heat flux is measured at a certain depth below surface, but the MEP model uses ground heat flux at the surface. Therefore, reconstructing the flux at the surface includes the uncertainty in estimating soil energy between the depth of the sensor and soil surface. The uncertainty also relates to the uncertainty in dynamic properties of soil in that layer, soil thermal properties and sol water content. A value of $I_S$ is directly affected by this uncertainty.

Some accidental events caused equipment failure and recorded missing values. The damage to the instrument caused erroneous data collection that required special calibration effort as shown in the Appendix.

# References


Agam, N., Kustas, W. P., Anderson, M. C., Norman, J. M., Colaizzi, P. D., Howell, T. A., Prueger, J. H., Meyers, T. P., & Wilson, T. B. (2010). Application of the priestley-taylor approach in a two-source surface energy balance model. *Journal of Hydrometeorology*, *11*(1), 185–198. https://doi.org/10.1175/2009JHM1124.1

ALLEN, R. G.; PEREIRA, L. S.; RAES, D.; SMITH, M. (1998). Guidelines for computing crop water requeriments. *Fao*, 308. http://www.kimberly.uidaho.edu/water/fao56/fao56.pdf%5Cnhttp://linkinghub.elsevier.com/retrieve/pii/S1161030110001103

Allen, R G; Pereira, L S; Raes, D; Smith, M. (1998). Crop evapotranspiration-Guidelines for computing crop water requirements-FAO Irrigation and drainage paper 56 H2Olive3s View project no title View project. In *Fao, Rome* (Vol. 300, Issue 9). http://www.fao.org/3/x0490e/x0490e00.htm

Allen, R. G., Tasumi, M., & Trezza, R. (2007). Satellite-Based Energy Balance for Mapping Evapotranspiration with Internalized Calibration (METRIC)—Model. *Journal of Irrigation and Drainage Engineering*, *133*(4), 380–394. https://doi.org/10.1061/(asce)0733-9437(2007)133:4(380)

Allen, R. G., Walter, I. A., Elliott, R. L., Howell, T. A., Itenfisu, D., Jensen, M. E., & Snyder, R. L. (2018). ASCE sandardized reference evapotranspiration equation. *ASCE Standardized Reference Evapotranspiration Equation*, 1–203. https://doi.org/10.1061/9780784408056

Anderson, M. C., Norman, J. M., Mecikalski, J. R., Otkin, J. A., & Kustas, W. P. (2007). A climatological study of evapotranspiration and moisture stress across the continental United States based on thermal remote sensing: 1. Model formulation. *Journal of Geophysical Research Atmospheres*, *112*(10), 10117. https://doi.org/10.1029/2006JD007506

Bastiaanssen, W. G. M., Pelgrum, H., Wang, J., Ma, Y., Moreno, J. F., Roerink, G. J., & Van Der Wal, T. (1998). A remote sensing surface energy balance algorithm for land (SEBAL): 2. Validation. *Journal of Hydrology*, *212–213*(1–4), 213–229. https://doi.org/10.1016/S0022-1694(98)00254-6

Brutsaert, W. (1982). Evaporation into the Atmosphere. In *Evaporation into the Atmosphere*. Springer Netherlands. https://doi.org/10.1007/978-94-017-1497-6

Businger, J. A., Wyngaard, J. C., Izumi, Y., & Bradley, E. F. (1971). *Flux-Profile Relationships in the Atmospheric Surface Layer in: Journal of the Atmospheric Sciences Volume 28 Issue 2 (1971)*. Journal of Atmospheric Sciences. https://journals.ametsoc.org/view/journals/atsc/28/2/1520-0469_1971_028_0181_fprita_2_0_co_2.xml

Christiansen, J. E. (1968). Pan Evaporation and Evapotranspiration from Climatic Data. *Journal of the Irrigation and Drainage Division*, *94*(2), 243–266.

https://doi.org/10.1061/jrcea4.0000568

El Sharif, H., Zhou, W., Ivanov, V., Sheshukov, A., Mazepa, V., & Wang, J. (2019). Surface Energy Budgets of Arctic Tundra During Growing Season. *Journal of Geophysical Research: Atmospheres*, *124*(13), 6999–7017. https://doi.org/10.1029/2019JD030650

Gonzalez-Dugo, M. P., Neale, C. M. U., Mateos, L., Kustas, W. P., Prueger, J. H., Anderson, M. C., & Li, F. (2009). A comparison of operational remote sensing-based models for estimating crop evapotranspiration. *Agricultural and Forest Meteorology*, *149*(11), 1843–1853. https://doi.org/10.1016/j.agrformet.2009.06.012

Good, E. J., Ghent, D. J., Bulgin, C. E., & Remedios, J. J. (2017). A spatiotemporal analysis of the relationship between near-surface air temperature and satellite land surface temperatures using 17 years of data from the ATSR series. *Journal of Geophysical Research: Atmospheres*, *122*(17), 9185–9210. https://doi.org/10.1002/2017JD026880

Gowda, P. H., Chavez, J. L., Colaizzi, P. D., Evett, S. R., Howell, T. A., & Tolk, J. A. (2008). ET mapping for agricultural water management: Present status and challenges. *Irrigation Science*, *26*(3), 223–237. https://doi.org/10.1007/s00271-007-0088-6

Haag, L., Duncan, S., Roozeboom, K., & Waite, J. (n.d.). *2013 Kansas Performance Tests with Cotton Varieties dryland irrigated*. Retrieved February 2, 2022, from http://www.ksre.ksu.edu/bookstore/pubs/MF2567.pdf

Hall, R. G. (2014). Corn growth stages with estimated calendar days and growing-degree units. *Https://Mygeohub.Org/Resources/878*, *V*, 4–6.

Hargreaves, G. H., & Allen, R. G. (2003). History and Evaluation of Hargreaves Evapotranspiration Equation. *Journal of Irrigation and Drainage Engineering*, *129*(1), 53–63. https://doi.org/10.1061/(asce)0733-9437(2003)129:1(53)

Hoeft, R. (2000). *Modern corn and soybean production* (1st ed.). MCSP Publications.

Holman, J. D., & Foster, A. J. (2017). *Kansas State University Agricultural Experiment Station and Cooperative Extension Service*.

Jackson, R. D., Kustas, W. P., & Choudhury, B. J. (1988). A reexamination of the crop water stress index. *Irrigation Science*, *9*(4), 309–317. https://doi.org/10.1007/BF00296705

Jiang, L., & Islam, S. (2001). Estimation of surface evaporation map over southern Great Plains using remote sensing data. *Water Resources Research*, *37*(2), 329–340. https://doi.org/10.1029/2000WR900255

*Kansas Mesonet*. (2019). Historical Weather. Kansas State University. http://mesonet.k-state.edu/weather/historical/

Ko, J., Piccinni, G., Marek, T., & Howell, T. (2009). Determination of growth-stage-specific crop coefficients (Kc) of cotton and wheat. *Agricultural Water Management*, *96*(12), 1691–

1697. https://doi.org/10.1016/j.agwat.2009.06.023

Koudahe, K., Sheshukov, A. Y., Aguilar, J., & Djaman, K. (2021). Irrigation-water management and productivity of cotton: A review. *Sustainability (Switzerland)*, *13*(18), 1–21. https://doi.org/10.3390/su131810070

Kumar, R., Shankar, V., & Kumar, M. (2011). Modelling of Crop Reference: A Review. *Universal Journal of Environmental Research and Technology*, *1*(3), 239–246. www.environmentaljournal.org

Lamm, F. R., Manges, H. L., Stone, L. R., Khan, A. H., & Rogers, D. H. (1995). Water requirement of subsurface drip-irrigated corn in northwest Kansas. *Transactions of the American Society of Agricultural Engineers*, *38*(2), 441–448. https://doi.org/10.13031/2013.27851

Menenti, M., & Choudhury, B. J. (1993). *Parameterization of land surface evaporation by means of location dependent potential evaporation and surface temperature range*. Exchange Processes at the Land Surface for a Range of Space and Time Scales. Proc. International Symposium, Yokohama, 1993. https://agris.fao.org/agris-search/search.do?recordID=GB9416706

Mildrexler, D. J., Zhao, M., & Running, S. W. (2011). A global comparison between station air temperatures and MODIS land surface temperatures reveals the cooling role of forests. *J. Geophys. Res*, *116*, 3025. https://doi.org/10.1029/2010JG001486

Monteith, J. L., Szeicz, G., & Waggoner, P. E. (1965). The Measurement and Control of Stomatal Resistance in the Field. *The Journal of Applied Ecology*, *2*(2), 345. https://doi.org/10.2307/2401484

Norman, J. M., Kustas, W. P., & Humes, K. S. (1995). Source approach for estimating soil and vegetation energy fluxes in observations of directional radiometric surface temperature [Agric. For. Meteorol., 77 (1995) 263–293]. *Agricultural and Forest Meteorology*, *80*(2–4), 297. https://doi.org/10.1016/0168-1923(96)02344-1

North Carolina Climate Office. (n.d.). *Earth's Energy Balance | North Carolina Climate Office*. Retrieved January 27, 2022, from https://climate.ncsu.edu/edu/EnergyBalance

O'Shaughnessy, S. A., Evett, S. R., Colaizzi, P. D., & Howell, T. A. (2012). A crop water stress index and time threshold for automatic irrigation scheduling of grain sorghum. *Agricultural Water Management*, *107*, 122–132. https://doi.org/10.1016/j.agwat.2012.01.018

Oosterhuis, D. M. (2015). *Growth and Development of a Cotton Plant* (pp. 1–24). Publications of the American Society of Agronomy, Madison, 1-24. https://doi.org/10.2134/1990.nitrogennutritionofcotton.c1

Panwar, A., Kleidon, A., & Renner, M. (2019). Do Surface and Air Temperatures Contain Similar Imprints of Evaporative Conditions? *Geophysical Research Letters*, *46*(7), 3802–3809. https://doi.org/10.1029/2019GL082248

Sellinger, C. E. (1996). Computer Programe for Estimating Evapotranspiration using the Thornthwaite Method (NOAA Technical Memorandum ERL GLERL-101). *Computer*, 9.

Senay, G. B., Bohms, S., Singh, R. K., Gowda, P. H., Velpuri, N. M., Alemu, H., & Verdin, J. P. (2013). Operational Evapotranspiration Mapping Using Remote Sensing and Weather Datasets: A New Parameterization for the SSEB Approach. *Journal of the American Water Resources Association*, *49*(3), 577–591. https://doi.org/10.1111/jawr.12057

Su, H., McCabe, M. F., Wood, E. F., Su, Z., & Prueger, J. H. (2005). Modeling evapotranspiration during SMACEX: Comparing two approaches for local- and regional-scale prediction. *Journal of Hydrometeorology*, *6*(6), 910–922. https://doi.org/10.1175/JHM466.1

Subedi, A., & Chávez, J. L. (2015). Crop Evapotranspiration (ET) Estimation Models: A Review and Discussion of the Applicability and Limitations of ET Methods. *Journal of Agricultural Science*, *7*(6). https://doi.org/10.5539/jas.v7n6p50

Temesgen, B., Eching, S., Davidoff, B., & Frame, K. (2005). Comparison of Some Reference Evapotranspiration Equations for California. *Journal of Irrigation and Drainage Engineering*, *131*(1), 73–84. https://doi.org/10.1061/(asce)0733-9437(2005)131:1(73)

United States Department of Agriculture. (2016). *USDA/NASS QuickStats Ad-hoc Query Tool*. National Agricultural Statistics Service. https://quickstats.nass.usda.gov/results/B7EDA0D6-0B8F-3535-8600-4B9B6F903F20%0Ahttps://quickstats.nass.usda.gov/#2D38CEAD-4589-386A-9CE9-82040BBFE5FA%0Ahttps://quickstats.nass.usda.gov/results/D137063F-E35A-32C3-9919-CB2865784714?pivot=short_desc%0Ahttps

*USDA/NASS 2020 State Agriculture Overview for Kansas*. (n.d.). Retrieved January 19, 2022, from https://www.nass.usda.gov/Quick_Stats/Ag_Overview/stateOverview.php?state=KANSAS

Wang, J., & Bras, R. L. (2009). A model of surface heat fluxes based on the theory of maximum entropy production. *Water Resources Research*, *45*(11), 1–15. https://doi.org/10.1029/2009WR007900

Wang, Jingfeng, & Bras, R. L. (2011). A model of evapotranspiration based on the theory of maximum entropy production. *Water Resources Research*, *47*(3), 1–10. https://doi.org/10.1029/2010WR009392

Wang, Jingfeng, Bras, R. L., Nieves, V., & Deng, Y. (2014). A model of energy budgets over water, snow, and ice surfaces. *Journal of Geophysical Research: Atmospheres*, *119*(10), 6034–6051. https://doi.org/10.1002/2013JD021150

Yang, J., Gong, P., Fu, R., Zhang, M., Chen, J., Liang, S., Xu, B., Shi, J., & Dickinson, R. (2013). The role of satellite remote sensing in climate change studies. *Nature Climate Change*, *3*(10), 875–883. https://doi.org/10.1038/nclimate1908

# Appendix A - Data Summary & Calibration

**Table A.1: Data preprocessing limits for variables (10 minutes dataset)**

| Variables | Maximum Limit | Minimum Limit | Unit |
|---|---|---|---|
| Battery Voltage | 20 | 8 | Volts |
| Logger temperature | 50 | -30 | °C |
| Shortwave Radiation Incoming | 2000 | 0 | $Wm^{-2}$ |
| Shortwave Radiation Outgoing | 2000 | -1000 | $Wm^{-2}$ |
| Shortwave Radiation Net | 2000 | -1000 | $Wm^{-2}$ |
| Longwave Radiation Incoming | 2000 | -1000 | $Wm^{-2}$ |
| Longwave Radiation Outgoing | 2000 | -1000 | $Wm^{-2}$ |
| Longwave Radiation Net | 2000 | -1000 | $Wm^{-2}$ |
| Net Radiation | 2000 | -1000 | $Wm^{-2}$ |
| Albedo | 1 | 0 | - |
| Air Temperature | 50 | -30 | °C |
| Relative Humidity | 100 | 0 | % |
| Canopy Temperature | 60 | -30 | °C |
| Subsurface Temperature | 60 | -30 | °C |

**Table A.2: Radiation fluxes adjustments**

| Sites | Sensors | Radiation Fluxes | Correction |
|---|---|---|---|
| East | Old Sensor | SWin | 0.9128 |
| | | SWout | 1.19638 |
| | | LWin | $LWin + 3 * 10^{-9} * (AirTC\_Avg)^4$ Temperature in K |
| | | LWout | N/A |
| | New Sensor | SWin | 1.0874 |
| West | Old Sensor | SWin | 0.912 |
| | | SWout | 1.19638 |
| | | LWin | $LWin + 3 * 10^{-9} * (AirTC\_Avg)^4$ Temperature in K |
| | | LWout | N/A |

**Table A.3 : Summary of radiation fluxes for growing season 2020 and 2021**

| Crop | Growing Season | Radiation Fluxes | Average | Minimum | Maximum | Total | Units |
|---|---|---|---|---|---|---|---|
| Cotton | 2020 | SWin | 193 | 14 | 463 | 30749 | W/m2/day |
| | | NR | 74 | -8 | 248 | 11779 | |
| | | G | -3 | -27 | 18 | -527 | |
| | 2021 | SWin | 231 | 31 | 325 | 37421 | |
| | | NR | 149 | -1 | 229 | 24084 | |
| | | G | 2 | -29 | 27 | 399 | |
| Corn | 2020 | SWin | 238 | 39 | 333 | 29949 | |
| | | NR | 120 | 6 | 193 | 15156 | |
| | | G | 2 | -40 | 61 | 278 | |
| | 2021 | SWin | 222 | 30 | 325 | 28414 | |
| | | NR | 99 | -47 | 228 | 12772 | |
| | | G | 1 | -30 | 30 | 155 | |

**Table A.4: Summary of temperature for growing season 2020 and 2021**

| Crop | Growing Season | Temperature | Average | Minimum | Maximum | Total | Units |
|---|---|---|---|---|---|---|---|
| Cotton | 2020 | Air at 20 cm | 16 | -8 | 30 | 2547 | °C/day |
| | | Air at 180cm | 16 | -8 | 30 | 2539 | |
| | | Canopy | 15 | -7 | 32 | 2476 | |
| | | Soil at 2 cm | 13 | -1 | 25 | 1787 | |
| | 2021 | Air at 20 cm | 21 | 3 | 31 | 3731 | |
| | | Air at 180cm | 21 | 3 | 30 | 3685 | |
| | | Canopy | 22 | 3 | 32 | 3758 | |
| | | Soil at 2 cm | 22 | 7 | 31 | 3828 | |
| Corn | 2020 | Air at 20 cm | 19 | 4 | 26 | 1577 | |
| | | Air at 180cm | 21 | 4 | 29 | 2690 | |
| | | Canopy | 21 | 4 | 29 | 2624 | |
| | | Soil at 2 cm | 20 | 8 | 25 | 1642 | |
| | 2021 | Air at 20 cm | 22 | 5 | 30 | 3474 | |
| | | Air at 180cm | 22 | 5 | 30 | 3411 | |
| | | Canopy | 23 | 5 | 50 | 3561 | |
| | | Soil at 2 cm | 24 | 11 | 32 | 3824 | |

# Appendix B - Python Scripts

## B.1 MEP for bare soil

```
import pandas as pd
import numpy as np
import matplotlib.pyplot as plt
from scipy.optimize import *

#importing dataset
cotton=pd.read_csv('Cotton 60min
mean_season1_and_2.csv',parse_dates=['Time'],na_values=['NAN'])

#masking data set
mask1=(cotton['Time'] >= '9/1/2021  12:00:00 AM') & (cotton['Time'] <=
'9/10/2021 11:00:00 PM')
cotton=cotton.loc[mask1]

#variables
gama=0.061 #psychrometric costant gama=0.061 KPaC-1
#material density, p
p=1334.18 #kg/m3

#thermal conductivity, K
K=1.3 #unit W/m/K

# specific heat, C
C=752.635 #J/Kg K
alpha=1 #range 0.75-1
gama2=12
beta=4.7
z=5 #unit m
g=9.81 #gravity in m/s2
k=0.4 #Von Karman constant
Tr=330 #reference temperature in kelvin
lamdda=2.5*10**6
R_v=461
epsilon=0.62
P=912.3 #mb
Tc=273 #K
Tcc=0 #c

cotton.loc[(cotton['NR_adj'] >= 0) , 'C1'] = np.sqrt(3)/alpha #unstable
cotton.loc[(cotton['NR_adj'] < 0) , 'C1'] = 2/(1+2*alpha) # stable
cotton.loc[(cotton['NR_adj'] >= 0) , 'C2'] = gama2/2 #unstable
cotton.loc[(cotton['NR_adj'] < 0) , 'C2'] = 2*beta #stable
```

```
#bowing ratio calculation
 #proportional coefficient
 #for delta,d calculation AirTC_2_Avg has been used to calculate mean T ,
Tmean=(Tmax+Tmin)/2


#saturation vapor pressure at reference temperature
e0=0.6108*10**((7.5*Tcc)/(Tcc+237.3))*10 #mbar

cotton=cotton.fillna(0)

exponential=(lamdda/R_v)*((1/Tc)-(1/(cotton['TargetTC_Avg']+273)))
#unsaturated condition
cotton['q_s']=epsilon*(e0/P)*np.exp(exponential)
cotton['sigma_unsat']=(lamdda**2*cotton['q_s'])/(1200*R_v*(cotton['TargetTC_A
vg']+273)**2)*(cotton['RH_2_Max']/100)
#saturated condition
#vapor pressure at skin temperature for baresoil skin temperature will be
taken AirTC_2_Avg
eo=0.6108*10**((7.5*cotton['TargetTC_Avg'])/(cotton['TargetTC_Avg']+237.3))
d1=(4098*eo)
d2=(cotton['TargetTC_Avg']+237.3)**2
d=(d1/d2)
cotton['sigma_sat']=d/0.067

#apparent thermal inertia of air Io; rho= 1000 J/Kg/K, cp=1
Io=1200*np.sqrt(k*cotton['C1']*z)*((cotton['C2']*k*z*g)/(1*1200*Tr))**(1/6)
cotton['Io']=Io
Is=1141
Iw=np.sqrt(1000*4200*0.58)#porosity
porosity=1-(p/2650) #cotton['VWC_1_Avg']
cotton['porosity']=porosity
Is_1=Is+np.sqrt(cotton['VWC_1_Avg'])*Iw
#I=0
I=Is_1/Io
Rn=cotton['NR_adj']

#Bowing ratio, B

#B=6*(np.sqrt(1+(11*sigma/36))-1)
#for saturated sat for unsaturated unsat
x=((11/36)*cotton['sigma_sat'])
cotton['B']=6*(np.sqrt(1+x)-1)
cotton['bowen']=cotton['B']**-1
B1=(cotton['B']/cotton['sigma_sat'])*I
B2=1
```

```
def myfunction(zGuess,*Params):
    B,B1,Rn = Params
    H=zGuess
    F=B*H+H+B1*H*abs(H)**(-1/6)-Rn
    return F

cotton['B1']=B1
cotton['B2']=B2
cotton['Rn']=cotton['NR_adj']
cotton['zguess']=cotton['NR_adj']/2
zGuess=cotton['zguess']


for index,coeffs in cotton.iterrows():
    params=(coeffs['B'],coeffs['B1'],coeffs['Rn'])
    z=fsolve(myfunction,zGuess,args=params,fprime=None,xtol=1.49012e-08)
    cotton.loc[index,['H_MEP']]=z[0]


print(cotton['H_MEP'])

cotton['E_MEP']=cotton['B']*cotton['H_MEP']
cotton['G_MEP']=cotton['B1'] *cotton['H_MEP']*abs(cotton['H_MEP']  )**(-1/6)
print(cotton['G_MEP'])
print(cotton['E_MEP'])

def plotting(axes,x,y,color,xlabel,ylabel,title,label):
    axes.plot(x,y,color=color,linestyle='--',label=label)
    axes.set_xlabel(xlabel)
    axes.set_ylabel(ylabel)
    axes.tick_params('x',direction='in',rotation=45)
    axes.tick_params('y',direction='in')
    plt.legend(loc='upper center',fontsize='x-small',ncol=8,frameon=False)
    axes.set_title(title)

fig,ax=plt.subplots()

plotting(ax,cotton['Time'],cotton['NR_adj'],'orange','Time','[W/m2]','Net
NR','Net Radiation Observed')
plotting(ax,cotton['Time'],cotton['E_MEP'],'r','Time','[W/m2]','ET','ET_MEP')


fig1,ax1=plt.subplots()

ax1.plot(cotton['sigma_sat'],cotton['B'])
ax1.set_xlabel('\u03C3')
ax1.set_ylabel('B(\u03C3)')
ax1.tick_params('x',direction='in',top=True)
ax1.tick_params('y',direction='in',right=True)

fig2,ax2=plt.subplots()

ax2.plot(cotton['sigma_sat'],cotton['B']/cotton['sigma_sat'])
```

```
ax2.set_xlabel('\u03C3')
ax2.set_ylabel('B(\u03C3)/\u03C3')
ax2.tick_params('x',direction='in',top=True)
ax2.tick_params('y',direction='in',right=True)
plt.show()
```

### B.2 MEP for full vegetation

```
import pandas as pd
import numpy as np
import matplotlib.pyplot as plt

cotton=pd.read_csv('Cotton 60min
mean_season1_and_2.csv',parse_dates=['Time'],na_values=['NAN'])
cotton_max=pd.read_csv('Cotton 60min
max_season1_and_2.csv',parse_dates=['Time'],na_values=['NAN'])
cotton_min=pd.read_csv('Cotton 60min
min_season1_and_2.csv',parse_dates=['Time'],na_values=['NAN'])

mask1=(cotton['Time'] >='6/17/2020 12:00:00 AM') & (cotton['Time'] <=
'12/10/2020 11:00:00 PM')
cotton=cotton.loc[mask1]
mask2=(cotton_min['Time'] >= '6/17/2020 12:00:00 AM') & (cotton_min['Time']
<= '12/10/2020 11:00:00 PM')
cotton_min_1=cotton_min.loc[mask2]
mask3=(cotton_max['Time'] >= '6/17/2021 12:00:00 AM') & (cotton_max['Time']
<= '12/10/2020 11:00:00 PM')
cotton_max_1=cotton_max.loc[mask3]


#Io calculation
rho_cp=1000 #from Dr.Wang's paper
k=0.4 #Von Karman Constant
z=5 #meter (may change later)
g=9.8 #m/s2
T_ref=300 # K
alpha=0.75
beta=4.7
gama2=9
lamdda=2.5*10**6
R_v=461
epsilon=0.62
P=912.3 #mbar
Tr=300
Iw=np.sqrt(1000*4180*0.58)
cotton['SWin_adj']=cotton['SWin_Avg']*0.91203
cotton['SWout_adj']=cotton['SWout_Avg']*1.19638
cotton['LWin_adj']=cotton['LWin_Avg']+3*10**-9*(cotton['AirTC_Avg']+273)**4
cotton['NR_adj']=cotton['SWin_adj']-cotton['SWout_adj']+cotton['LWin_adj']-
cotton['LWout_Avg']

cotton.loc[(cotton['NR_adj'] >= 0) , 'C1'] = np.sqrt(3)/alpha #unstable
```

```
cotton.loc[(cotton['NR_adj'] < 0) , 'C1'] = 2/(2+alpha) # stable
cotton.loc[(cotton['NR_adj'] >= 0) , 'C2'] = gama2/2 #unstable
cotton.loc[(cotton['NR_adj'] < 0) , 'C2'] = 2*beta #stable
#bowing ratio calculation
 #proportional coefficient
 #for delta,d calculation AirTC_2_Avg has been used to calculate mean T ,
Tmean=(Tmax+Tmin)/2
#eo=0.6108*10**((7.5*corn['AirTC_2_Avg'])/(corn['AirTC_2_Avg']+237.3))
exponential=(lamdda/R_v)*((1/273)-(1/(cotton['AirTC_Avg']+273)))
#eo=0.6108*10**((7.5*27)/(27+237.3)) #saturation vapor pressure at reference
temperature
eo=6.11 #mbar
#exponential=(lamdda/R_v)*((1/T_ref)-(1/(corn['AirTC_2_Avg']+273)))
cotton=cotton.fillna(0)
eta_s=10/3*((cotton['VWC_1_Avg']-0.09)/(0.231-0.09))
cotton['q_s']=epsilon*(eo/P)*np.exp(exponential)*eta_s
cotton['sigma_unsat']=(lamdda**2*cotton['q_s'])*(cotton['RH_Max']/100)/(1000*
R_v*(cotton['AirTC_Avg']+273)**2)
d1=(4098*eo)
d2=(cotton['AirTC_Avg']+237.3)**2
d=(d1/d2)
print(d)
cotton['sigma_sat']=d/0.067


#Bowing ratio, B
cotton['B']=6*(np.sqrt(1+(11/36*cotton['sigma_unsat']))-1)
cotton['bowen']=cotton['B']**-1


#MEP model
#B1=1
Rn=cotton['NR_adj']
B=cotton['B']
cotton['Rn']=Rn
cotton['rmse']=0
lst=[]
I=0
B2=1
cotton['H_MEP']=cotton['Rn']/(1+cotton['B'])
cotton['E_MEP']=cotton['Rn']/(1+cotton['bowen'])
print(cotton['E_MEP'])
cotton=cotton.fillna(0)

plt.plot(cotton['Time'],cotton['E_MEP'])
plt.show()
```

### B.3 Crop Water Stress Index

```
import pandas as pd
import matplotlib.pyplot as plt
import numpy as np

cotton=pd.read_csv('corn_data_edited_daily_2021.csv',parse_dates=['Time'],low
_memory=False)

mask=(cotton['Time'] >= '5/28/2021') & (cotton['Time'] <= '10/31/2021')
cotton=cotton.loc[mask]

cotton['SWin_adj']=cotton['SWin_adj'].astype('float')
cotton['AirRH_Avg']=cotton['AirRH_Avg'].astype('float')
cotton['AirTC_Avg']=cotton['AirTC_Avg'].astype('float')

#Tc-Ta
cotton['AirTC_Avg']=cotton['AirTC_Avg'].astype('float')
cotton['TT_C_Avg']=cotton['TT_C_Avg'].astype('float')

cotton['Tc-Ta']=cotton['TT_C_Avg']-cotton['AirTC_Avg']

#Tc-Ta ul
P=91230 #Pa
Temperature=(cotton['AirTC_Avg']+273)

r_dry=287.058 #j/kg/k
rho=P/(Temperature*r_dry)
# rho_dry=P/(Temperature_dry*r_dry)
cp=1013 #J/kg/C
k=0.41
height=0.12 #mean crop height
d=(2/3)*height
zom=0.123*height
zoh=0.1*zom
zm=zh=2 #m
lon=(np.log((zm-d)/zom)*np.log((zh-d)/zoh))/k**2
ra=lon/(cotton['WS_ms_Avg'])
albedo=0.23
R_s=cotton['SWin_adj']  #w/m2#*0.0864#MJ/m2/day
R_ns=(1-albedo)*R_s #w/m2

sigma=4.903*10**-9
es_max= 0.6108*10**((7.5*cotton['TT_C_Avg'])/((cotton['TT_C_Avg'])+237.3))
#unit KPa
es_min= 0.6108*10**((7.5*cotton['AirTC_Avg'])/((cotton['AirTC_Avg'])+237.3))
es=(es_min+es_max)/2

ea=(cotton['AirRH_Avg']/100)*es

T=((cotton['AirTC_Avg']+273)**4+(cotton['TT_C_Avg']+273)**4)/2

e=0.34-0.14*np.sqrt(ea)
```

```
#radiation calc
G_sc=0.0820 #MJm-2min-1
doy=cotton['Time'].dt.dayofyear
d_r=1+0.033*np.cos(doy*2*np.pi/365)

phi=38.026*np.pi/180 #latitude
delta=0.409*np.sin(2*np.pi/365*doy-1.39)

# lz=90
# lm=100.872
ws=np.arccos(-np.tan(phi)*np.tan(delta))
R_a=(24*60/np.pi)*G_sc*d_r*(ws*np.sin(phi)*np.sin(delta)+np.cos(phi)*np.cos(d
elta)*np.sin(ws))
R_so=(0.75+2*10**-5*885)*R_a*11.6 #w/m2
cotton['Rs/Rso']=R_s/R_so
cotton.loc[(cotton['Rs/Rso'] <= 1)& (cotton['Rs/Rso'] > 0.3) , 'r']
=1.35*cotton['Rs/Rso']-0.35
cotton.loc[(cotton['Rs/Rso'] <=0.3) , 'r'] =1.35*0.30-0.35
cotton.loc[(cotton['Rs/Rso'] > 1) , 'r'] =1

L_n=(sigma*T*e*cotton['r'])*11.6
R_n=R_ns-L_n
cotton['Rn']=R_n
cotton['G']=R_n*0.1 #MJ/m2/day
g=cotton['Rn']-cotton['G']
cotton['Tc-Ta_ul']=(ra*g)/(rho*cp)

#Tc-Ta ll
gama=0.067
d1=(4098*es)
d2=(cotton['AirTC_Avg']+237.3)**2
d=(d1/d2)

cotton['Tc-Ta_ll']=(cotton['Tc-Ta_ul']*(gama/(gama+d)))-(((es-ea)/(gama+d)))
print(rho)
cotton['cwsi']=(cotton['Tc-Ta']-cotton['Tc-Ta_ll'])/(cotton['Tc-Ta_ul']-
cotton['Tc-Ta_ll'])
cotton.loc[(cotton['cwsi'] <=0) , 'cwsi'] =0

ax.plot(cotton['Day'],cotton['cwsi'],label='corn_cwsi',color='b')
ax.plot(cotton['Day'],np.linspace(0.45,0.45,157),color='r',linestyle='--')
ax.legend()
ax1.legend(loc='upper center',fontsize='small',ncol=8,frameon=False)
plt.title('Growing Season 2021')
plt.xlabel('Days After Planting',fontsize=10)
ax.set_ylabel('CWSI')
ax.set_xlim(-2,160)
ax.set_xlabel('Days After Planting',fontsize=10)
plt.tight_layout()
ax.tick_params('x',direction='in')
ax.tick_params('y',direction='in')
ax1.tick_params('y',direction='in')
plt.show()
```